

Experimental and Modelling Study of Gerbil Middle ear

Nima Maftoon

Department of BioMedical Engineering

McGill University, Montréal

May 2014

A thesis submitted to McGill University in partial fulfillment

of the requirements of the degree of

Doctor of Philosophy

*To my mother Showleh
and the memory of my father Habib (1946-2013)
for engraving a high regard for knowledge in my values*

Abstract

This thesis presents *in vivo* experimental measurements of vibrations on the surgically exposed tympanic membrane (TM) in the gerbil and a finite-element model of the gerbil middle ear. The TM is composed of the pars tensa and pars flaccida and is connected to the middle-ear bones via the manubrium of the malleus. Measurements were done on the pars flaccida and at several points along the manubrium and on the pars tensa using a laser Doppler vibrometer. Measurements were first done with a closed middle-ear cavity. The manubrial points show an increasing displacement magnitude from the lateral process toward the umbo, with the apparent axis of rotation shifting at high frequencies. Above 5 kHz, phase differences between points along the manubrium may indicate flexing in the manubrium. The simple low-frequency vibration pattern of the pars tensa breaks up at between 1.8 and 2.8 kHz.

The effects of progressive opening of the middle-ear cavity were then explored. In all responses, opening the cavity causes an increase in the low-frequency magnitude and a shift of the main middle-ear resonance to lower frequencies, and introduces an antiresonance. However, opening the cavity has little or no effect on either the mode of vibration of the manubrium or the breakup frequency of the pars tensa. An identification method was developed for eliminating the effect of the antiresonance. It was validated and then applied to manubrial and pars-tensa responses.

The finite-element model developed in this study uses a set of baseline parameters based primarily on *a priori* estimates from the literature. Responses from the model were validated against our measurements and against measurements from other groups. The responses of the model are mostly within the range of variability seen in the experimental data. A sensitivity analysis ranked the parameters of the model based on their effects on the model results.

Résumé

Cette thèse présente des mesures expérimentales *in vivo* des vibrations du tympan chirurgicalement exposé de la gerbille et un modèle aux éléments finis de l'oreille moyenne de la gerbille. Le tympan est composé du pars tensa et du pars flaccida et est relié aux osselets de l'oreille moyenne par le manubrium du malleus. Des mesures ont été effectuées sur le pars flaccida, et sur plusieurs points le long du manubrium et sur le pars tensa, utilisant un vibromètre laser Doppler. Les mesures ont été d'abord effectuées avec la cavité de l'oreille moyenne fermée. Les points sur le manubrium montrent une amplitude de déplacement augmentant du processus latéral à l'umbo, avec un axe apparent de rotation qui se déplaçait à des fréquences élevées. Au-dessus de 5 kHz, les différences de phase entre les points le long du manubrium indiquent possiblement la flexion du manubrium. Le type simple de vibration de basse fréquence du pars tensa commence à devenir plus complexe ('breaks up') entre 1.8 et 2.8 kHz.

Les effets de l'ouverture progressive de la cavité de l'oreille moyenne ont été ensuite explorés. Dans toutes les réponses, l'ouverture de la cavité provoque une augmentation de l'amplitude à basse fréquence et un décalage de la résonance principale de l'oreille moyenne aux fréquences plus basses, et aussi introduit une antirésonance. Toutefois, l'ouverture de la cavité a un effet minimal sur le mode de vibration du manubrium et sur la fréquence 'break-up' du pars tensa. Une méthode d'identification a été développée pour éliminer l'effet de l'antirésonance. Elle a été validée et ensuite a été appliquée aux mesures sur le manubrium et le pars tensa.

Le modèle aux éléments finis développé dans cette étude utilise un ensemble de paramètres de référence basés principalement sur des estimations *a priori* de la littérature. Les réponses du modèle ont été validées contre nos mesures expérimentales et celles d'autres groupes. Les réponses du modèle sont

pour la plupart à l'intérieur de la gamme de variabilité observée dans les données expérimentales. Une analyse de sensibilité a classé les paramètres du modèle selon leurs effets sur les résultats du modèle.

Table of Contents

Abstract.....	ii
Résumé.....	iii
Acknowledgements.....	viii
Contributions of authors.....	x
1 Introduction.....	1
1.1 Motivation.....	1
1.2 Objectives.....	2
1.3 Thesis outline.....	3
2 Anatomy.....	4
2.1 Introduction.....	4
2.2 Gerbil middle ear.....	4
2.3 Differences from human middle ear.....	10
3 Literature review.....	13
3.1 Introduction.....	13
3.2 Measurements of tympanic-membrane vibrations.....	13
3.3 Effects of middle-ear cavity on tympanic-membrane motion.....	18
3.4 Related gerbil measurements.....	19
3.4.1 Anatomical measurements.....	19
3.4.2 Quasi-static deformation of the tympanic membrane.....	20
3.4.3 Middle-ear impedance and admittance measurements.....	21
3.4.4 Sound-pressure distribution.....	22
3.4.5 Cochlear input impedance.....	22
3.4.6 Vibration measurements.....	22
3.5 Modelling of middle-ear mechanics.....	24
4 Experimental study of vibrations of gerbil tympanic membrane with closed middle-ear cavity.....	28
Preface.....	28
Abstract.....	29
4.1 Introduction.....	30
4.2 Materials and methods.....	32
4.2.1 Preparation.....	32
4.2.2 Instrumentation.....	35
4.2.3 Measurement and analysis procedures.....	36
4.3 Results.....	38
4.3.1 Effects of using beads.....	38
4.3.2 Repeatability and temporal effects.....	39
4.3.3 Umbo and pars-flaccida vibrations.....	40
4.3.3.1 Low frequencies.....	40
4.3.3.2 Mid and high frequencies.....	43
4.3.4 Manubrial vibrations.....	45
4.3.5 Pars-tensa vibrations.....	48
4.3.5.1 Low-frequency response.....	48
4.3.5.2 High-frequency response.....	49
4.4 Discussion.....	52
4.4.1 Umbo and pars-flaccida responses.....	52

4.4.2 Pars-flaccida retraction.....	54
4.4.3 Manubrial response.....	58
4.4.4 Pars-tensa response.....	59
4.5 Acknowledgements.....	59
Appendix.....	60
5 Effect of opening middle-ear cavity on vibrations of gerbil tympanic membrane.....	61
Preface.....	61
Abstract.....	62
5.1 Introduction.....	63
5.2 Materials and methods.....	64
5.2.1 Preparation and measurement.....	64
5.2.2 Estimation of ideal open-cavity responses.....	67
5.3 Results.....	72
5.3.1 Umbo vibrations.....	72
5.3.2 Pars-flaccida vibrations.....	77
5.3.3 Manubrial vibrations.....	78
5.3.4 Pars-tensa vibrations.....	80
5.3.5 Estimated ideal open-cavity responses.....	82
5.3.5.1 Validation of the method.....	82
5.3.5.2 Umbo response.....	85
5.3.5.3 Sensitivity to the fitting range.....	88
5.3.5.4 Effect of enlarging the opening.....	89
5.3.5.5 Manubrium response.....	91
5.3.5.6 Pars-tensa response.....	91
5.4 Discussion.....	92
5.4.1 Effects of opening the middle-ear cavity on manubrium and TM vibrations	92
5.4.2 Estimation of ideal open-cavity responses.....	95
5.4.3 Implications of ideal open-cavity responses.....	97
5.5 Acknowledgements.....	98
6 Finite-element modelling of the response of the gerbil middle ear to sound.....	99
Preface.....	99
Abstract.....	100
6.1 Introduction.....	101
6.2 Materials and methods.....	102
6.2.1 Geometry, model components and mesh.....	102
6.2.2 Boundary conditions.....	106
6.2.3 Calculation of frequency responses.....	106
6.2.3.1 Procedure.....	106
6.2.3.2 Time dependence.....	107
6.2.3.3 Mesh dependence.....	108
6.2.3.4 Effect of viewing angle.....	108
6.2.4 Baseline material properties.....	109
6.2.4.1 Stiffness.....	109
6.2.4.1.1 Pars tensa.....	109
6.2.4.1.2 Pars flaccida.....	112
6.2.4.1.3 Other structures.....	113
6.2.4.2 Mass.....	114

6.2.4.3 Damping.....	115
6.2.4.4 Cochlear load.....	116
6.2.5 Sensitivity analysis.....	116
6.3 Results.....	116
6.3.1 Umbo and pars-flaccida responses.....	116
6.3.1.1 Low frequencies.....	117
6.3.1.2 Mid and high frequencies.....	120
6.3.2 Manubrial response.....	121
6.3.3 Pars-tensa response.....	122
6.3.4 Stapes response.....	125
6.3.5 Sensitivity analysis.....	127
6.4 Discussion.....	135
6.4.1 Study approach.....	135
6.4.1.1 Baseline model.....	135
6.4.1.2 Sensitivity analysis.....	135
6.4.2 Model parameters.....	137
6.4.3 Model responses.....	139
6.4.3.1 Pars flaccida and umbo.....	139
6.4.3.2 Manubrium.....	140
6.4.3.3 Pars tensa.....	140
6.4.3.4 Stapes.....	141
6.4.4 Model sensitivity.....	141
6.5 Acknowledgements.....	142
7 Conclusion.....	144
7.1 Summary.....	144
7.2 Original contributions.....	144
7.3 Significance.....	146
7.4 Future work.....	147
7.4.1 Future gerbil studies.....	148
7.4.2 Application to the human middle ear.....	151
References.....	152

Acknowledgements

I am finishing my PhD studies with a big wish that some day I will be so knowledgeable, so professional, so thoughtful, so selfless, so supportive and so dedicated that I can provide the same level of supervision that I received from Dr. W. Robert J. Funnell, to others. Thank you!

This work wouldn't be possible without the clinical insight of my co-supervisor Dr. Sam J. Daniel. I deeply appreciate his supervision and support, especially for the measurements that I made at the Montréal Children's Hospital.

I greatly benefited from collaborating with Dr. Willem F. Decraemer of the University of Antwerp, Belgium. His smart comments had significant impact on the quality of my work.

I would like to thank my advisory committee members Dr. Robert Kearney, Dr. Tony Leroux and Dr. Luc Mongeau. I deeply appreciate the time that they spent on reviewing my work and I am grateful for their excellent questions that encouraged me to learn more and think more deeply about my research. I am very honoured that distinguished researchers, Dr. Sunil Puria and Dr. Luc Mongeau, agreed to be my PhD examiners.

I would also like to thank my friends and colleagues in the Auditory Mechanics Laboratory and McGill Auditory Science Laboratory. I thank Hamid Motallebzadeh, for so many hours of inspiring discussions that we had about vibration and modelling and for our outside fun. I would also like to thank Zinan He and Richard Shapiro for discussions that we had about experiments. I especially thank Richard for his great job on the French translation of my abstract. I thank Shruti Nambiar for the surgery lessons that I received from her when I started my studies. Long hours

of surgery and measurements always had a perfect start with the help of Dr. Dan Citra – thanks, Dan!

I would like to express my gratitude to Nancy Abate and Pina Sorrini. My studies, like those of many others in the department, wouldn't have gone so smoothly without their help and support.

I am thankful to my family and friends for their love, support and understanding. My special thanks go to my two little angels, Armita and Vianna, for the understanding they showed during this time.

I cannot finish this acknowledgement without expressing my deepest gratitude to my wife and best friend Parisa. Without her constant encouragement, support and sacrifice I couldn't even have started this chapter of my life.

This work was supported in part by the Canadian Institutes of Health Research, the Fonds de recherche en santé du Québec, the Natural Sciences and Engineering Research Council of Canada, the Montréal Children's Hospital Research Institute and the McGill University Health Centre Research Institute.

Contributions of authors

Chapters 4 & 5:

Experimental study of vibrations of gerbil tympanic membrane with closed middle-ear cavity, *Journal of the Association for Research in Otolaryngology*, August 2013, Volume 14, Issue 4, 467-481.

Effect of opening middle-ear cavity on vibrations of gerbil tympanic membrane, *Journal of the Association for Research in Otolaryngology*, June 2014, Volume 15, Issue 3, 319-334.

First author: Nima Maftoon

Involved in designing and building the experimental setup and in designing experimental protocols; performed experiments (anaesthesia, surgery and measurements); designed data-analysis procedure, analyzed and interpreted data; conceived and developed an algorithm for estimating ideal open-cavity responses; wrote the manuscripts.

Second author: W. Robert J. Funnell

Conceived the study, supervised the research and writing.

Third author: Sam J. Daniel

Helped conceive the study, provided the experimental facilities, provided comments and suggestions, reviewed the manuscripts.

Fourth author: Willem F. Decraemer

Provided comments and suggestions, reviewed the manuscripts.

Chapter 6:

Finite-element modelling of the response of the gerbil middle ear to sound, Submitted to *Journal of the Association for Research in Otolaryngology*, 2014 May 26

First author: Nima Maftoon

Developed the finite-element model, designed and performed simulations, analyzed and interpreted results, designed validation protocol, validated the model, wrote the manuscript.

Second author: W. Robert J. Funnell

Conceived the study, reconstructed the geometry of the model, supervised the research and writing.

Third author: Sam J. Daniel

Helped conceive the study, provided suggestions and comments, reviewed the manuscript.

Fourth author: Willem F. Decraemer

Provided the μ CT imaging data, provided comments and suggestions, reviewed the manuscript.

1 Introduction

1.1 Motivation

In Canada alone, more than two thousand children are born with some degree of hearing loss every year (The Hearing Foundation of Canada, 2010). In the first six months of life, hearing is crucial for the development of language skills (e.g., Kuhl et al., 1992). In order to detect hearing loss as early as possible, universal newborn hearing screening (UNHS) is increasingly becoming a standard practice in many countries. UNHS aims at identification of permanent bilateral or unilateral, sensorineural (disorders of the inner ear, auditory nerve and/or brain) or conductive (disorders of the external or middle ear) hearing loss (Joint Committee on Infant Hearing et al., 2000; Joint Committee on Infant Hearing, 2007). Screening is done using either otoacoustic emissions (OAEs) or the auditory brain-stem response (ABR). Because different types of hearing loss need different interventions, distinction between types of hearing loss is very important. Unfortunately the screening versions of both OAE and ABR tests cannot distinguish between conductive and sensorineural hearing loss effectively. A low positive predictive value of 0.02 to 0.4 (Akinpelu et al., 2014) is another concern with UNHS. This can be attributed to the transient condition of the middle ear due to some fluid and residual tissue in the first 48 hours postpartum (e.g., Stuart et al., 1994). False positives result in wasting time and money and cause emotional distress for families (e.g., Paradise, 1999). New screening tools and methods that can distinguish between conductive and sensorineural hearing loss and can differentiate between transient and permanent losses are required.

The auditory organ is a complex system. In order to develop new screening tools and methods, quantitative models that can describe it are required. These quantitative models should embody our understanding about the system and help us both to predict responses of the system in different conditions and to interpret new experimental observations. Building and validating these quantitative models require experimental data that often need to be collected invasively. The gerbil is a frequently used species in auditory research and the wealth of knowledge and data that exist about its auditory system can be used in developing reliable models. In this thesis, experimental data collection was done in the gerbil middle ear and a quantitative model of the gerbil middle ear was developed and validated. The set of parameter values established in this thesis and the validated modelling methodology can guide development of human middle-ear models.

1.2 Objectives

The sound stimulus, collected by the external ear, vibrates the tympanic membrane. This primary vibration is then passed through the ossicles to stimulate the inner ear. In order to obtain a better understanding of middle-ear function, understanding vibrations of the tympanic membrane is crucial. Despite the extensive literature about the auditory system of the Mongolian gerbil (*Meriones unguiculatus*), very little is known about the vibrations of its tympanic membrane.

There are some circuit models in the literature that tried to describe the dynamic function of the gerbil middle ear. However, these models are not direct representations of the biomechanical characteristics of the middle ear and cannot reproduce its 3-D motions. The finite-element method has been proven to be a powerful method for making models of mechanical systems including the middle ear.

The objectives of this thesis are the following:

1. To study vibrations of the gerbil tympanic membrane in response to sound stimuli *in vivo* with an intact middle-ear cavity.
2. To study the effects of opening the middle-ear cavity on the vibrations of the gerbil tympanic membrane *in vivo*.
3. To develop a method for estimating tympanic-membrane vibrations in the limit of no middle-ear cavity from experimental data collected with a partial opening in the cavity wall. This will facilitate comparisons of the experimental responses with responses from the models with no middle-ear cavity.
4. To develop and validate a finite-element model of the gerbil middle ear.

1.3 Thesis outline

Chapter 2 provides a brief overview of middle-ear anatomy and serves as a nomenclature guide. Related works from the literature are reviewed in Chapter 3. Chapter 4 covers the experimental study of tympanic-membrane vibrations with a closed middle-ear cavity. Chapter 5 explores the effects of opening the middle-ear cavity on tympanic-membrane vibrations. It also presents a theoretical framework for estimating tympanic-membrane vibrations in the limit of no middle-ear cavity. Chapter 6 presents a finite-element model of the gerbil middle ear. Finally, Chapter 7 presents conclusions and suggests some future work.

2 Anatomy

2.1 Introduction

The peripheral auditory system collects acoustic information from the environment and converts it to signals that are channelled to the brain via cranial nerve VIII. This system is divided into three parts: external, middle and inner. The external ear collects sounds from the air and transfers them to the middle ear via the ear canal. The middle ear consists of the tympanic membrane (TM) or eardrum, the ossicles (malleus, incus and stapes) and their suspensory attachments, the middle-ear cavity, and tendons and muscles. The TM is the interface between the middle and external ears. The sound impinging on the TM sets it and its attached ossicles into motion. The last bone in the ossicular chain (the stapes) is connected to the oval window of the cochlea. Vibrations of the stapes are transferred to the lymph filled in the cochlea. The lymph motion finally stimulates hair cells in the cochlea to generate signals that can be processed in the brain to perceive the sound. The anatomy of the human middle ear can be found in standard temporal-bone anatomy textbooks (e.g., Gulya & Schuknech, 1994). This section describes the anatomy of the gerbil middle ear and highlights its differences from the human middle ear.

2.2 Gerbil middle ear

In the following description of middle-ear anatomy, the number in parentheses following the name of each middle-ear component refers to its corresponding 3-D representation in Figures 2.1 and 2.2.

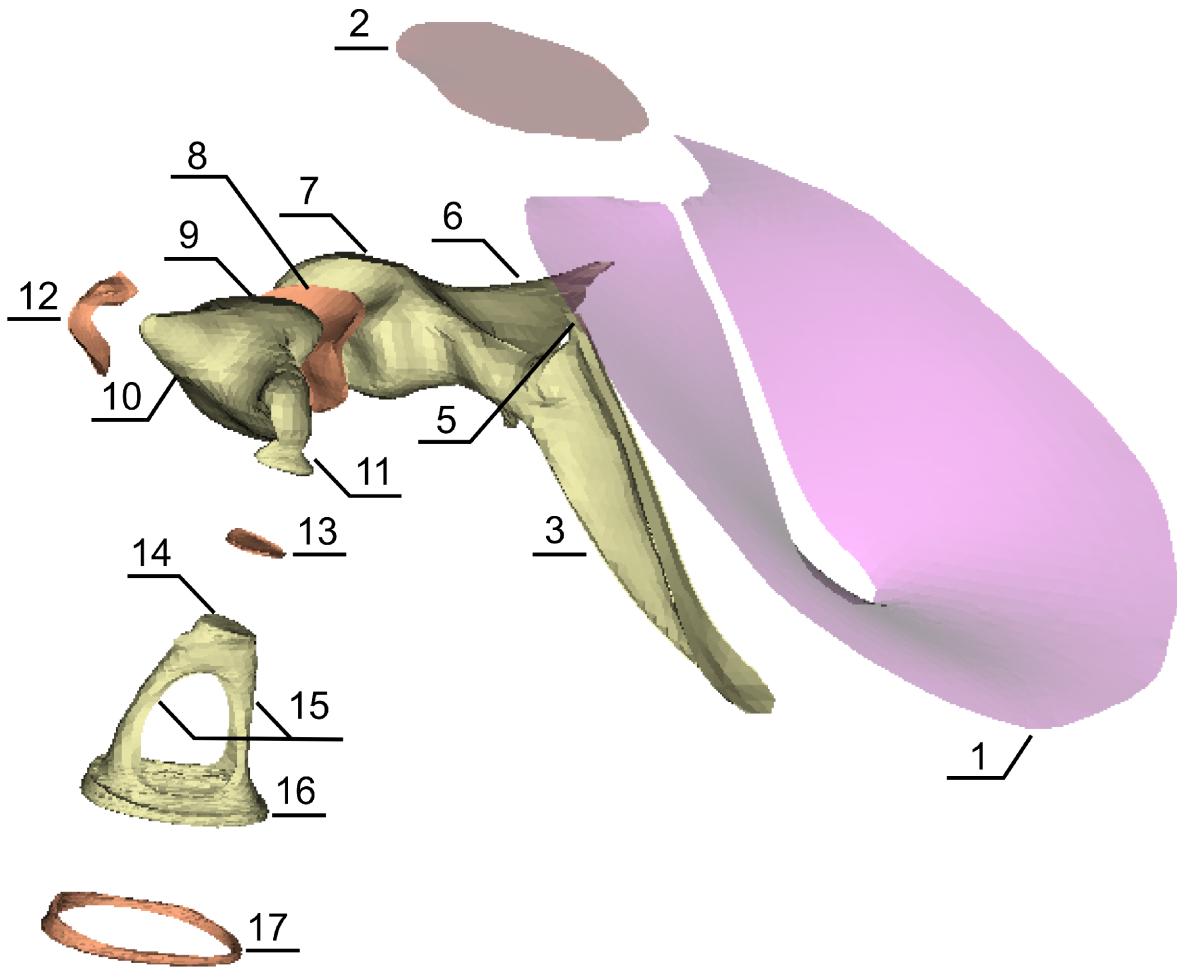


Figure 2.1: Exploded view 1 of TM, ossicles and ligaments in gerbil middle ear prepared based on our finite-element model. 1: pars tensa, 2: pars flaccida, 3: manubrium of malleus, 5: lateral process of the manubrium, 6: anterior process of malleus, 7: malleus head, 8: incudomalleal joint, 9: incus body, 10: short process of incus, 11: lenticular process of incus, 12: posterior incudal ligament, 13: incudostapedial joint, 14: stapes head, 15: stapes crura, 16: stapes footplate, 17: stapedial annular ligament.

The TM is divided into two parts that have different micro-structures: pars tensa (1) and pars flaccida (2). The pars tensa is the bigger part and is tightly connected to the malleus via its handle, which is called the manubrium (3). The manubrium is connected to the pars tensa along its length. The pars tensa forms a surface that connects the manubrium to the fibrocartilaginous ring in the bony tympanic ring. The shape of this surface resembles a minimal-energy surface

(like the surfaces formed by soap films). It was hypothesized that this shape results from minimization of the surface elastic energy during the development process (Decraemer & Funnell, 2008). The umbo is the deepest part of the pars tensa, where the inferior tip of the manubrium is. The pars tensa is made up of three layers: a lateral epidermal layer, an intermediate fibrous layer (lamina propria) and a medial mucosal layer (Lim, 1968a). The lamina propria is composed of four sublayers: subepidermal and submucosal loose connective-tissue sublayers, and two sublayers composed of highly organized collagen fibres in radial and circumferential directions. In the radial collagenous sublayer, collagen fibres start from the fibrocartilaginous ring and go almost straight toward the manubrium. In the circumferential collagenous sublayer, collagen fibres start from the manubrium, curve around the inferior end of the manubrium, and end in the opposite side of the manubrium.

The pars flaccida is located superior to the pars tensa and the manubrium. The pars flaccida is also composed of a lateral epidermal layer, a lamina propria and a medial mucosal layer but its lamina propria does not have the highly organized sublayers of the pars tensa and is abundant in elastic fibres (Lim, 1968b). More information about the tympanic membrane and related measurements can be found in Funnell & Laszlo (1982) and Decraemer and Funnell (2008).

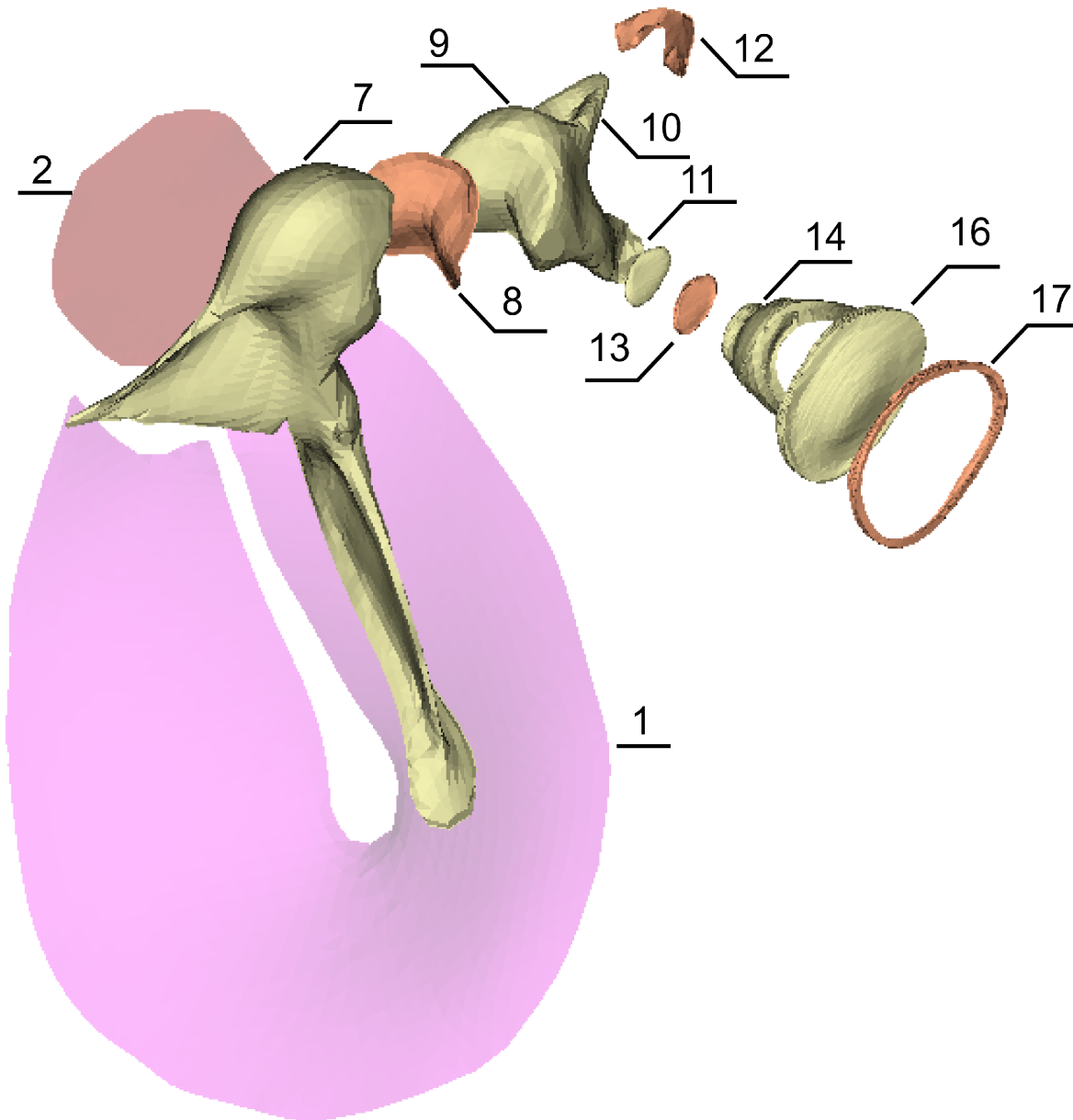


Figure 2.2: Exploded view 2 of TM, ossicles and ligaments in gerbil middle ear prepared based on our finite-element model. 1: pars tensa, 2: pars flaccida, 7: malleus head, 8: incudomalleal joint, 9: incus body, 10: short process of incus, 11: lenticular process of incus, 12: posterior incudal ligament, 13: incudostapedial joint, 14: stapes head, 16: stapes footplate, 17: stapedial annular ligament.

The ossicular chain is composed of the three smallest bones of the body. The first bone in this chain is the malleus. The anterior process of the malleus is long and is attached to the bony cavity with a thin bony attachment (Rosowski et al., 1999). The bony attachment can be seen in

Figure 2.3. The incudomalleolar joint is a synovial joint between the malleus head (7) and the incus body (9). The short process of the incus (10) is connected to the middle-ear cavity wall by means of the posterior incudal ligament (12). The long process of the incus ends in the lenticular process (11). The lenticular process (Figure 2.4) is composed of the pedicle and the lenticular plate (e.g., Funnell et al., 2005). The pedicle in gerbils is so thin that it is almost transparent. The incudostapedial joint (13), another synovial joint, is between the lenticular plate and the head of the stapes (14). The capsules of both of these joints are mainly composed of elastic fibres (e.g., Davies, 1948; Harty, 1953; Kawase et al., 2012; Takanashi et al., 2013). The stapes head branches into two crura (15) that connect the head to the stapes footplate (16). The almost oval periphery of the stapes footplate is attached to the stapedial annular ligament (17). This ligament holds the stapes within the oval window of the inner ear. It is mainly composed of elastic fibres (e.g., Davies, 1948; Harty, 1953; Ohashi et al., 2006; Takanashi et al., 2013).

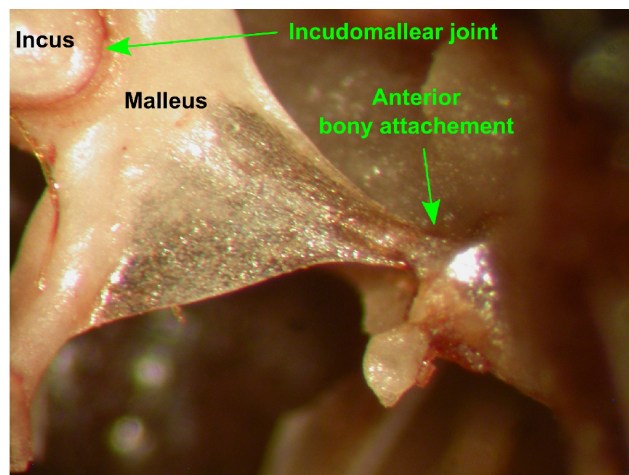


Figure 2.3: Anterior bony attachment of the malleus in one of our gerbil preparations.

The middle-ear cavity is the air space that contains all middle-ear components. In the gerbil this space is formed by a hypertrophied bone referred to as a bulla (Lay, 1972). The bony surface of this cavity is lined with a mucosal layer (Sadé & Ar, 1997). The air pressure in the middle-ear

cavity is applied on the medial surface of the TM and the pressure in the ear canal is applied on its lateral surface. The Eustachian tube connects the cavity to the nasopharynx. This tube is normally closed but it opens occasionally to ventilate the cavity and equalize its pressure with the ambient pressure which, in a natural condition, is the same as the pressure in the ear canal.

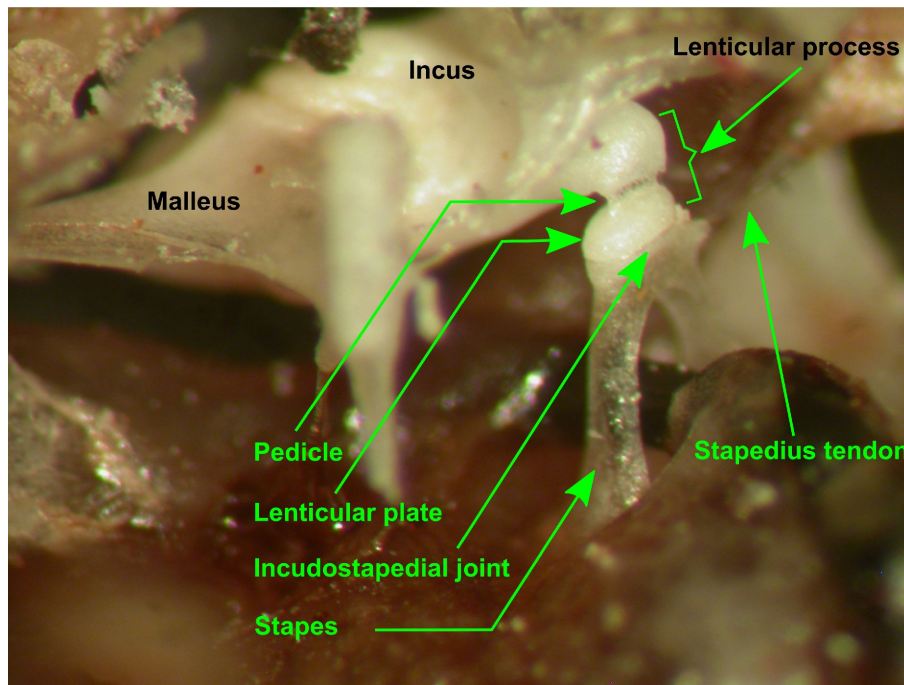


Figure 2.4: Malleus, incus, lenticular process (pedicle and lenticular plate), incudostapedial joint, stapedius tendon and stapes in one of our gerbil preparations after removing the TM and parts of the cavity wall.

The smallest skeletal muscle of the body (stapedius muscle) is connected to the stapes by the stapedius tendon (see Figures 2.4 and 2.5). The tensor tympani muscle is buried in the cavity wall and is connected to the malleus via the tensor tympani tendon. These muscles contract in response to high-intensity sounds (acoustic reflex) to reduce sound conduction to the cochlea (e.g., Borg, 1968). Furthermore, their contractions are associated with body motion (Carmel & Starr, 1963), vocalization (Borg & Zakrisson, 1975) and chewing and swallowing (Djupestrand, 1965). Contraction of the muscles reduces masking of high-frequency sounds by low-frequency sounds (e.g., Irvine, 1976; Pang & Guinan, 1997).

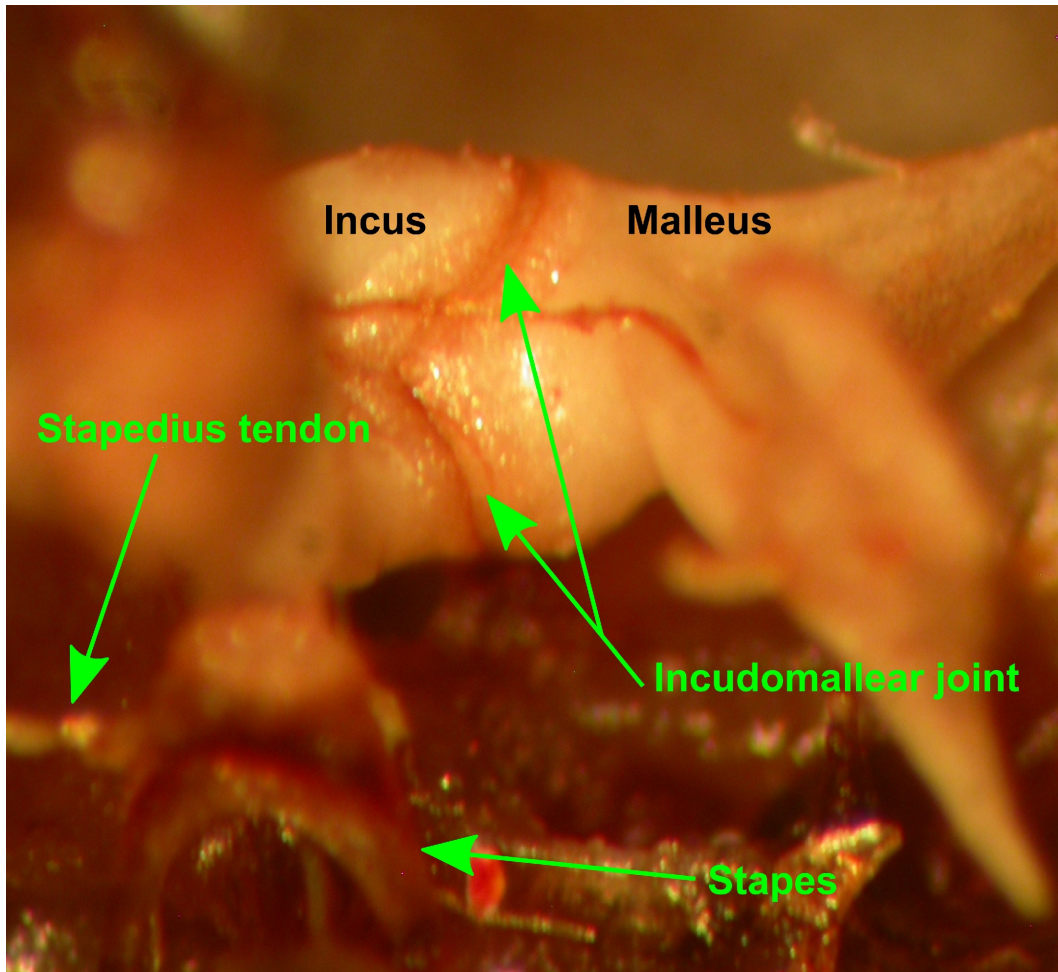


Figure 2.5: Malleus, incus, incudomalleal joint, stapedius tendon and stapes in one of our gerbil preparations after removing the TM and parts of the cavity wall.

2.3 Differences from human middle ear

The human middle ear (Figure 2.6) is generally similar to the gerbil middle ear except for the following aspects:

1. The human middle ear is larger than the gerbil middle ear as schematically shown in Figure 2.7.
2. In the gerbil the middle-ear cavity is composed of a hypertrophied bulla (g in Figure 2.7). In the human the tympanic cavity (b in Figure 2.7) is the air space medial to the TM. Inferior and superior to it are located the hypotympanum (a) and the epitympanic recess (c), respectively. The hypotympanum opens to the eustachian tube. The epitympanic

recess (c) is the air space where the head of the malleus and the short process of incus are encased and it is connected to the mastoid air cells (e) via the antrum (d).

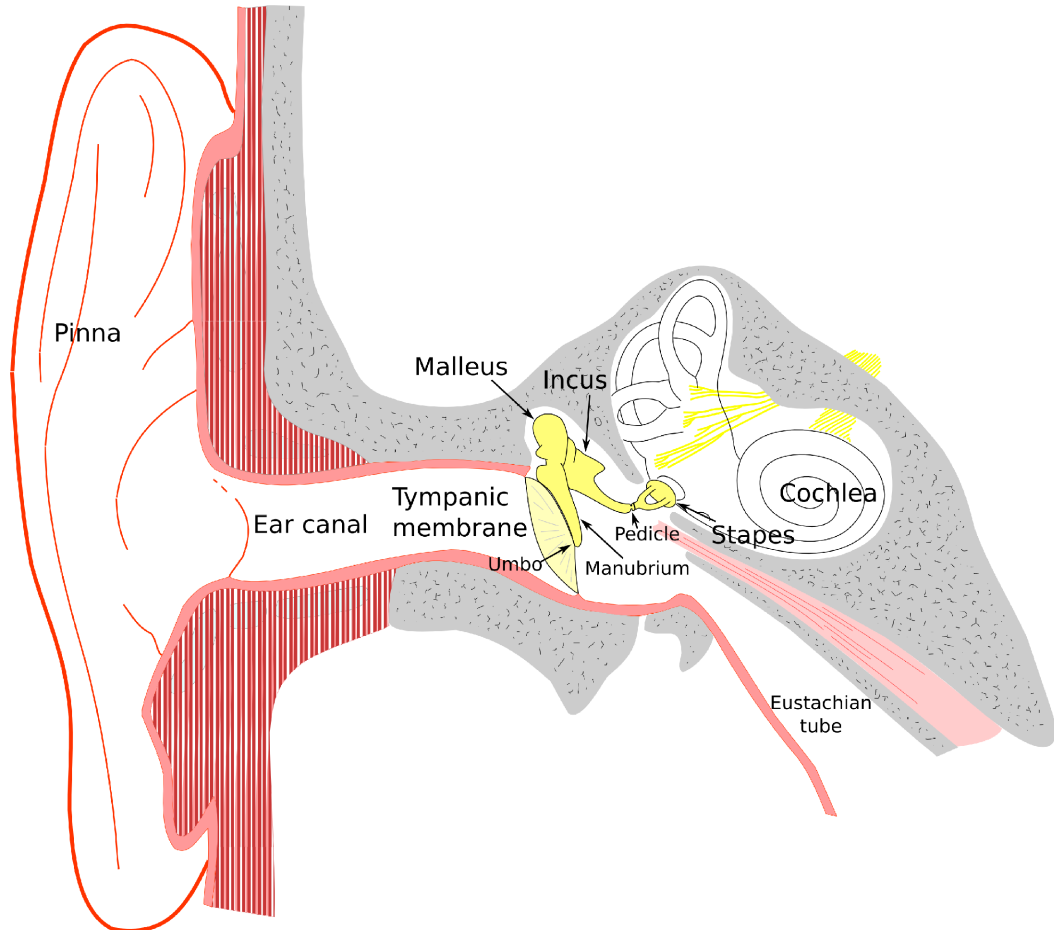


Figure 2.6: Human ear. (After Funnell, http://audilab.bme.mcgill.ca/AudiLab/teach/me_saf/me_saf.html, date viewed: 2014 May 12)

3. The human pars flaccida is relatively much smaller than that of the gerbil.
4. The human TM contains more and denser collagen than does that of the gerbil (Chole & Kodama, 1989).
5. Unlike the case in the gerbil, the human manubrium is tightly connected to the pars tensa only in two regions: at the umbo and at the lateral process of the manubrium (5) .

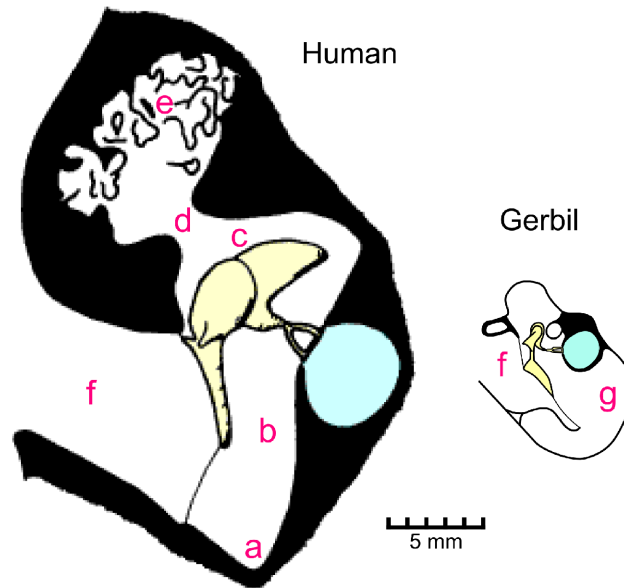


Figure 2.7: Sizes of human and gerbil middle ears are compared. Air spaces in the ear: (a) hypotympanum; (b) tympanic cavity; (c) epitympanic recess; (d) antrum; (e) mastoid air cells; (f) ear canal; (g) hypertrophied bulla. (after Funnell, http://audilab.bme.mcgill.ca/AudiLab/teach/me_saf/me_saf.html, date viewed: 2014 May 12.)

6. In the adult human the anterior process of the malleus (6) is very short and is connected to the middle-ear cavity wall by means of the anterior malleolar ligament, rather than by a direct bony attachment.
7. Instead of being one entity surrounding the short process of the incus, the posterior incudal ligament (12) in the human is composed of a medial bundle and a lateral bundle (e.g., Bryant, 1890; Fumagalli, 1949; Kobayashi, 1955; Winerman et al., 1980).
8. Some authors (e.g., Guilford & Anson, 1967; Hartwein & Rauchfuss, 1987; Nandapalan et al., 2002; Dai et al., 2007; Sim & Puria, 2008; Schwab et al., 2012) have discussed other ligaments such as the superior malleolar, lateral malleolar and superior incudal ligaments in the human middle ear, but other authors doubt whether they have any considerable mechanical contributions (Rosowski, 2010). Mikhael (2005) reviewed the controversies that exist in the literature about the middle-ear ligaments.

3 Literature review

3.1 Introduction

This chapter reviews the studies in the literature that are related to the vibrations in the middle ear. Previous measurements of TM vibrations are reviewed in the first section, then studies that dealt with the effects of opening the middle-ear cavity on TM vibrations are surveyed. While these two sections are about TM vibration measurements done in all mammalian species, the next section deals with all measurements done in gerbils that were related to vibrations or might help modelling of the system. A final section briefly reviews efforts in finite-element modelling of the middle ear.

3.2 Measurements of tympanic-membrane vibrations

Early measurements of tympanic-membrane vibrations were reviewed by Funnell and Laszlo (1982). Here we only mention a few key studies that are also discussed in that article and then review measurements that were done after the publication of that article.

In 1941 von Békésy used a capacitive probe to measure TM vibration. He described the low-frequency (up to 2 kHz) motion of the TM as a rotation of “a stiff surface along with the manubrium” about an axis superior to the TM and observed that due to this rotation, the maximum vibration magnitude occurs inferior to the manubrium (von Békésy, 1960, p. 101). He described how above 2.4 kHz “the conical portion of the eardrum loses its stiffness” and the manubrium lags behind the pars tensa portions adjacent to the manubrium (ibid, p. 102).

Tonndorf and Khanna (1972) and Khanna and Tonndorf (1972) used time-averaged laser holography to study vibrations of the TM in cat and cadaveric human ears. This interferometric

technique revealed iso-amplitude contours on the vibrating TM. They showed that even at low frequencies (at 525 and 600 Hz respectively) the TM does not move as a stiff surface as von Békésy described. They observed two regions of higher magnitudes in the posterior and anterior regions of the pars tensa with a maximum on the posterior side. This simple pattern remained almost unchanged up to about 2 kHz. At about 3 kHz the simple vibration patterns started to break up into more complex ones. They measured up to 5 and 6 kHz and observed increasing complexity in the vibration patterns. A discussion of the possible causes of the discrepancy between von Békésy's observations and those of Tonndorf and Khanna is given in Funnell and Laszlo (1978).

In the Mössbauer technique a very small gamma-ray source is placed on the vibrating structure to produce a measure of vibration velocity. Manley (1972a, 1972b) and Manley and Johnstone (1974) applied this method to lizard and guinea pig TMs. They measured TM motions at multiple points of the TM and provided displacement contour plots of the entire TM based on interpolation. They concluded that in the guinea pig the TM displacements are greater than manubrial ones and are greatest in the region inferior to the umbo.

Time-averaged laser holography was used by a number of other researchers to study TM vibrations. Okano (1990), Suehiro (1990) and Maeta (1991) reported break-up frequencies of 3 kHz for the posterior part of the dog TM and 4 kHz for the anterior part.

Dancer et al. (1975) used holography with a pulsed ruby laser to study the transient displacements of the TM in guinea pigs. However, because they presented acoustic impulse responses in the time domain it is hard to compare their results with those from other reports. Using a double-pulsed ruby laser holography system in a human temporal-bone preparation with pure-tone excitation, von Bally (1977, 1979) was able to extract both magnitude and phase

information. In these studies the laser pulses were synchronized with the sound stimulus. The technique was used to monitor the healing process in tympanoplasty surgery as well as to study the differences in the vibrations patterns of healthy and pathologic human middle ears. von Bally and Baumeister (1979) and Fritze et al. (1979) used this method to study vibration patterns of the human TM *in vivo*. In order to obtain a better optical access to the TM in living humans, von Bally (1982) developed a fibre endoscope equipped with the double-pulsed laser holography system. Løkberg et al. (1979, 1980) used time-averaged electronic speckle pattern interferometry with phase modulation in living humans and presented preliminary magnitude and phase results. There were some attempts to integrate this technique with fibre optics to develop a clinical tool (e.g., Castracane et al., 1993; Conerty et al., 1995). Wada et al. (2002) used phase-modulated time-averaged laser speckle interferometry to study the magnitude and phase of the TM vibrations in the guinea pig. They made measurements up to 4 kHz and observed that complex vibration patterns appeared at frequencies above 2.5 kHz.

Point-by-point laser interferometry provides more precise magnitude and phase information than do holographic techniques. This technique can also provide finer frequency resolution. Tonndorf and Khanna (1968) developed a laser interferometer and studied vibrations of the umbo in the cat at the umbo. Buunen and Vlaming (1981) used a laser Doppler vibrometer (LDV) to measure the magnitude and phase of the umbo vibrations in the cat. Later Vlaming and Feenstra (1986a, 1986b) studied the umbo response of normal and reconstructed middle ears in human temporal-bone preparations. In a series of *in vivo* studies in healthy and pathological human ears (Rosowski et al., 2003; Whittemore Jr. et al., 2004; Rosowski et al., 2008), the potential clinical diagnostic utility of LDV measurements at the umbo was demonstrated. In this review we focus on measurements dealing with TM vibrations rather than umbo or manubrial vibrations.

Konrádsson et al. (1987) studied vibrations of the entire human TM surface using a scanning LDV and presented data at 578, 3107 and 3113 Hz. The observations were consistent with earlier studies. Huber et al. (2001) evaluated the potential of scanning LDV for middle-ear diagnosis by studying TMs from subjects with normal hearing and from subjects with conductive or sensorineural hearing loss. Although they scanned the TM surface, their discussions and conclusions were based on the umbo response. They suggested that scanning LDV can detect conductive hearing loss and can distinguish among a few middle-ear conditions.

Decraemer et al. (1989) utilized a homodyne laser interferometer and reported phase and magnitude for a wide frequency range (130 Hz to 20 kHz) for a few points on the cat pars tensa and manubrium using reflective objects to increase the signal-to-noise ratio. They observed that up to 1 kHz all points on the pars tensa move almost in phase, but beyond that frequency the phase differences increase and for frequencies above 5 kHz each point moves very differently. Decraemer et al. (1999) used an improved interferometer so that the measurements could be done without the need for reflective objects, allowing them to measure TM vibrations with a high spatial resolution. They concluded that the motion ‘looks more like a traveling wave than like a standing wave’.

In measurements from our group, Akache et al. (2007) performed *post mortem* LDV measurements on the rat TM. They used microbeads to enhance the signal quality and presented displacement magnitudes in the frequency range of 1 to 10 kHz. They observed no break up in the TM simple vibration pattern up to 10 kHz. This observation might be due to the drying of the middle-ear structures in their postmortem measurements. Ellaham (2008) and Nambiar (2010) performed post-mortem LDV measurements on the pars tensa and manubrium in gerbil ears. Maftoon et al. (2011) presented some preliminary *in vivo* pars tensa and manubrium vibration

data measured in gerbil ears. LDV measurements were performed *in vivo* by He (2012) on a wider area of the pars tensa than those of Ellaham, Nambiar and Maftoon et al.

de La Rochefoucauld and Olson (2010) made measurements along the manubrium and on the pars tensa near the umbo in the gerbil in the frequency range of 250 Hz to 50 kHz. They concluded that the TM motion ‘could be approximated as the combination of a wave-like motion and an in-and-out piston-like motion’. They also observed that the manubrium does not move as a rigid body, exhibiting bending at some frequencies.

Recent advances in software and hardware have revived TM holographic measurements and enabled measuring at higher frequencies. Rosowski et al. (2009) performed computer-assisted time-averaged holographic measurements in cadaveric chinchilla, cat and human as well as live chinchilla ears. Based on their observations, they classified the TM motions into three regimes. At the lowest frequency (they showed results at 400 and 500 Hz), the entire TM shows a motion pattern with up to three displacement maxima. At 4 kHz in the human and cat and 1 kHz in the chinchilla they observed more complex patterns composed of areas of concentric rings of high-magnitude motions separated by rings of low-magnitude motions. This regime was described in the previous studies (e.g., Tonndorf & Khanna, 1972) as the breakup of the simple low-frequency motion. Their observations in these two regimes were consistent with the ones from previous time-averaged holographic studies. At higher frequencies (above 8 kHz in the cat and human and above 4 kHz in the chinchilla) they observed another regime of vibration pattern that they named ‘ordered pattern’. In this regime the vibration pattern is composed of a multitude of displacement maxima alternating with displacement minima. These repeated vibration features were distributed in an orderly fashion in the radial and circumferential directions. Rosowski and co-workers later integrated stroboscopy in their holographical setup (Furlong et al., 2009;

Hernandez-Montes et al., 2011) to measure the phase of the motion as well. Cheng et al. (2010) then used the stroboscopic holography system to study the TM motions in cadaveric human ears at a few frequencies. They interpreted their results as a combination of standing waves and ‘some smaller traveling-wave like components’. Their interpretation was similar for later stroboscopic holographic measurements of the TM motions in cadaveric human ears (Rosowski et al., 2011). They added that the standing waves have large amplitudes and the superposed travelling waves produce a small modulation over the standing waves. This means that even at 8 to 12 kHz large areas of the TM are in-phase. Khaleghi et al. (2013) and Rosowski et al. (2013) performed TM shape and vibration measurements in the same preparation and calculated the 3-D motion of the TM assuming a simple shell model for the TM.

Optical coherence tomography (OCT) has recently been used for measuring vibrations of the TM. Subhash et al. (2012) showed the feasibility of measuring TM and ossicle motions at 500 Hz using OCT. Chang et al. (2013) applied OCT vibrography to simultaneously measure the 3-D shape and the motions of the TM and ossicles. They performed measurements in cadaveric chinchilla ears in the frequency range of 0.5 to 5 kHz. Consistent with previous studies, it was seen that the vibration pattern becomes more complex when the frequency increases. They interpreted their TM vibrations at 1910 and 3050 Hz as travelling waves or ‘damped modal motions’. They observed that the TM vibration pattern was changed after ossicular manipulation but they could not find a simple relationship between the manipulations and the respective vibration patterns.

3.3 Effects of middle-ear cavity on tympanic-membrane motion

Ishihara (1989) studied the effects of alterations in the cross-sectional area of the aditus ad antrum and the volume of the middle-ear cavity on the vibrations of the human TM using

holography. It was observed that the break-up frequency of the TM ‘was not affected much’ by these alterations. No other vibration measurements dealing with the effects of the middle-ear cavity have been found. However, the effects of the middle-ear cavity on the response of the middle-ear have been studied by many groups using impedance or admittance measurements. Examples in various species include: human (Zwislocki, 1962), guinea pig (Zwislocki, 1963), rabbit (Møller, 1965), cat (Møller, 1965; Lynch et al., 1994), lion (Huang et al., 1997), gerbil (Ravicz et al., 1992; Teoh et al., 1997) and chinchilla (Rosowski et al., 2006). In these studies it was found that opening the middle-ear cavity has the following effects on the response of the middle ear: (1) the stiffness of the middle ear at low frequencies is reduced; (2) the middle-ear resonance moves to lower frequencies; (3) an antiresonance is introduced in the admittance; (4) at high frequencies there is not much difference between open-cavity and closed-cavity admittances (except for the presence of the antiresonance); (5) in species with large pars flaccida (like the gerbil, cf. Teoh et al., 1997) the admittance peak associated with the pars flaccida becomes more prominent.

3.4 Related gerbil measurements

3.4.1 Anatomical measurements

Lay (1972) performed morphological and neurophysiological measurements on the auditory organ of more than 13 gerbilline species. Among other things, he measured the dimensions of the ossicles and TM and the volume of the middle-ear cavity. The auditory organ of one of these gerbilline species, the Mongolian gerbil (*Meriones unguiculatus*) has been the subject of many studies (including the present thesis).

The pars flaccida of the TM in gerbil is known to be planar and almost circular (e.g., Dirckx et al., 1997). Kuypers et al. (2005) studied the TM thickness distribution in gerbil. Because

measurement all over the eardrum was resource intensive they performed measurements only along a few straight lines.

Cohen et al. (1992) reported values for the masses of the malleus (1.17 mg) and incus (0.67 mg) in gerbils. The masses reported by Nummela (1995) for the gerbil middle-ear ossicles (malleus 1.15 mg, incus 0.63 mg) are very close to the ones reported by Cohen, and Nummela also provided the mass of the stapes (0.12 mg). Buytaert et al. (2011) performed orthogonal-plane fluorescence optical-sectioning microscopy (OPFOS) for imaging the ligaments, tendons and muscles, and micro-scale X-ray computed tomography (μ CT) for imaging the TM and bony structures of the gerbil middle-ear. They reported average densities for the malleus and incus complex (1740 kg/m^3) and for the stapes (1370 kg/m^3) using the mass data from Nummela (1995).

3.4.2 Quasi-static deformation of the tympanic membrane

Quasi-static deformation of the gerbil tympanic membrane under static pressure was measured in several studies using moiré interferometry; we will mention a few of them that are related to the current study. von Unge et al. (1993) studied gerbil pars-tensa deformation under static pressure. Their measurements show hysteresis between the loading and unloading cycles. Dirckx et al. (1997, 1998) studied gerbil pars-flaccida deformation under static pressure and showed that its deformed surface could always be approximated with high accuracy as a spherical cap. Hysteresis was again found between loading and unloading. The results showed that much of the pars-flaccida deformation takes place due to small pressure changes of few hundred Pa. Dirckx & Decraemer (2001) studied how removal of different middle-ear structures affects the displacement pattern of the TM under static pressure. More recently Gea et al. (2009) studied boundary deformations in the gerbil ear under static pressure using μ CT.

3.4.3 Middle-ear impedance and admittance measurements

Ravicz et al. (1992) measured the middle-ear input impedance in gerbil in the frequency range of 10 Hz to 18 kHz. They performed measurements before and after various manipulations to study contributions of the middle-ear cavity and other middle-ear structures. They concluded that the middle-ear input impedance is stiffness-dominated below 1.5 kHz and resistance-dominated at higher frequencies. They suggested a lumped-parameter model for the gerbil middle ear. They showed that the middle-ear cavity is responsible for about 70% of the acoustic stiffness of the auditory periphery below the middle-ear resonance frequency. The middle-ear cavity was not observed to have a significant effect above 4 kHz. Comparing with low-frequency acoustic stiffness and anatomical dimensions in other species they concluded that the large middle-ear cavity in gerbil reduces the middle-ear stiffness at low frequencies.

Teoh et al. (1997) measured middle-ear input admittance to study the role of the pars flaccida in the sound conduction in the gerbil ear. They suggested that the pars flaccida acts as a resonator. They modified the model suggested by Ravicz et al. to have a branch for the pars flaccida parallel to the input admittance for the pars tensa, ossicles and cochlea. Below its resonance, the admittance of the compliance-like pars flaccida is comparable to the collective admittance of the pars tensa, ossicles and the cochlea. Therefore, at these frequencies the pars flaccida increases the overall input admittance of the middle ear. Above its resonance, the pars flaccida input admittance is mass-like and its effect on the overall input admittance of the middle ear is insignificant. They concluded that the pars flaccida has the effect of reducing the hearing sensitivity at low frequencies.

3.4.4 Sound-pressure distribution

Ravicz et al. (2007) measured the sound pressure distribution in the bony ear canal of gerbil with both a probe-tube microphone and a fibre-optic miniature microphone. They concluded that the ear-canal sound field can be described as a one-dimensional standing wave and the sound pressure is almost uniform across the TM below 60 kHz.

Recently Bergevin and Olson (2014) measured sound pressure in the ear canal and middle-ear cavity in gerbils. They used a probe-tube microphone and a fibre-optic miniature microphone. They showed that the pressure distribution across the medial side of the TM (in the middle-ear cavity) is not uniform even below 10 kHz. They also concluded that the variations of pressure across the lateral side of the TM (in the ear canal) are ‘relatively small’.

3.4.5 Cochlear input impedance

Overstreet and Ruggero (2002) measured stapes vibrations and calculated the input impedance of the cochlea based on these data and the pressure measurements in the scala vestibuli near the oval window by Olson (1998). They concluded that the input impedance of the cochlea in the gerbil is ‘principally dissipative’ below 10 kHz. Later studies by Decraemer et al. (2007), de La Rochefoucauld et al. (2008) and Ravicz et al. (2008) also came to that conclusion, consistent with older studies in other species (e.g., Lynch et al., 1982, in cat; Aibara et al., 2001, in human; Slama et al., 2010, in chinchilla).

3.4.6 Vibration measurements

Rosowski et al. (1997, 1999) performed LDV measurements at the umbo, at the centre of the pars flaccida and on the posterior crus of the stapes. Later, Lee and Rosowski (2001) and Rosowski and Lee (2002) pressurized the middle ear and studied the vibrations at the umbo and

at the centre of the pars flaccida using a LDV. Results from these four studies are discussed in detail and compared with our results in Chapters 4 and 5 of this thesis.

Ravicz et al. (2008) studied the middle-ear transfer admittance (ratio of stapes velocity to the sound pressure near the umbo) by measuring the velocity at the posterior crus of the stapes using a LDV and the sound pressure near the umbo. Except for a narrow frequency range around 10 kHz, the stapes motion was observed to be primarily piston-like. They observed that the magnitude of the middle-ear transfer admittance increased up to 1 kHz, remained constant between 5 and 35 kHz and decreased significantly between 35 and 50 kHz. They concluded that there was a linear phase decrease between 5 and 35 kHz consistent with 20 to 29 μs delay. The acoustical effect of the opening in the middle-ear cavity wall obscured the responses in the 1 to 5 kHz frequency range.

Decraemer et al. (2007) measured the pressure in the scala vestibuli as well as the motion of the stapes. The measurements were not done simultaneously. They did not find any correlation between the non-piston-like vibration components of the footplate and the pressure inside the scala vestibuli. Later de la Rochefoucauld et al. (2008) changed the protocol to do the same measurements but simultaneously. They concluded that the pressure in the scala vestibuli follows the piston-like vibration component of the stapes with 'high fidelity'. de la Rochefoucauld et al. (2010) studied middle-ear delays by measuring vibrations at various points along the ossicular chain from the umbo to the stapes footplate. They concluded that the delay between the pressure in the ear canal and the velocity of the stapes footplate is almost constant in the frequency range of 7 to 30 kHz. However, below 17 kHz most of the delay was between the ear canal and the umbo, and above 17 kHz most of the delay was along the ossicular chain.

The 3-D measurements of malleus and incus vibrations by Decraemer et al. (2011a, 2014) complement their previous 3-D measurements of the stapes vibrations to provide a complete view of the ossicular motion in the gerbil. They showed that the axis of rotation of the malleus is close to anatomical axis of rotation only at frequencies below a few kilohertz. They did not conclude that there is a constant delay but reported a frequency-dependent and ear-dependent slippage between the malleus and incus equivalent to a delay on the order of 2 to 3 μ s.

3.5 Modelling of middle-ear mechanics

There have been lumped-parameter models of the middle-ear where dependent variables are functions only of time (e.g., Zwislocki, 1957, 1962; Møller, 1965). In these models each middle-ear structure is usually lumped as an equivalent electrical circuit element. In distributed models, on the other hand, dependent variables are functions of both time and spatial coordinates. Finite-element models are inherently distributed and can incorporate the detailed anatomical and biomechanical properties of the middle-ear structures, so their results can be connected to the physiological characteristics of the system. We have provided an introduction to the fundamentals of modelling of middle-ear mechanics elsewhere (Funnell et al., 2012). We have also published a recent thorough review of models of the middle ear (Funnell et al., 2013), and Vollandri et al. (2011) recently reviewed finite-element models of the TM. Here only a brief review of previous finite-element models of the middle ear is provided.

Funnell and Laszlo (1978) presented the first finite-element model of the middle ear and investigated the low-frequency behaviour of the cat TM. Funnell (1983) extended this model to higher frequencies. In these models the eardrum geometry was approximated by circular arcs. Results from these models were qualitatively similar to the experimental observations of Khanna and Tonndorf (1972). Funnell et al. (1987) added damping to this model. Comparing with laser

interferometric point measurements on the cat TM, it was found that mass-proportional damping could represent the damping in the TM fairly well. Lesser and Williams (1988), Williams and Lesser (1990) and Lesser et al. (1991) presented models of the human TM and ossicles using the finite-element method in 2-D. However, it was known from previous studies that 3-D geometry has an important effect on the behaviour of the middle ear. Wada et al. (1992) presented a 3-D model of the human middle ear that included the TM and ossicles. Ladak and Funnell (1996) investigated ossicular reconstruction using the finite-element method in the cat. To increase the accuracy with which TM shape was represented in FE models, Funnell and Decraemer (1996) presented a method for using TM shape from moiré measurements. Daniel et al. (2001) used moiré measurements for reconstructing the TM shape and histological sections and high-resolution magnetic resonance microscopy data for reconstructing the ossicles and ligaments in a model of the human middle-ear. Later Sun et al. (2002) used histological sections, and Kelly et al. (2003) used magnetic resonance imaging, to reconstruct the TM geometry. Decraemer et al. (2003) and Mikhael et al. (2004) used μ CT imaging data to reconstruct the ossicle and TM geometries, respectively. Elkhouri et al. (2006) used a combination of phase-shift moiré topography, magnetic resonance microscopy and μ CT to reconstruct the TM, ossicles and stapes annular ligament, respectively. For a recent review of the image segmentation methods used for 3-D reconstruction of the ear see Ferreira et al. (2012).

The TM is often modelled as a single layer of isotropic material. However, there were models that treated it as an orthotropic material (e.g., Funnell & Laszlo, 1978; Gan et al., 2006). Fay et al. (2006) and Tuck-Lee et al. (2008) presented multilayered models of the TM.

Nonlinear deformations of the TM were modelled by considering only the geometric nonlinearity (Ladak et al., 2006) or in combination with hyperelastic materials (e.g., Wang et al., 2007; Qi et

al., 2008). Finite-element method was used in conjunction with tensile testing (e.g., Cheng et al., 2007) or indentation (e.g., Huang et al., 2008; Daphalapurkar et al., 2009) for material characterization of the TM. TM material characterizations using finite-element models will be described later in Chapter 6.

Most finite-element models have not considered the acoustic effects of the ear canal and the middle-ear cavity. Prendergast et al. (1999) presented a model that included the ear canal also. Koike et al. (2002) and Gan et al. (2004) integrated the ear canal and middle-ear cavity in their finite-element models of the human ear. A model that included the middle-ear cavity enabled Gan and Wang (2007) to study otitis media with effusion.

In earlier finite-element models the damping effect of the cochlea was distributed in the damping of TM and ossicles and there was no explicit load representing the cochlea (e.g., Funnell, 1983). Koike et al. (2002) represented the cochlear load in their middle-ear models by one dashpot connected to the footplate. Gan et al. (2002) modelled the cochlear load as “viscoelastic constraints with linear springs and dashpots”. For this purpose they attached a number of branches, each composed of a spring and dashpot. Recently fluid models of the cochlea have been incorporated in the finite-element models (Gan et al., 2007; Kim et al., 2011).

Daniel et al. (2001) discussed the clinical applications of finite-element modelling of the human middle ear. In addition to modelling otitis media (Gan & Wang, 2007), finite-element models were applied to study middle-ear prostheses (e.g., Ladak & Funnell, 1996; Ferris & Prendergast, 2000; Kelly et al., 2003), TM perforations (e.g., Gan et al., 2009), TM reconstructions (e.g., Lee et al., 2006, 2007) and ligament fixation (Huber et al., 2003; Dai et al., 2007). Zhao et al. (2009) reviewed the application of the finite-element method to middle-ear pathologies.

Although most middle-ear FE models have been developed for the human, validation of FE models requires experimental data that can be collected with a higher quality in other species. There have been some models for animal middle ears. Cat was at one time the mainstream animal model (e.g., Funnell & Laszlo, 1978; Funnell, 1983; Funnell et al., 1987; Ladak & Funnell, 1996; Tuck-Lee et al., 2008). Recently a model for the rabbit (Aernouts et al., 2010) and a model for the rat (Ghadarghadar et al., 2013) were published. Further to many experimental studies on the gerbil middle ear, reviewed in Section 3.4, it has been the subject of a number of finite-element studies. Funnell et al. (1999, 2000) presented some preliminary results of the middle-ear response at low frequencies. The model was later refined by Elkhouri et al. (2006). Material characterization was done using FE modelling in conjunction with pressurization by Decraemer et al. (2010) for the pars flaccida and in conjunction with indentation by Aernouts and Dirckx (2011, 2012) for the pars flaccida and pars tensa. Decraemer et al. (2011b) studied the effects of the tympanic-membrane (TM) geometrical asymmetry on ossicle-motion asymmetry in response to high static pressures. Maftoon et al. (2011) presented some results concerning the response of the gerbil middle ear at audio frequencies. They were a preliminary version of the results presented in Chapter 6 of this thesis.

4 Experimental study of vibrations of gerbil tympanic membrane with closed middle-ear cavity

Published in the *Journal of the Association for Research in Otolaryngology*,
2013 August, Volume 14, Issue 4, 467–481

Preface

This chapter introduces the methodology for the experimental data collection and analysis that is also used in the next chapter. It also presents our tympanic-membrane vibration measurements in the closed middle-ear cavity condition. This is the natural condition of the middle-ear cavity in living gerbils. This chapter establishes the basis for the experimental study of tympanic-membrane vibrations with an open middle-ear cavity that is presented in Chapter 5.

Although the hearing range of the gerbil extends well beyond 40 kHz, the studies presented in this thesis are limited to 10 kHz. There are two reasons for this limitation. (1) Beyond 10 kHz the sound-pressure fields in the gerbil ear canal and middle-ear cavity may not be uniform and each point of the TM may be excited by a different sound pressure. With current equipment, simultaneously measuring point-wise sound pressures and vibrations would be very difficult, if not impossible. Furthermore, taking the non-uniform sound pressure into account would greatly complicate the analysis and modelling. (2) The main motivation of this thesis is to establish a basis for similar human studies. The human hearing range is limited to 20 kHz and most of the information vital for comprehending speech is below 10 kHz.

Abstract

The purpose of the present work is to investigate the spatial vibration pattern of the gerbil tympanic membrane as a function of frequency. *In vivo* vibration measurements were done at several locations on the pars flaccida and pars tensa, and along the manubrium, on surgically exposed gerbil tympanic membranes with closed middle-ear cavities. A laser Doppler vibrometer is used to measure motions in response to audio-frequency sine sweeps in the ear canal. Data are presented for two different pars-flaccida conditions: naturally flat, and retracted into the middle-ear cavity. Resonance of the flat pars flaccida causes a minimum and a shallow maximum in the displacement magnitude of the manubrium and pars tensa at low frequencies. Compared with a flat pars flaccida, a retracted pars flaccida has much lower displacement magnitudes at low frequencies and does not affect the responses of the other points. All manubrial and pars-tensa points show a broad resonance in the range of 1.6 to 2 kHz. Above this resonance, the displacement magnitudes of manubrial points, including the umbo, roll off with substantial irregularities. The manubrial points show an increasing displacement magnitude from the lateral process toward the umbo. Above 5 kHz, phase differences between points along the manubrium start to become more evident, which may indicate flexing of the tip of the manubrium or a change in the vibration mode of the malleus. At low frequencies, points on the posterior side of the pars tensa tend to show larger displacements than those on the anterior side. The simple low-frequency vibration pattern of the pars tensa becomes more complex at higher frequencies, with the break-up occurring at between 1.8 and 2.8 kHz. These observations will be important for the development and validation of middle-ear finite-element models for the gerbil.

4.1 Introduction

Understanding the response of the middle ear to sound stimuli is highly dependent on knowledge of the tympanic membrane (TM) vibrations and they have been the subject of a number of studies, with laser-based methods being particularly valuable. Tonndorf & Khanna (1972) and Khanna & Tonndorf (1972) were the first to study vibration patterns of the human and cat TM by time-averaged laser holography, at frequencies up to 5 and 6 kHz respectively. They observed that in both species the maximum displacement happens in the posterior region, and for frequencies beyond 2.5 kHz the simple low-frequency vibration pattern starts to break up and vibration patterns become more complex. Funnell & Laszlo (1982) reviewed other applications of holography (as well as other techniques). Later, Ishihara (1989) observed that the break-up frequency of the human TM ‘was not affected much’ by the cross-sectional area of the aditus ad antrum, the sound pressure level or the volume of the middle-ear cavity. Okano (1990), Suehiro (1990) and Maeta (1991) reported break-up frequencies of 3 kHz for the posterior part of the dog TM and 4 kHz for the anterior part. Wada et al. (2002) used time-averaged laser speckle interferometry to study guinea-pig TM vibrations up to 4 kHz. It was seen that complex vibration patterns appear at frequencies above 2.5 kHz.

Point-by-point laser interferometry provides more precise magnitude and phase information than do holographic techniques. Konrádsson et al. (1987) studied vibration of the human TM using scanning laser Doppler vibrometry (LDV) and presented data at 578, 3107 and 3113 Hz that were consistent with earlier studies. Decraemer et al. (1989) utilized a homodyne laser interferometer and reported phase and magnitude for a wide frequency range (130 Hz to 20 kHz) for a few points on the cat pars tensa and manubrium. They observed that up to 1 kHz all points on the pars tensa move almost in phase, but that beyond that frequency the phase differences

increase and for frequencies above 5 kHz each point moves very differently. Decraemer et al. (1999) used an improved interferometer so that the measurements could be done without the need for reflective objects to increase the signal-to-noise ratio, allowing them to measure TM vibrations with a high spatial resolution. They concluded that the motion ‘looks more like a traveling wave than like a standing wave’.

Recently Rosowski et al. (2009) used time-averaged holography to study TM vibrations up to 25 kHz in human, cat and chinchilla. They found increasingly complicated vibration patterns for frequencies higher than 0.8 kHz for chinchilla and 2 kHz for cat and human; for frequencies higher than 1 kHz for chinchilla and 4 kHz for cat and human, the patterns were ring-like. Later, using stroboscopic holography, they were also able to study the phase at a few frequencies in human temporal bones (Cheng et al., 2010) and interpreted their results as indicating a combination of standing waves and ‘some smaller traveling-wave like components’.

The gerbil is a commonly used species in hearing research. For example, Cohen et al. (1993) investigated the effects of developmental changes on the gerbil umbo velocity response using LDV. Admittance measurements (e.g., Ravicz et al., 1992, 1996; Ravicz & Rosowski, 1997; Teoh et al., 1997) and LDV umbo and pars-flaccida measurements (e.g., Rosowski et al., 1997, 1999; Lee & Rosowski, 2001; Rosowski & Lee, 2002) were used to study the gerbil middle and external ears. Quasi-static deformation of the gerbil tympanic membrane under static pressure was measured in several studies using moiré interferometry (e.g., von Unge et al., 1993; Dirckx & Decraemer, 2001). The gerbil has also been used as an animal model for middle-ear infection in several studies (e.g., Fulghum & Marrow, 1996; von Unge et al., 1997; Larsson et al., 2005).

Although there have been many experimental studies of the gerbil middle ear, the only measurements of the vibration patterns of the gerbil TM have been those made at a few points on

the pars tensa near the umbo by de La Rochefoucauld & Olson (2010) and *post mortem* studies in our lab (Ellaham et al., 2007; Nambiar, 2010). The present work, therefore, was performed to investigate the vibrations of the gerbil TM more extensively. Measurements were done *in vivo* using LDV at several locations on the pars tensa, along the manubrium and on the pars flaccida. All measurements were done with the middle-ear cavity both closed and open, but only closed-cavity data are reported here. The open-cavity observations will be reported in a subsequent paper.

4.2 Materials and methods

4.2.1 Preparation

TM vibration was measured *in vivo* in 12 ears of 11 female Mongolian gerbils (*Meriones unguiculatis*) supplied by Charles River Laboratories (St-Constant, Québec). Body weights were from 64 to 100 g. The study protocol was approved by the McGill University Animal Care Committee.

The animal was weighed and analgesics (buprenorphine 0.05 mg/kg and carprofen 5 mg/kg) were administered subcutaneously. After fifteen minutes, 10 mg/kg xylazine plus 35 mg/kg sodium pentobarbital were given to the animal by intraperitoneal injection. In order to maintain normal body temperature, the gerbil rested on a SnuggleSafe microwave-heated heating pad (Lenric C21 Ltd.) during the whole procedure. A low flow of oxygen was provided to the animal through a tube near the nose. Anaesthesia was maintained for several hours of measurements by administering a 5–10 mg/kg sodium pentobarbital bolus injection every 45 minutes. A diluted local anaesthetic (lidocaine) was applied on the exposed tissues to control pain locally and to keep the tissue hydrated. A reflex check was done every 5–10 minutes during the experiment to

verify the depth of the anaesthesia and, if the animal showed any reaction, an additional dose of 5–10 mg/kg of sodium pentobarbital was injected.

Once the animal reached an appropriate level of anaesthesia, the surgery was started. The skin over the skull was excised and a wooden block (2.5×1×1 cm) was attached to the skull with dental cement (IRM, Dentsply Caulk). During measurements, the wooden block was fixed in a positioning device located under the microscope, which was equipped with a vibrometer sensor head. The soft tissues covering the bulla were removed under an operating microscope. Then, a surgical ear drill was used to remove the bony ear canal and expose the TM. To equalize pressure in the bulla, a ventilation hole was made on the bulla away from the TM; to cancel the acoustic effects of the hole, a 15-cm-long polyethylene tube with an inner diameter of 0.58 mm and an outer diameter of 0.96 mm was inserted into the hole. The ventilation tube was checked for patency at the time of insertion by passing a wire through it. Glass-coated plastic beads of diameter of 90 to 150 μm with a density of 1.02 g/cm^3 (Sigma-Aldrich, model G4519) were used as targets for the laser. They increased reflection of the laser beam and thus improved the signal-to-noise ratio of the vibrometer signal. The beads also served as markers of the measurement locations. Placing of the beads was done manually under an operating microscope using a paint brush reduced to a single bristle and there were inevitably some differences in bead positioning from ear to ear. In using beads in our measurements and drawing conclusions from our data, we have assumed that the beads stick perfectly to the TM or manubrium and do not move with respect to the surface. Decraemer et al. (1989) showed that their beads followed the underlying structure, and beads have been used by many groups since then (e.g., Bigelow et al., 1996; Qin et al., 2010).

We used an aluminum acoustic coupler, the interior air space of which had a resonance frequency beyond 10 kHz. A metal washer (9.6 mm O.D., 3.8 mm I.D., 1.1 mm thickness) was attached to the bony ear canal with dental cement and the coupler was attached to the washer, again with dental cement (see Figure 4.1). At the other end of the coupler there was a seat for placing an anti-reflective coated glass window. Euthanasia with sodium pentobarbital overdose was performed immediately after the completion of the data collection.

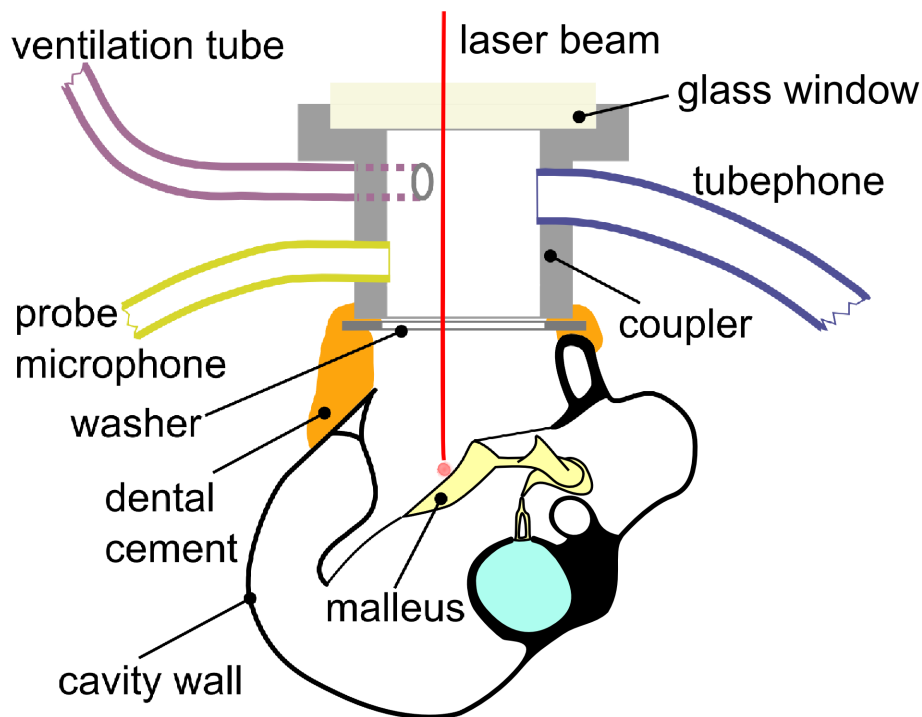


Figure 4.1: Schematic diagram showing the acoustic coupler attached to the bony ear canal.

In a few ears, whose results were excluded from this report, upon exposing the TM we observed liquid drops on the lateral surface of the TM, sitting on the annulus anteriorly and posteriorly, touching the ear-canal wall and extending about 20% of the distance to the manubrium. These drops, which were associated with significant ripples in the frequency responses, might be caused by exudation due to mechanical stimulation of the ear canal as observed by Emgård & Hellström (1997) in rats.

4.2.2 Instrumentation

A 128-ms linear sinusoidal sweep from 0.2 to 12.5 kHz was used as the stimulus. Sound was delivered by an ER-2 tubephone (Etymotic Research) into the acoustic coupler through a hole in its wall, and the sound pressure about 2–3 mm away from the TM was picked up by an ER-7C (Etymotic Research) probe microphone connected through another hole in the coupler wall. A third hole was made in the coupler wall for insertion of a ventilation tube to prevent the build-up of pressure and moisture. Both ER-2 and ER-7C have almost flat magnitude responses in the frequency range of interest. The ER-7C probe microphone was calibrated against a Brüel & Kjær 1/4" model 4939 condenser microphone using a Brüel & Kjær sound intensity calibrator model 3541. A cubic polynomial and a straight line were fitted to the calibration measurement points below 600 Hz and above 600 Hz respectively ($R^2=0.995$ for each part).

A single-point LDV (HLV-1000, Polytec) attached to an operating microscope (OPMI 1-H, Zeiss) was used inside a double-walled audiometric examination room (model C-24, Génie Audio, St-Laurent, Québec), which attenuated acoustical noise. Measurements were performed from a single viewing direction. Owing to animal-to-animal variability of the anatomy and of the experimental procedures, there were slight differences between the measurement angles in different ears. The data-acquisition board of the LDV system used delta-sigma-modulating analog-to-digital convertors (e.g., Aziz et al., 2002) with 128-times oversampling, which avoided aliasing. An effective sampling frequency of 25 kHz was used. An extremely flat, linear-phase, low-pass digital filter automatically adjusts its cutoff frequency to remove frequency components above half the requested sampling rate. The frequency range of interest in this study is 200 Hz to 10 kHz.

4.2.3 Measurement and analysis procedures

Measurements always started with the middle-ear cavity closed, that is, with a small ventilation hole and a ventilation tube in place, as described in Section 4.2.1. Before collection of the vibration data began, the probe-microphone signal recorded near the tympanic membrane was inspected to ensure absence of any acoustical artifacts. To assess the noise floor, the laser beam was pointed at the acoustic coupler or at the cavity wall, and the resulting vibration signal was compared with the signal measured from the bead at the umbo. The umbo response was always 30 and 40 dB above the noise floor for frequencies higher than 400 and 600 Hz respectively. Averaging (20 to 60 times) was used to reduce the low-frequency noise that mainly influenced responses in the frequency range of 200 to 300 Hz. The frequency-response function was estimated as the cross spectral density of the excitation and response signals divided by the power spectral density of the excitation signal. The linearity was checked by varying the sound-stimulus amplitude and ensuring that the normalized displacement magnitudes at the umbo remained the same.

To minimize drying effects, we covered the exposed bulla between the soft tissue and the acoustic coupler with a cotton pad moistened with diluted lidocaine solution (our local anaesthetic as described in Section 4.2.1). The cotton was re-moistened every half hour.

In each ear 3 or 4 target beads were placed on the manubrium. One bead was placed approximately at the centre of the pars flaccida. Up to 3 beads were placed on each of the posterior and anterior parts of the pars tensa at the level of the middle of the manubrium, and a few more were placed in the region just posterior, anterior and inferior to the umbo. The picture of the TM shown on the left-hand side of Figure 4.2 is focused on the beads inferior to the umbo

on the pars tensa, while the picture on the right is focused on the beads at the level of the middle of the manubrium on the pars tensa.

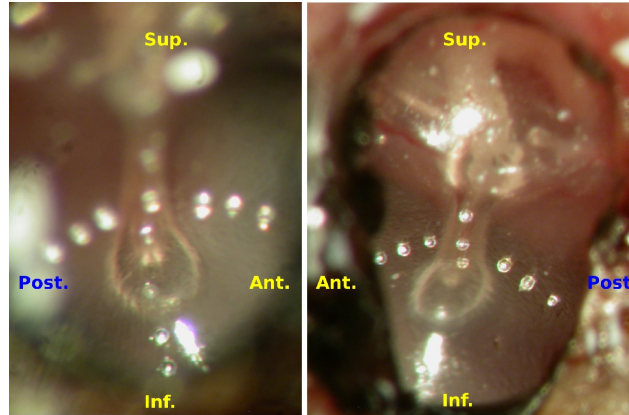


Figure 4.2: Lateral views of two tympanic membranes. Beads are positioned on the manubrium and the pars tensa.

One or two reference beads were always measured at both the start and the end of the measurements on the beads in each region. These reference measurements were used to screen the results both for gradual temporal effects and for possible abrupt changes due to unwanted changes in the system. For points around the umbo on the pars tensa, and for points along the manubrium and on the pars flaccida, the umbo was taken as the reference. For points across the manubrium, both the umbo and the closest bead on the manubrium were taken as reference points. The signal from each bead was recorded several times in a row to confirm repeatability, but only the first recorded signals have been reported here.

A 1600-line FFT was used to transfer the recorded vibrometer and microphone time-domain signals to the frequency domain. A two-pass (forward and reverse) moving-average filter with a window length of five was applied to the real and imaginary parts of the complex signal, and the magnitude and phase responses were then calculated from the filtered complex signal. Such calculated phases are ‘wrapped’ within a range of 360° and their unwrapping can be uncertain in the presence of noise and rapid phase changes. We have checked the configuration and continuity

of the Nyquist plots (Cartesian plots of the real part vs. the imaginary part of the complex response) to increase our confidence in the validity of the phase unwrapping process. Examples of Nyquist plots are given in Figure 4.8 and discussed in the Appendix.

4.3 Results

4.3.1 Effects of using beads

The mass of the beads used as reflective targets may affect the behaviour of the TM. The effect of adding beads was assessed in four ears. First we placed one bead on the umbo and another one on the posterior or anterior part of the pars tensa, and recorded the vibrometer signals at these two points; we then successively added up to four more beads near the first bead on the pars tensa. To have access to the pars tensa for adding each bead, we had to remove the acoustic coupler, place the bead and then seal the coupler again. After the addition of each bead we measured the motion of the first pars-tensa bead and of the umbo bead. These measurements were done *post mortem*. We observed that, with the addition one at a time of up to four additional beads at one location, structures in the response shifted to higher frequencies due to temporal effects but differences between the shifted structures remained within 3 dB and 10°. In our regular experiments we placed no more than three beads on the pars tensa on each side of the manubrium and leave some distance between them (about 100 µm) so the response of the pars tensa is not expected to be greatly modified. We were not able to do measurements without any beads on the pars tensa, so these data do not address what happens as the first bead is added to the pars tensa.

In using beads in our measurements and drawing conclusions from our data, we have assumed that the beads stick perfectly to the TM or manubrium and do not move with respect to the

surface. Decraemer et al. (1989) showed that the beads follow the underlying structure, and beads have been used by many groups since then (Bigelow et al., 1996 e.g., ; Qin et al., 2010).

4.3.2 Repeatability and temporal effects

Our data show a high degree of short-term repeatability in all ears. Except on very rare occasions, the repeat average magnitudes and phases within 5 minutes were within 1 dB and 3° of the first average, except above the break-up frequency on the pars tensa where they were usually within 2 dB and 7°. For the sharpest features the differences were sometimes up to 5 dB and 12° but the shapes of the frequency responses were essentially unchanged.

Dehydration of the middle-ear structures is probably one of the main mechanisms that affects the long-term repeatability. Drying is caused by altering the normal physiological conditions, by removal of the cartilaginous ear canal and the soft tissues covering the bulla, and manifests itself in the frequency-response data as a decrease in magnitude and a frequency shift of the response features to higher frequencies (Voss et al., 2000; Ellaham et al., 2007). In the closed-cavity condition, over a time span of 90 minutes, most features of the umbo response typically showed a maximum shift of about 2 Hz/min to higher frequencies, a maximum magnitude decrease of about 0.2%/min, and a maximum phase change of about 0.02 deg/min over the entire frequency range of interest. The umbo-response feature caused by the pars flaccida, consisting of a magnitude minimum and a phase maximum as discussed in Section 4.3.3.1, moved to higher frequencies at a somewhat higher rate (approximately 3 Hz/min). Teoh et al. (1997) also reported faster changes with drying for this feature.

4.3.3 Umbo and pars-flaccida vibrations

The response of the umbo is better understood when it is compared with the pars-flaccida response, so we present both responses together. Responses are reported for two different pars-flaccida conditions: when it is naturally flat and when it is retracted into the middle-ear cavity.

4.3.3.1 Low frequencies

In some of our experiments the normally flat pars flaccida was retracted into the middle-ear cavity. A retracted pars flaccida has an obvious inverted dome-like geometry when examined under the microscope. Typical responses of a flat pars flaccida (gerbil K) and of a retracted pars flaccida (gerbil J) are presented in Figure 4.3, together with the corresponding umbo responses. In both the flat case and the retracted case, the pars flaccida and the umbo both had a flat magnitude response below 300 Hz and both had a phase of about 0° up to 700 Hz. The response of the flat pars flaccida in Figure 4.3 shows a resonance peak at 850 Hz with a width (full width at half maximum) of 220 Hz. In the ears with a flat pars flaccida the resonance peak was observed to be between 500 and 900 Hz with a width of 140 to 270 Hz. The resonance of a flat pars flaccida corresponds to a minimum and a more or less shallow maximum in the umbo magnitude response, seen at 750 Hz and 950 Hz respectively in Figure 4.3, and a maximum in the umbo phase response, seen at 840 Hz in Figure 4.3. In contrast, the response of the retracted pars flaccida in Figure 4.3 shows a gentle increase in magnitude from 300 Hz up to a small peak at about 850 Hz. This small peak is located between 850 and 1700 Hz in different ears with a retracted pars flaccida. In this ear, the almost flat magnitude response of the umbo continues up to about 600 Hz and is then followed by a gentle rise up to about 1650 Hz. In ears with a retracted pars flaccida like gerbil J in Figure 4.3, the magnitude response is smaller than that in ears with a flat pars flaccida; it is even smaller than that of the umbo. For example, in Figure 4.3

at 300 Hz the displacement magnitude of the retracted pars flaccida is 35 nm/Pa, which is much less than the 500 nm/Pa of the flat pars flaccida and less than the 70 nm/Pa of the umbo.

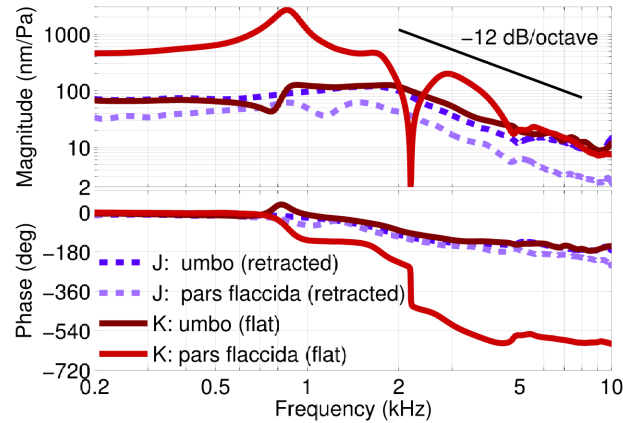


Figure 4.3: Displacement response of the centre of the pars flaccida and of the umbo, normalized by sound pressure, in two ears. The pars flaccida was retracted in gerbil J (dashed lines) and was flat in gerbil K (solid lines).

Figure 4.4 shows umbo displacement responses for twelve gerbil ears. The responses at low frequencies show an almost flat response, except in a few ears at the lowest frequency, and a phase close to zero (within 30°), which is characteristic of a stiffness-dominated system. In 7 ears (gerbils A, B, F, G, I and J, with dashed lines in Figure 4.4) the pars flaccida was retracted into the middle-ear cavity. At 300 Hz the magnitudes in this group ranged between 50 and 90 nm/Pa. In the other 5 ears (gerbils C, D, E, H and K, with solid lines in Figure 4.4) the pars flaccida was flat and a distinct feature was observed in the umbo magnitude response, with a magnitude minimum between 400 and 700 Hz and a phase maximum between 450 and 750 Hz. The magnitudes at 300 Hz in this group ranged between 45 and 60 nm/Pa, mostly lower than in the group with a retracted pars flaccida. Note that for gerbil K the umbo response shown in Figure 4.4 was measured about 95 minutes later than the one shown in Figure 4.3. Temporal effects changed the resonance frequency of the pars flaccida, so in Figure 4.4 the umbo-response feature related to the pars flaccida is about 300 Hz higher in frequency than it is in Figure 4.3.

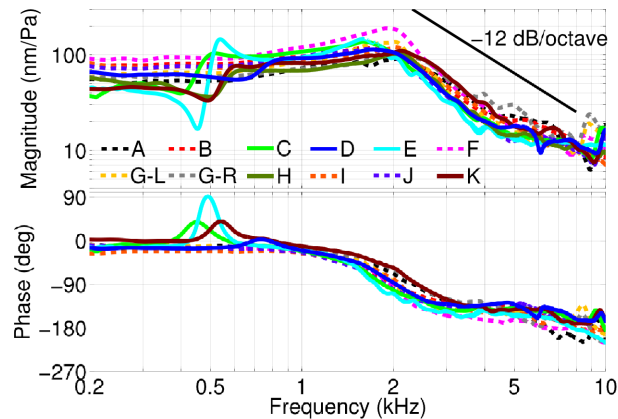


Figure 4.4: Umbo displacement response normalized by sound pressure in 12 ears. The responses measured in ears with a flat pars flaccida are shown with solid lines and the responses measured in ears with a retracted pars flaccida are shown with dashed lines.

The magnitude-minimum/phase-maximum feature in the umbo response became gradually less distinct with a greater degree of retraction. For example, the pars flaccida in gerbil D was partially retracted and a shallow minimum in the umbo magnitude response is still visible at 610 Hz in Figure 4.4. During measurements in two ears (C and H), each with an initially flat pars flaccida, we noticed that over a time interval of about one minute the low-frequency umbo magnitude gradually increased and the minimum associated with the pars-flaccida resonance disappeared. The effect in gerbil H can be appreciated by comparing Figures 4.4 and 4.5.

The low-frequency results provided in Figures 4.3 and 4.4 are in general agreement with the findings of Rosowski et al. (1997), Lee & Rosowski (2001) and Rosowski & Lee (2002). In all three studies the results were reported in terms of velocities and for comparison with our data we have converted them to displacements. Except for the results from Rosowski et al. (1997), which are only for one ear, the data from the other studies involved pressure sweeps and can be compared with our results only with caution because the directions of the pressure sweeps affected the observations at zero static pressure. The low-frequency umbo-displacement magnitude was reported to be approximately 55 nm/Pa at 200 Hz (Rosowski et al., 1997, Figure

6), 56.7 ± 6.7 (S.E.M.) nm/Pa at 250 Hz (Lee & Rosowski, 2001, Figure 7, zero static pressure, average of the two pressure-sweep directions), and 35 to 48 nm/Pa (95% confidence interval) at 200 Hz (Rosowski & Lee, 2002, Figure 2, zero static pressure, positive-to-negative sweep). These values are consistent with the range of 45 to 60 nm/Pa that we report here for the umbo displacement magnitude with a flat pars flaccida at 300 Hz. In Rosowski & Lee (2002, Figure 3, zero static pressure, positive-to-negative sweep) the umbo displacement magnitude with an immobilized pars flaccida was reported to be from about 45 to 60 nm/Pa (95% confidence interval) at 200 Hz, similar to the range of 50 to 90 nm/Pa that we report here for the umbo response with a retracted pars flaccida at 300 Hz.

4.3.3.2 Mid and high frequencies

As shown in Figure 4.3, near and above the resonance of the flat pars flaccida its phase departs from that of the umbo. The pars-flaccida displacement remains higher than that of the umbo up to about 4.5 kHz, except around 2.2 kHz where it shows a sharp and deep antiresonance. This antiresonance was absent in some ears (e.g., gerbil E, not shown here). When the antiresonance is present, it causes a phase shift of almost half a cycle (180°). At higher frequencies, in this animal the pars-flaccida magnitude went down to about the level of that of the umbo, while in other animals the pars-flaccida magnitude was as much as 7.5 dB lower than that of the umbo.

In the response of the retracted pars flaccida of Figure 4.3, the phase follows the umbo phase closely up to 3.5 kHz except for a divergence with a minimum at about 1 kHz, but at higher frequencies the phase difference increases up to about 70° at 10 kHz. The 1-kHz minimum of the divergence in the pars-flaccida phase is accompanied by a minimum in the magnitude at a slightly higher frequency. Similar behaviour in both magnitude and phase was seen in all ears, with phase minima in the range of 1 to 1.7 kHz.

Figure 4.4 shows that, for both flat and retracted pars flaccida, the umbo response has a rather broad resonance with a peak between 1.6 and 2.0 kHz. The maximum displacement at the resonance is from 90 to 190 nm/Pa. The ratio of the displacement at the resonance peak to the displacement at the low-frequency asymptote is from 1.6 to 2.1 in different ears. We quantify the width of the resonance as the full width at half maximum of the velocity response. (We use velocity because for the displacements the low-frequency magnitude is sometimes greater than the half-maximum magnitude.) The width computed in this way varies from 1.5 to 2.8 kHz in the different ears.

For frequencies above the resonance frequency, the umbo magnitude generally decreases with increasing frequency, but with substantial irregularities. These irregularities typically have bandwidths of a few hundred hertz, magnitude changes of a few decibels and phase changes of a few tens of degrees; these changes are quite stable in time and are much larger than the short-term variations described in Section 4.3.2. In the range of 8.5 to 9.1 kHz, 3 ears (gerbils F and G) show a distinct maximum and 6 ears (gerbils A, C, D, H, J and K) show a distinct minimum.

Ravicz et al. (1992) and Teoh et al. (1997) also reported a gerbil middle-ear resonance frequency of about 2 kHz in their impedance and admittance measurements. The three studies mentioned in Section 4.3.3.1 presented mid- and high-frequency response shapes that, when converted to displacement, are similar to those presented here. At the resonance peak, Rosowski et al. (1997, Figure 6) reported umbo displacement magnitudes of approximately 110 nm/Pa at about 2.1 kHz, which is consistent with our observed range of 90 to 190 nm/Pa. Other reported values in the literature are 67.0 ± 7.8 (S.E.M.) nm/Pa at 2 kHz (Lee & Rosowski, 2001, Figure 7, zero static pressure, average of the two pressure-sweep directions); and 55 to 80 nm/Pa (95% confidence interval) with normal pars flaccida and 45 to 65 nm/Pa (95% confidence interval) with

immobilized pars flaccida, both between about 1.7 and 2.1 kHz (Rosowski & Lee, 2002, zero static pressure, positive-to-negative sweep: Figure 2, normal pars flaccida; Figure 3, immobilized pars flaccida). These are lower than the ranges reported in the current study but, as mentioned in Section 4.3.3.1, values from these two studies that involved pressure sweeps can be compared with our results only with caution.

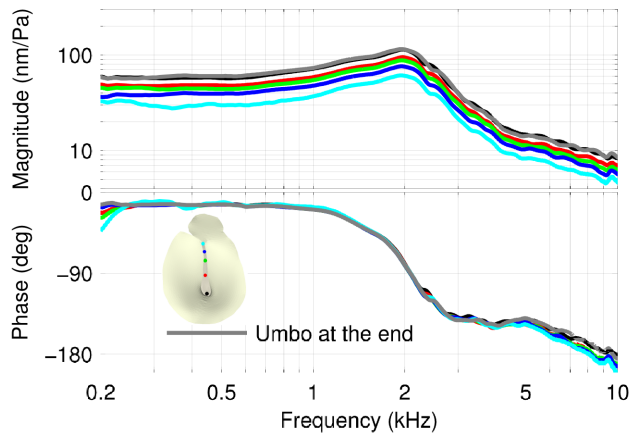


Figure 4.5: Displacement response normalized by sound pressure along the manubrium in gerbil H.

4.3.4 Manubrial vibrations

Figure 4.5 shows manubrial displacement responses for gerbil H. We measured the umbo displacement at the start of the measurement series (black curve) and, to check for temporal effects, we measured it again 32 minutes later at the end of the series (grey curve). Comparison of the two umbo responses shows that the details were almost completely preserved, indicating that temporal effects were very small over the time period required to measure all of the points on the manubrium. As mentioned in Section 4.3.3.1, the state of the pars flaccida in this ear changed from flat (Figure 4.4) to retracted (Figure 4.5). As seen in this figure, all points along the manubrium moved in phase with each other (within 5°) up to at least 5 kHz while the magnitude increased from the lateral process to the umbo. Similar differences along the

manubrium were observed in all ears. This gradual increase is consistent with the classical view of rotation of the malleus around a fixed axis of rotation.

In order to estimate the position of the axis of rotation from the experimental data, we used an improved version of the 3-D gerbil middle ear model of Gea et al. (2009), reconstructed based on a microCT dataset. We oriented the model to correspond to the angle of view in our experiments and then used it to estimate the distances between the measurement locations on the manubrium. Using the ratio of the displacement magnitude of the umbo to that of the lateral process of the malleus (Figure 4.5) averaged over the frequencies from 0.3 to 4 kHz, and using distances taken from the model, the low-frequency axis of rotation was estimated to be approximately 1.7 mm superior to the lateral process of the malleus, measured along an extension of the line from the umbo to the lateral process (as projected onto the plane perpendicular to the direction of the laser beam). In the 3-D model, the anatomical axis of rotation (running from the tip of the anterior malleolar process to the posterior incudal ligament) is estimated to lie approximately 1.9 mm superior to the lateral process of the malleus (measured along a line in the same direction as described above). This is quite comparable to the value of 1.7 mm found from the experimental data. It should be noted that for an accurate estimation of the location and orientation of the axis of rotation, 3-D measurements like those of Decraemer et al. (1994a, 2011a) are required.

In our results, for frequencies higher than 5 kHz, the trend continues of increasing displacements from the lateral process to the umbo, but phase differences among the points along the manubrium start to become more evident, with the phase difference between the umbo and the short process increasing with frequency up to about 19° at 10 kHz. In Figure 4-B of de La Rochefoucauld & Olson (2010) a phase difference of about 7° at 5 kHz and a maximum phase difference of about 15° between the umbo and the lateral process in the range of 5 to 10 kHz can

be seen, which is comparable to the findings here. They observed much greater phase differences at frequencies beyond those considered here.

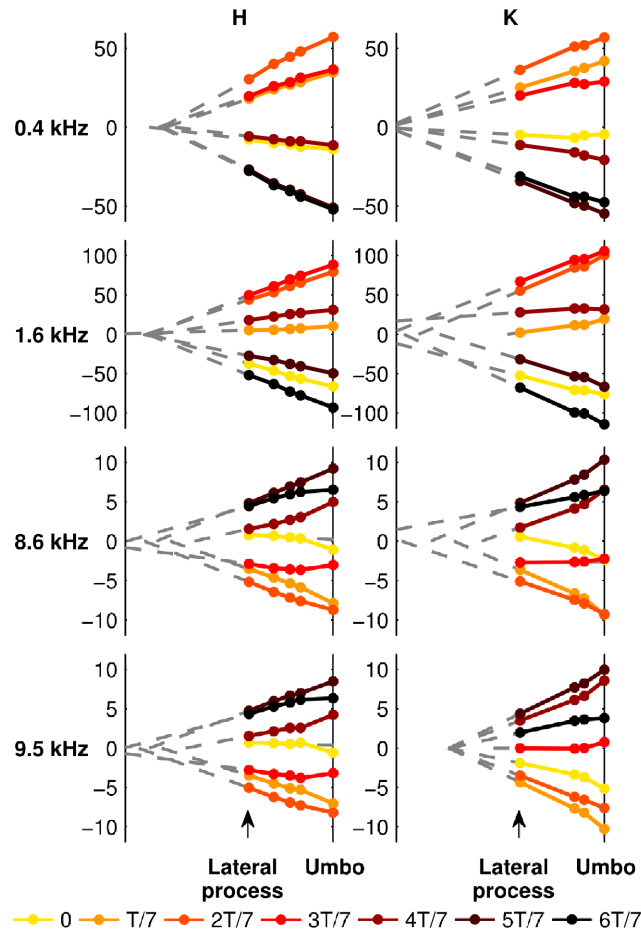


Figure 4.6: Sinusoidal motion of the manubrium at seven time instants (multiples of $T/7$) throughout the cycle in gerbils H and K at frequencies of 400, 1600, 8600 and 9500 Hz.

These differences in phase indicate mode changes of the malleus and flexing of the tip of the manubrium at high frequencies, as can be seen in Figure 4.6 for gerbil H (as in Figure 4.5) and gerbil K. In this figure, the displacements of the points on the manubrium are drawn for four frequencies and for seven equally spaced time instants within each cycle. The manubrium appears to be moving more or less as a rigid body with a fixed axis of rotation at the lowest frequency (400 Hz). In gerbil H at 1600 Hz, the manubrium again appears to be almost rigid and the axis of rotation is again almost fixed at the same position as for 400 Hz. At this frequency in

gerbil K, however, the axis of rotation clearly moves throughout the cycle. Non-straight lines seen at 8600 and 9500 Hz can be attributed to flexing in the region of the umbo, changes in the rigid-body vibration mode of the malleus, or both. Our data are consistent with a recent study by Decraemer et al. (2011a) in which complex motions of the gerbil malleus were observed.

4.3.5 Pars-tensa vibrations

As described in Section 4.2.3, vibrations of the pars tensa were studied by placing beads on its posterior and anterior parts at the level of the middle of the manubrium, and in the region just posterior, anterior and inferior to the umbo.

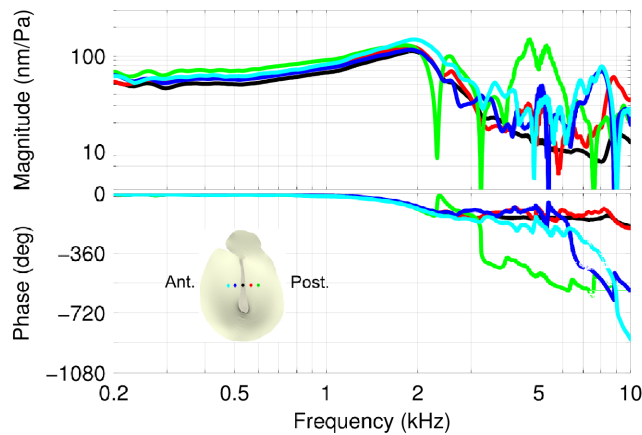


Figure 4.7: Pars-tensa displacement responses, normalized by sound pressure, at locations in a line perpendicular to the manubrium in the left ear of gerbil G.

4.3.5.1 Low-frequency response

Figures 4.7 and 4.8 illustrate vibrations at the level of the middle of the manubrium in gerbils G and J. These figures show that points on the pars tensa and the manubrium move in phase up to about 2 kHz. The relationships among the magnitudes at the different points are more clearly shown in Figure 4.9, with the magnitudes of the pars-tensa points in all ears, normalized by the respective displacements at the manubrium, at a low frequency (0.5 kHz). All curves have a minimum at the manubrium and, for approximately the same distances from the manubrium,

beads on the posterior side show larger displacements than the ones on the anterior side. Note that, although the relative positions of the beads are approximately constant from ear to ear, we did not measure the actual distances between the measurement points so the curves are presented based on bead numbers rather than positions.

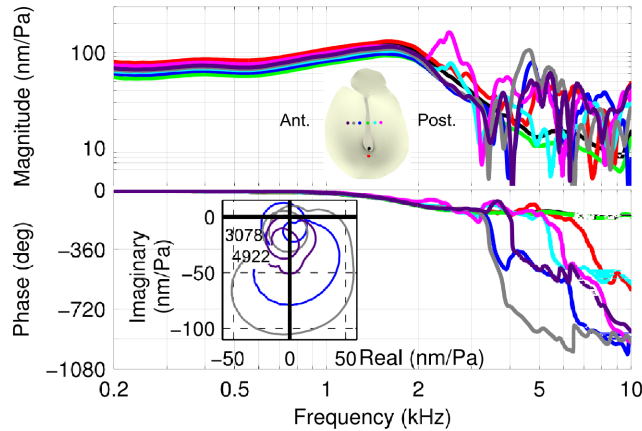


Figure 4.8: Pars-tensa displacement responses, normalized by sound pressure, at locations in a line perpendicular to the manubrium, at the umbo, and at a location inferior to the umbo in gerbil J. The inset shows the Nyquist plots for three anterior pars-tensa points in the frequency range of 3078 to 4922 Hz, as discussed in the Appendix.

4.3.5.2 High-frequency response

Beyond 2.1 kHz in Figure 4.7 and 1.9 kHz in Figure 4.8, different points of the pars tensa move out of phase with each other and the manubrium, and show frequency-dependent magnitude differences, indicating that the simple vibration pattern has broken up. Table 4.1 shows the break-up frequencies for all ears, based on the frequency at which the phase curves for different points diverge by more than 15° (5 times the short-term repeatability described in Section 4.3.2).

Because of the length of the experiment and the difficulty of keeping the animal alive, measurements on both ears could only be done in one animal (gerbil G). Table 4.1 shows that both the resonance frequencies and the break-up frequencies of the two ears of this animal were very similar.

Table 4.1: Estimation of break-up frequencies in 12 gerbil ears

Gerbil ear	Middle-ear resonance frequency (kHz)	Break-up frequency (kHz)
A	2.0	2.3
B	1.7	2.5
C	1.6	1.9
D	1.8	2.8
E	1.6	1.8
F	1.9	2.3
G-left	1.9	2.1
G-right	2.0	2.2
H	1.9	2.1
I	2.0	2.8
J	1.7	1.9
K	1.8	2.8

Figure 4.10 shows the pars tensa motions at the level of the middle of the manubrium in two ears at seven time instants throughout the cycle for four frequencies. In this figure displacements were normalized by the displacement magnitudes at the manubrium. The first row shows the low-frequency displacement at 0.5 kHz, with points moving in phase and displacement increasing when moving further away from the manubrium, similar to what was seen in Figure 4.9. The second row shows the displacements at the onset of break-up as defined earlier. At this frequency the magnitude envelopes are still similar to the ones at low frequencies but phase differences between points start to make the displacement pattern more complex. The last two rows show displacements at frequencies 1.3 and 1.5 times the break-up frequencies, respectively, that is, at 2.7 and 3.2 kHz for gerbil H and at 3.6 and 4.2 kHz for gerbil K. At these frequencies, the anterior and posterior parts vibrate in very different ways. In the posterior part a displacement maximum appears at the second point from the manubrium. At the frequencies shown here, the phase differences seen from point to point indicate that there is not a pure standing wave.

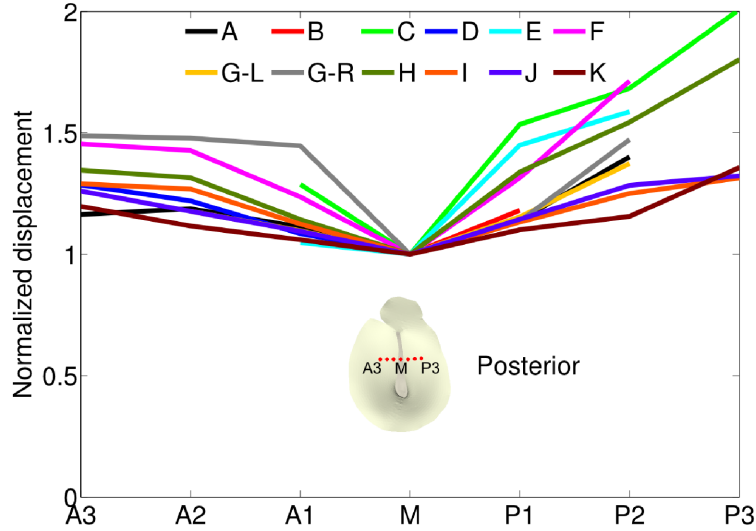


Figure 4.9: Pars-tensa motion at a low frequency (0.5 kHz) in all gerbil ears. The horizontal axis shows the bead number on the pars tensa, and the vertical axis shows the displacement magnitude normalized by that of the manubrium.

In addition to pars-tensa points at the level of the middle of the manubrium, Figure 4.8 also shows the response of a point inferior to the umbo. The magnitude of motion of this point is comparable to the magnitudes of other points on the pars tensa while its phase stays closer to that of the manubrium up to higher frequencies (within 16° up to about 4 kHz).

Figure 4.11 provides more data about the vibrations of the pars tensa in the region of the umbo, for gerbil F. This figure confirms that, similar to responses of the pars-tensa points at the level of the middle of the manubrium, responses in this region break up beyond a particular frequency. In this ear, a break-up frequency of 2.3 kHz is seen in the figure, which is the same as for points at the level of the middle of the manubrium (not shown). The similarity of the phase in the inferior region to that at the umbo, seen in Figure 4.8 beyond the break-up frequency, is not seen here but was observed in some other ears.

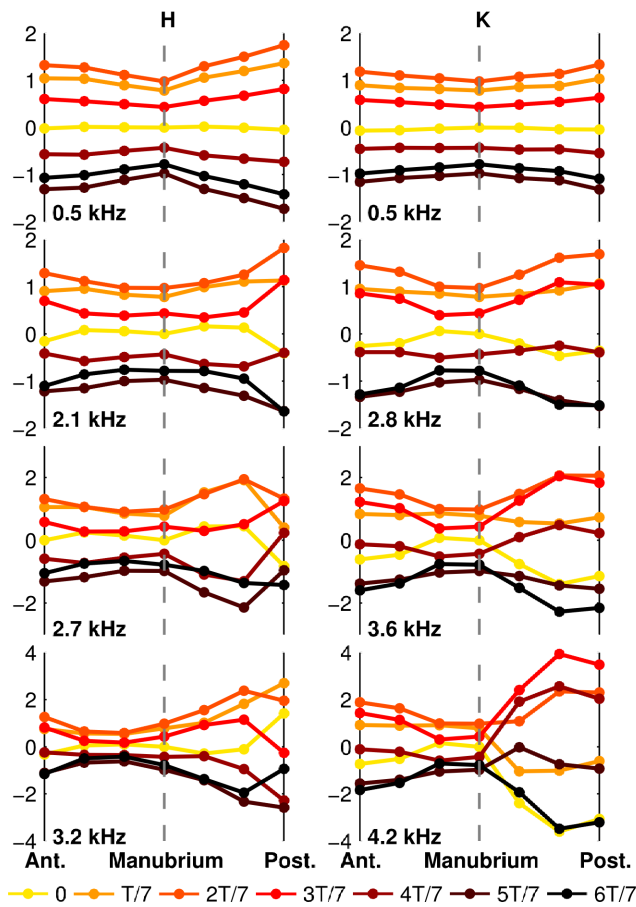


Figure 4.10: Sinusoidal motion of the pars tensa points at the level of the middle of the manubrium at seven time instants (multiples of $T/7$) throughout the cycle in gerbils H and K at four frequencies (from top to bottom: low frequency, break-up frequency, 1.3 times the break-up frequency and 1.5 times the break-up frequency).

4.4 Discussion

4.4.1 Umbo and pars-flaccida responses

Kohllöffel (1984) performed anatomical measurements of the pars flaccida and suggested that, among other possible roles, the pars flaccida may act as a shunt around the pars tensa at low frequencies in some species. Teoh et al. (1997) adapted Kohllöffel's generic circuit model to the gerbil middle ear and determined model parameters based on their admittance measurements. They showed that the large pars flaccida in this species is responsible for reducing the hearing

sensitivity around the pars-flaccida resonance frequency, which is between 500 and 900 Hz in our observations, and at lower frequencies.

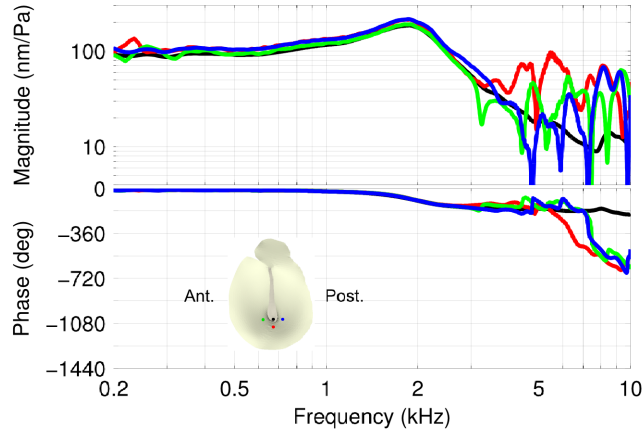


Figure 4.11: Pars-tensa displacement responses, normalized by sound pressure, at locations at and around the umbo in the left ear of gerbil F.

Our results confirm that a flat pars flaccida has larger displacements than the umbo, as was observed by Rosowski et al. (1997), and also show that it has larger displacements than the pars tensa in this low frequency range. A flat pars flaccida is manifested by the presence of a distinct feature in the umbo response below 900 Hz: as the frequency approaches and passes the pars-flaccida resonance frequency, the umbo magnitude response passes through a minimum and the phase passes through a maximum. Above its resonance frequency, the motion of the pars flaccida is more or less mass-dominated, and as it rolls off its effect on the umbo response becomes negligible.

Near and above its resonance, the phase of the flat pars flaccida departs from that of the umbo and its magnitude remains higher up to about 4.5 kHz, except for an antiresonance in some ears. This antiresonance was not observed in all ears, presumably because it is very sensitive to the location of the bead near the centre of the pars flaccida: a small difference between the bead locations from one ear to the other may cause the presence or absence of this feature. For

frequencies higher than 4.5 kHz, the pars-flaccida magnitude is either lower than or at the same level as that of the umbo.

When the pars flaccida is retracted inside the middle-ear cavity, it becomes stiffer and cannot play its normal role of shunting low-frequency sound around the pars tensa. In this situation, at low frequencies the umbo response looks like the response of a stiffness-dominated system. This is consistent with earlier observations of an artificially stiffened pars flaccida (Teoh et al., 1997; Rosowski & Lee, 2002).

The phase of the retracted pars flaccida shows a divergence from that of the umbo at about 1.0 to 1.7 kHz accompanied by a minimum in the magnitude. Modelling studies may shed some light on the cause of this behaviour. For frequencies beyond this feature, the response of a retracted pars-flaccida is more or less like a mass-dominated system.

The umbo magnitude response shows a relatively broad resonance at about 2 kHz, indicative of heavy damping, followed by an overall decrease with irregularities. These irregularities are presumably the result of complex motions of the pars tensa (see Section 4.3.5) and of the ossicular chain (Decraemer et al., 2011a).

4.4.2 Pars-flaccida retraction

Some of the ears in this study had a retracted pars flaccida. (During measurements in two ears, we noticed that over a time interval of about one minute the initially flat pars flaccida became retracted into the middle-ear cavity.) So far we have not been able to control the shape of the pars flaccida *in vivo*. Nambiar (2010) carried out a *post mortem* study on the gerbil TM in which rapid euthanasia by a carbon dioxide overdose was performed before the surgery was started. In that study the pars flaccida was always flat and the pars-flaccida effect was always evident in the

umbo responses. Effects on the umbo response that are similar to those of pars-flaccida retraction can be produced by applying static pressure to the middle-ear cavity (Lee & Rosowski, 2001) or by immobilizing the pars flaccida (Teoh et al., 1997; Rosowski & Lee, 2002). In the impedance measurements of Ravicz et al. (1992), the distinctive umbo-response feature caused by the pars-flaccida was absent except in one ear. Teoh et al. (1997) attributed this absence to the effects of drying because Ravicz et al. (1992) did not moisten the pars flaccida. However, we also did not moisten the pars flaccida, and drying did not eliminate the pars-flaccida effect. Therefore, it may be that the pars flaccida was retracted in most of the (1992) measurements but that the retraction was not noticed.

It has been seen in different species that, in the presence of liquid in the middle-ear cavity, the pars flaccida is retracted into the cavity (e.g., Tos & Poulsen, 1980, in humans; Stenfors et al., 1981, in rats; Larsson et al., 2005, in gerbils). Such retractions might have been caused by the development of negative pressures inside the cavity. Indeed, only a very small pressure is needed to retract the pars flaccida (Dirckx et al., 1998). Although negative pressure can initiate the retraction, it cannot be responsible for keeping the membrane retracted in our case, because equalization of the middle-ear pressure by creation of a ventilation hole in the cavity wall did not cause the flat shape to be recovered. Although we checked that our ventilation tubes were patent when inserted, as mentioned in Section 4.2.1, it is possible that they became blocked at some point in the two ears in which a previously flat pars flaccida became retracted after creation of the ventilation hole and insertion of the ventilation tube. However, removing the ventilation tube as soon as the retraction happened did not change the state of the pars flaccida. Indeed, we have observed that applying a positive static pressure to the ventilation tube moves the pars flaccida back to its natural flat state and causes the pars-flaccida contribution to the frequency response to

be recovered, but when the pressure is released the pars flaccida is retracted again. The surface tension of a liquid film that forms on the cavity wall near the pars flaccida may pull it inward and keep it retracted. When the liquid film behind the pars flaccida is removed, the flat shape is recovered and maintained, but this removal requires a wide opening of the cavity wall, which cannot be done until the very end of our data-collection protocol. The removal also carries the risk of tearing the pars flaccida.

In the literature different mechanisms have been suggested as being responsible for the emergence of liquid in the middle-ear cavity. One of those mechanisms is the development of negative pressure inside the cavity. Flisberg et al. (1963) showed that, with a negative pressure of 20–30 mmHg, 15 minutes were enough for transudation to start in the human ear. Hiraide & Paparella (1972) and Hiraide & Eriksson (1978) reported that as little as one minute at –5 mmHg in guinea pigs caused transudation. Hutchings (1987) applied negative pressure in the gerbil middle-ear cavity for 30 to 90 minutes and observed that any pressure more negative than –11 mmHg caused transudation.

In our experiments we use pentobarbital, which is known to disable the muscles of the Eustachian tube (e.g., Doyle et al., 1995). Zheng et al. (1997) reported that pentobarbital caused negative middle-ear pressure in gerbils, and they suggested that this might be due to the inactivity of the tube muscles. Occlusion of the Eustachian tube is thus one of the candidates for causing the development of a negative pressure in the cavity and the subsequent accumulation of liquid. A good description of the underlying mechanism of the gas-exchange process can be found in Sadé & Ar (1997).

Theoretically, nitrogen partial pressure dominates the gas-exchange process in the long term and, even without a functional Eustachian tube for the length of our experiments, it should not allow

the development of large enough negative pressures to cause transudation. Doyle et al. (1999) measured the trans-mucosal gas-exchange rate of nitrogen and calculated that opening of the Eustachian tube once a day is enough to prevent middle-ear effusion in monkeys. When Hiraide & Paparella (1972) closed the Eustachian tube in guinea pigs and monkeys, they found that transudation did not occur in less than 24 hours. Although these two studies suggest that negative pressures that are large enough to initiate transudation should not build up in short periods of time after Eustachian tube occlusion, Eriksson et al. (2003) reported liquid in the middle ear within only 3 hours of the occlusion of the Eustachian tube in rats, which is consistent with the retraction of the pars flaccida during our experiments.

Another factor in our experiments is that the stream of oxygen that we kept in front of the animal's nose might have affected the gas exchange by causing hyperventilation, hyperoxia and/or hypocapnia. It would be necessary to monitor the animal's respiration to confirm this.

Yet other mechanisms might be responsible for the emergence of liquid in the cavity. Alm et al. (1983) demonstrated that mechanical scratching of the external ear canal in rats caused the emergence of liquid in the cavity and the ear canal, and retraction of the pars flaccida within 30 minutes. They also showed that irritation of the ear canal with an air flow of 5 L/min at 15 °C had the same effect. Later Hellström et al. (1985) studied the effect of air-flow temperatures of 14, 24 and 34 °C and concluded that the phenomenon is temperature-dependent with the greatest effect at 14 °C and no effect at 34 °C, which is the normal temperature for the ear canal. Although their study emphasized the impact of temperature, and they mentioned the similarity of the response to that of the mucosa of the bronchi and nasal cavity, they still attributed these effects to the irritation of the ear canal and not to the possibility of a temperature-related response of the middle-ear mucosa caused by conductive heat transfer across the TM.

Our experiments involve both mechanical stimulation of the external ear and changes in temperature inside the middle-ear cavity and ear canal. The temperature changes are caused by inserting the ventilation tube, which introduces air at room temperature into the cavity, and by removing the cartilaginous ear canal and attaching an aluminum coupler, the high thermal conductivity of which keeps the canal environment near room temperature.

In summary, although negative pressure may initiate pars-flaccida retraction, we think that formation of a liquid film near the pars flaccida may be the cause of maintenance of the retraction and possibly also for its initiation. One or more of the mechanisms discussed above may be responsible for the emergence of liquid in the middle-ear cavity in our experiments. It remains unexplained, however, why retraction of the pars flaccida does not occur in some gerbils. Since the pars flaccida influences the responses of the manubrium and pars tensa, its status is very important for the interpretation of the measurements.

4.4.3 Manubrial response

The results presented here show that, for frequencies up to at least 5 kHz, the displacement magnitude increases from the lateral process to the umbo and all manubrial points move in phase with each other. The location of the axis of rotation that was calculated from experimental results at low frequencies was shown to be close to the location of the anatomical axis of rotation in a reconstructed 3-D model of the gerbil middle ear. Beyond 5 kHz, although the trend of increasing magnitudes is preserved, there is an increasing phase difference with frequency that may indicate a change of the vibration mode of the malleus and some flexing of the tip of the manubrium consistent with observations in the cat (Decraemer et al., 1991, 1994b) and, more recently, in the gerbil (Decraemer et al., 2011a). The flexing of the manubrium in the cat has been shown to be consistent with the geometry of the manubrium and with plausible material

properties (Funnell et al., 1992), but a similar analysis has not been done for the gerbil. Changes in the vibration mode of the malleus are compatible in principle with the elastic suspension of the ossicles but have not yet been modelled quantitatively.

4.4.4 Pars-tensa response

At low frequencies, we observed a fundamental mode with all pars-tensa points moving in phase with the manubrium. The magnitude at the manubrium is lower than that on the pars tensa, and the posterior side tends to have larger displacements than the anterior side. The vibration pattern becomes more complex at higher frequencies, which is consistent with previous experimental results (e.g., Tonndorf & Khanna, 1972) and modelling results (Funnell, 1983). The break-up occurred between 1.8 and 2.8 kHz in the ears studied here, which is similar to what has been found in other species. These observations will be important for the development and validation of middle-ear finite-element models for the gerbil, in conjunction with the 3-D ossicle measurements of Decraemer et al. (2011a).

4.5 Acknowledgements

The authors would like to thank Ms. Shruti Nambiar and Ms. Zinan He for their contributions to the development of the surgical and measurement techniques; Dr. Jim Gourdon for advice on the anaesthesia procedure; and Dr. Dan Citra for his help dealing with the animals. This work was supported in part by the Canadian Institutes of Health Research, the Fonds de recherche en santé du Québec, the Natural Sciences and Engineering Research Council (Canada), the Montréal Children's Hospital Research Institute, the McGill University Health Centre Research Institute and the Research Fund of Flanders (Belgium).

Appendix

An inset in Figure 4.8 shows the Nyquist plots for three anterior beads in the frequency range of 3078 to 4922 Hz, as an example of their use for verification of the phase response as mentioned in Section 4.2.3. The unwrapped phases shown for these three beads follow what the Nyquist plots display regarding the phase evolution, which can be described in terms of ‘phasors’, that is, vectors drawn from the origin to points on the Nyquist plot. When for increasing frequency the phasor rotates clockwise, the phase angle decreases (becomes more negative), and vice versa. All three curves start in the same quadrant and end in that same quadrant, but the trajectories in between are quite different. At the beginning of the violet trajectory on the Nyquist plot, the phasor rotates clockwise through a small angle then counterclockwise, corresponding to a phase decrease up to about 3300 Hz and then a phase increase up to about 3650 Hz. After this frequency it rotates clockwise, which corresponds to a decrease in phase up to a point where the phasor becomes extremely short and the trajectory becomes almost tangent to the real axis, at about 4100 Hz. Approaching and passing this tangent zone, with the phasor still rotating clockwise and encircling the origin, causes a sharp drop in the phase plot, after which the phasor becomes longer and continues to rotate clockwise, corresponding to a smooth phase drop. (When the phasor becomes very short, a very small difference in the real or imaginary parts, due to noise or frequency resolution, can change whether it encircles the origin or not, which in turn causes a difference of 360° in the phase.) The phasors for the blue and grey trajectories start rotating clockwise and both of them make circles, but the grey trajectory encircles the origin while the blue trajectory does not. This corresponds to a continuous drop of the grey phase plot but an increase at about 4 kHz in the blue phase plot.

5 Effect of opening middle-ear cavity on vibrations of gerbil tympanic membrane

Published in the *Journal of the Association for Research in Otolaryngology*,
2014 June, Volume 15, Issue 3, 319–334

Preface

In Chapter 4, measurements of tympanic-membrane and manubrium vibrations with a closed middle-ear cavity were presented. Since our finite-element model (presented in the next chapter) does not include the middle-ear cavity, it is important to know how our observations with a closed cavity are affected by opening the cavity. In this chapter, the effects of progressive opening in the cavity wall on vibrations of the tympanic membrane and manubrium are presented. In order to be able to validate the responses from the model described in the next chapter, we present a method in this chapter to estimate tympanic-membrane responses at the limit of no middle-ear cavity, based on experimental results collected with a partial opening in the cavity wall.

Abstract

This paper presents *in vivo* experimental measurements of vibrations on the pars flaccida, along the manubrium and at several points on the pars tensa in the gerbil with open middle-ear cavity. The effects of progressive opening of the middle-ear cavity are presented, with up to five different extents of opening. In all manubrial, pars-tensa and pars-flaccida responses, opening the cavity causes an increase in the low-frequency magnitude and a shift of the main middle-ear resonance to lower frequencies, and introduces an antiresonance. However, opening the cavity has little or no effect on either the mode of vibration of the manubrium or the breakup frequency of the pars tensa. When the opening is gradually widened the antiresonance frequency moves to higher frequencies. When the opening is made as wide as anatomically possible, the antiresonance moves to almost 10 kHz. The main increase in the low-frequency response magnitude happens upon making the smallest hole in the cavity wall, and further progressive enlarging of the opening has little or no effect on the low-frequency magnitude. The antiresonance interferes with the response shapes. An identification method is suggested for eliminating the effect of the antiresonance in order to estimate the ideal open-cavity response. The method is validated and then applied to manubrial and pars-tensa responses. Estimating the ideal open-cavity responses will simplify comparison of the data with numerical models which do not include the air cavity. The data collected at intermediate stages of opening will be useful in validating models that do include the cavity.

5.1 Introduction

In auditory research on the mechanical response of the ear, it is usually the condition with a naturally closed middle-ear air cavity that is of interest but there are many instances where the methodology of the study demands opening of the cavity. Examples include removing some parts of the cavity wall to expose the ossicles, to study artificial otitis media with effusion, to expose the round window membrane or manipulating the cochlea. In some preparations it is possible to easily reverse the effects of the opening by resealing, for example with a glass coverslip, but in other cases it would be very difficult and time-consuming. Understanding the effects that the opening has on frequency responses and on spatial vibration patterns is essential in deciding whether to spend effort resealing the opening.

When the cavity is opened, different sizes of the opening may be involved, ranging from a very small hole made in the cavity wall to an almost complete removal of the cavity wall. To permit comparison of experimental results with different sizes of opening, it is important to know how that affects the results.

The effects of the middle-ear cavity on the response of the ear have been investigated using admittance, impedance and other measurements in human (Zwislocki, 1962), guinea pig (Zwislocki, 1963), rabbit (Møller, 1965), cat (Møller, 1965; Guinan & Peake, 1967; Lynch et al., 1994), lion (Huang et al., 1997), gerbil (Ravicz et al., 1992; Teoh et al., 1997) and chinchilla (Rosowski et al., 2006). In these studies it was found that opening the middle-ear cavity has the following effects on the response of the middle ear: (1) the stiffness of the middle ear at low frequencies is reduced; (2) the middle-ear resonance moves to lower frequencies; (3) an antiresonance is introduced in the admittance; (4) at high frequencies there is not much difference between open-cavity and closed-cavity admittances (except for the antiresonance); (5)

in species with large pars flaccida (like the gerbil, cf. Teoh et al., 1997) the admittance peak associated with the pars flaccida becomes more prominent.

In Chapter 4, we briefly summarized previous studies that dealt with vibration patterns of the TM and presented our closed-cavity measurements. However, there have been no measurements reported for the effects of opening the middle-ear cavity on the vibration patterns of the TM and manubrium. The present study explores how opening the middle-ear cavity, and the extent of the opening, affect the vibration patterns of the TM.

Models of the middle ear without the cavity are less complex and require fewer parameters than models including the cavity. Validating these simpler models is an important step in developing comprehensive models that include the cavity. For this purpose, experimental data with a completely open middle-ear cavity should be used but usually only a partial opening of the cavity is possible. There is a need, therefore, for a method that can exclude the effects of the partial opening on the responses and estimate the ideal open-cavity responses. This paper demonstrates a method for estimating an ideal open-cavity response from measurements made with a partial cavity opening.

5.2 Materials and methods

5.2.1 Preparation and measurement

The materials and methods used in this study are similar to those described in detail in Chapter 4, with additional steps for studying the effects of opening the middle-ear cavity. Here we briefly summarize what is common to this and the closed-cavity study and then explain the steps specific to this study. TM vibration was measured *in vivo* in 12 ears of 11 female Mongolian gerbils (*Meriones unguiculatis*) supplied by Charles River Laboratories (St-Constant, Québec).

Body weights were from 64 to 100 g. The study protocol was approved by the McGill University Animal Care Committee. Analgesics and anaesthetics were administered and, once the animal reached an appropriate level of anaesthesia, the bulla was exposed by removing soft tissue. Then, using a surgical ear drill, the bony ear canal was removed and the TM was exposed. A wooden block attached to the skull using dental cement (IRM, Dentsply Caulk) was used to fix the head under an operating microscope (OPMI 1-H, Zeiss) equipped with the sensor head of a single-point LDV (HLV-1000, Polytec). Measurements were performed from a single viewing direction. In order to equalize pressure in the bulla, a ventilation hole was made on the bulla about 3 mm away from the TM; to cancel the acoustical effects of the hole, a 15-cm-long polyethylene tube with an inner diameter of 0.58 mm and an outer diameter of 0.96 mm was inserted into the hole.

The TM was stimulated by 128-ms sinusoidal sweeps from 0.2 to 12.5 kHz delivered to the ear canal by an ER-2 tubephone (Etymotic Research) through an aluminum acoustic coupler. The measured vibration amplitudes are normalized by the sound pressure measured about 2–3 mm away from the TM by an ER-7C (Etymotic Research) probe microphone connected through a hole in the coupler wall. The upper limit of the frequency range of interest in this study is 10 kHz. Within that range, replacement of the normal ear-canal wall by a coupler is not expected to have a significant effect on the normalized vibration measurements.

Glass-coated plastic beads of diameter of 90 to 150 μm (Sigma-Aldrich, model G4519) were used to increase reflection of the laser beam and mark the measurement locations. In each ear three or four target beads were placed on the manubrium. One bead was placed approximately at the centre of the pars flaccida. Up to three beads were placed on each of the posterior and anterior parts of the pars tensa at the level of the middle of the manubrium, and a few more were

placed in the region just posterior, anterior and inferior to the umbo. Images of the TM with beads were shown in Figure 4.2.

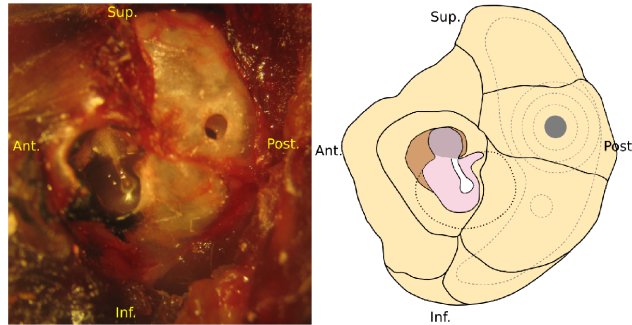


Figure 5.1: Left panel: lateral view of the gerbil middle-ear cavity wall and the tympanic membrane. A ventilation hole of about 1 mm in diameter has been made in the cavity wall. Right panel: a schematic representation of the cavity wall, the tympanic membrane, and our progressive opening of the cavity wall. The ventilation hole (about 1 mm in diameter) is shown as a grey filled circle. Progressive enlargement of the hole is shown by concentric circles and an additional 1-mm circle (grey dashed lines). The final maximal opening is shown by the large irregular closed curve (grey dashed line). The approximate boundary of the pars tensa is indicated by a dashed black curve and the approximate positions of the internal compartment borders of the middle-ear cavity are indicated by solid black lines.

A 1600-line FFT was used to transform the recorded vibrometer and microphone time-domain signals to the frequency domain. A two-pass (forward and reverse) moving-average filter with a window length of five was applied to the real and imaginary parts of the complex signal and the magnitude and phase responses were then calculated.

As mentioned above, in the ‘closed-cavity’ condition the cavity wall had a small ventilation hole and a ventilation tube in place. After finishing the closed-cavity data collection, as reported in Chapter 4, the cavity was opened to varying extents. To start, we simply removed the ventilation tube from the cavity wall, which left a hole about 1 mm in diameter. This hole can be seen in the cavity wall shown in the left panel of Figure 5.1 and it is shown as a grey filled circle in the right panel of that figure. The umbo response was recorded several times at this stage, and again after replacing the ventilation tube, and then after removing it again, to ensure repeatability of this process. The hole was then enlarged progressively, as shown schematically in the right panel of

Figure 5.1 by concentric circles and an additional 1-mm circle (grey dashed lines), and finally the cavity wall was removed as much as possible, shown by the large irregular closed curve (grey dashed line) in the figure. The approximate boundary of the pars tensa is indicated by a dashed black curve in the figure. The figure also indicates the approximate positions of the internal compartment borders of the middle-ear cavity (solid black lines). As can be seen in this figure, even at the maximum possible opening some portion of the walls of the middle ear remained intact. The complete removal of the middle-ear cavity wall was impossible due to surgical constraints. At each intermediate stage, measurements were taken several times. To speed up the process and thus avoid temporal effects, these intermediate measurements were done only at the umbo. As in Chapter 4, responses are reported for two different pars-flaccida conditions: when it is naturally flat (gerbils D, E and K) and when it is retracted into the middle-ear cavity. The state of the pars flaccida is not affected by opening the middle-ear cavity, as discussed in the above-mentioned article: if a pars flaccida is retracted in the closed-cavity condition then it remains retracted after the cavity is opened, and if flat then it remains flat.

5.2.2 Estimation of ideal open-cavity responses

The major feature added to the frequency responses upon partially opening the middle-ear cavity is a minimum, or notch, which is the acoustical signature of the opening and is seen in results from all measurement points. To estimate the ideal open-cavity response, this feature (referred to below as the ‘opening feature’) should be identified and removed. One way to approach this problem is to (1) develop a model for the middle ear which is based on physical and physiological properties of the structures and which includes a representation of the opening in the cavity wall (e.g., Ravicz et al., 1992); (2) adjust the model parameters to fit the model to the experimental data; and then (3) eliminate the part of the model that corresponds to the opening.

The disadvantage of this approach is that motions in the middle ear are complex and the development of a model that can closely fit all of the experimental results over the entire frequency range in each individual ear is very difficult, and indeed may not be possible in principle. Another approach for estimating the ideal open-cavity response, which we follow here, consists of direct mathematical identification and removal of the specific feature that corresponds to the partial opening.

We propose a method for finding the frequency-response function H_o corresponding to the opening feature, such that if the measured frequency response with a partially open cavity (H_{po}) is divided by H_o then the response H_{io} of a cavity with an ideal complete opening is obtained:

$$H_{io} = \frac{H_{po}}{H_o} \quad (1)$$

The method described here was implemented using MATLAB and the Signal Processing Toolbox (version 2012a, The MathWorks Inc.). The identification is performed by curve fitting to H_{po} in the frequency range where the targeted feature resides. We employed the so-called ‘rational fraction polynomials (RFP) method’ developed by Richardson & Formenti (1982) to perform the frequency-domain curve fitting. The RFP method is extensively used in identification of vibrating systems (e.g., Maia & Ewins, 1989; Formenti & Richardson, 2002; Meruane, 2013). Fitting by a rational fraction of polynomials results in a system of equations that is generally ill-conditioned (Richardson & Formenti, 1982). The use of orthogonal polynomials improves the numerical robustness of the method, in part by uncoupling the equations for the numerator and denominator coefficients. It also permits use of the Hermitian symmetry of the frequency responses about the origin to reduce the size of the problem by half. Furthermore, the method of Richardson and Formenti uses the Forsythe orthogonal polynomial (Forsythe, 1957).

Rolain et al. (1995) proved that, in the rational-fraction frequency-response form, no other polynomial basis can provide a better conditioning than the Forsythe polynomials do. We have used a MATLAB implementation of the RFP method by Gutiérrez Acuña (2003). In this method the frequency response within a frequency range is fitted by a rational fraction of orthogonal polynomials:

$$H(\omega_i) = \frac{\sum_{k=0}^m c_k \varphi_{i,k}}{\sum_{k=0}^n d_k \theta_{i,k}}, i=1, \dots, L \quad (2)$$

where L is the number of positive-frequency data points, c_k and d_k are polynomial coefficients to be found in the curve fitting process. Each of φ_i and θ_i is a set of orthogonal polynomial functions generated recursively with a simplified version of the method of Forsythe (1957), using real polynomials instead of complex ones. Each polynomial in the φ and θ sets is orthogonal to the other polynomials in its set with respect to a weighting function defined at each frequency. In the RFP method the weighting functions are equal to one for φ_i and to the magnitude squared of the frequency-response data for θ_i . The curve fitting involves minimizing the squared error between the fitted curve and the experimental response over a specified frequency range. Once the polynomial coefficients are found, the frequency response is converted to the ordinary rational fraction polynomial form (Kelly, 1967, chapter 5):

$$H(\omega) = \frac{\sum_{k=0}^m a_k (j\omega)^k}{\sum_{k=0}^n b_k (j\omega)^k} \quad (3)$$

where $j^2 = -1$ and ω is the angular frequency.

In our application of the method, in order to facilitate the subsequent removal of the opening feature, we convert Equation 3 to the pole-zero form (e.g., Chen, 2010; Funnell et al., 2012), leading to

$$H(\omega) = g \frac{\prod_{k=1}^m (j\omega - z_k)}{\prod_{k=1}^n (j\omega - p_k)} \quad (4)$$

where g is the gain; m and n are the same as in Equations 2 and 3; and z_k and p_k are zeroes and poles, respectively, which either are real-valued or occur in complex-conjugate pairs p_k, \bar{p}_k and z_k, \bar{z}_k . The conversion is done using the `tf2zp` MATLAB function.

In this paper the quality of the fit (Q) in a frequency range between ω_a and ω_b is assessed by the normalized root-mean-square error:

$$Q = \left[1 - \frac{\|H_{po}(\omega) - H_f(\omega)\|}{\|H_{po}(\omega) - \overline{H_{po}(\omega)}\|} \right], \quad \omega_a \leq \omega \leq \omega_b \quad (5)$$

where H_f is the fitted curve, the overbar indicates the mean, and $\|\cdot\|$ is the L^2 norm. To find the appropriate number of poles and zeroes, the fitting was always done starting from the lowest order for the polynomials and only if the quality of the fit was not acceptable ($Q \leq 90\%$) was the order increased. Some of the poles and zeroes of the fitted curve are used to construct the frequency-response function H_o of the opening feature, as will be described below.

$$Q = \left[1 - \frac{\|H_{po}(\omega) - H_f(\omega)\|}{\|H_{po}(\omega) - \overline{H_{po}(\omega)}\|} \right], \quad \omega_a \leq \omega \leq \omega_b \quad (6)$$

A good fit ($Q > 90\%$) to the opening feature can be obtained with polynomials of orders $m=3$, $n=4$. Using Equation 4, the pole-zero form of H_f can then be written as

$$H_f(\omega) = g \frac{\prod_{k=1}^3 (j\omega - z_k)}{\prod_{k=1}^4 (j\omega - p_k)}. \quad (7)$$

H_f usually consists of a real zero, a complex-conjugate pair of zeroes, and two complex-conjugate pairs of poles. In some cases the fitting algorithm produces two real poles and one complex conjugate pair of poles instead of two complex-conjugate pairs of poles. For constructing H_o we keep only the poles and zeroes that are close to the fitting frequency range.

The complex-conjugate pair of zeroes, to be denoted here as (z_a, \bar{z}_a) , occurs at the central frequency of the opening feature. This is consistent with our expectation that such a sharp minimum in the response should be related to a complex-conjugate pair of zeroes at that frequency. Therefore z_a and \bar{z}_a are taken as two constituents of H_o . The pair of zeroes is always accompanied by a complex-conjugate pair of poles at a slightly higher frequency (p_a, \bar{p}_a) . Including this pair of poles ensures that the magnitude of H_o approaches 1 and that its phase approaches 0 at low and high frequencies, as required. Based on the selected poles and zeroes, H_o can be written as

$$H_o(\omega) = \frac{(j\omega - z_a)(j\omega - \bar{z}_a)}{(j\omega - p_a)(j\omega - \bar{p}_a)}. \quad (8)$$

This function generates a minimum and a maximum at the frequencies of the zero and pole respectively, as will be seen in Section 5.3.5. Once H_o is known, the ideal open-cavity response H_{io} can be found using Equation 1.

We assume that the opening feature is shared among all pars-tensa and manubrial responses and that it can be identified from any of these responses. Since other features in the manubrium responses are less prominent than those of the pars-tensa responses (e.g. Figure 5.5 vs. Figure 4.7, and similar results in this chapter), identification of the opening feature is done based on the response of a manubrial point. The identified frequency response of the opening feature is then removed from all pars-tensa and manubrium frequency responses.

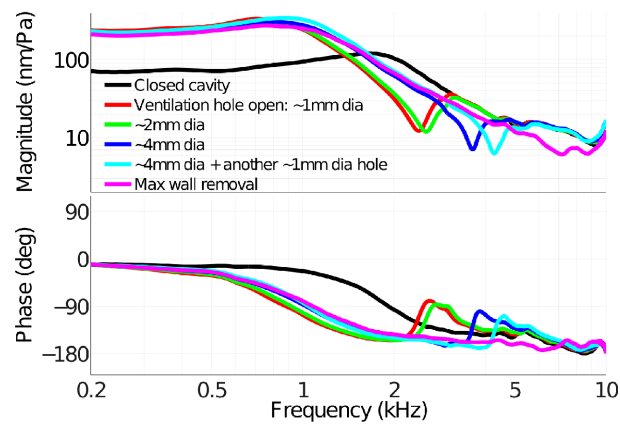


Figure 5.2: Closed and open-cavity umbo displacement responses, normalized by sound pressure, for various sizes of the cavity-wall opening in gerbil J. In this ear the pars flaccida was retracted.

5.3 Results

5.3.1 Umbo vibrations

As seen in the typical result shown in Figure 5.2 for an ear with a retracted pars flaccida, removing the ventilation tube from the cavity wall and leaving a hole of about 1 mm in diameter causes a jump in the low-frequency umbo response from about 70 nm/Pa to 230 nm/Pa. In all ears, to ensure that the observed changes were due to removal of the ventilation tube, the tube was removed and replaced a few times to check for repeatability. Progressive enlarging of the opening does not cause much further change to the response at low frequencies.

To illustrate the more complicated case of a flat pars flaccida, Figure 5.3 shows the results of progressive opening in gerbil E. As for the case with a retracted pars flaccida, there is a low-frequency magnitude jump due to opening the middle-ear cavity, from 26 to 76 nm/Pa in this ear. In the maximally open-cavity condition the pars flaccida affects the umbo response in a narrower frequency range (440 to 650 Hz, with a minimum at 490 Hz) than in the closed-cavity condition (in which it affects the umbo response from the lowest frequency up to about 900 Hz). When the middle-ear cavity is progressively opened, the minimum corresponding to the pars flaccida contribution to the umbo response becomes progressively shallower.

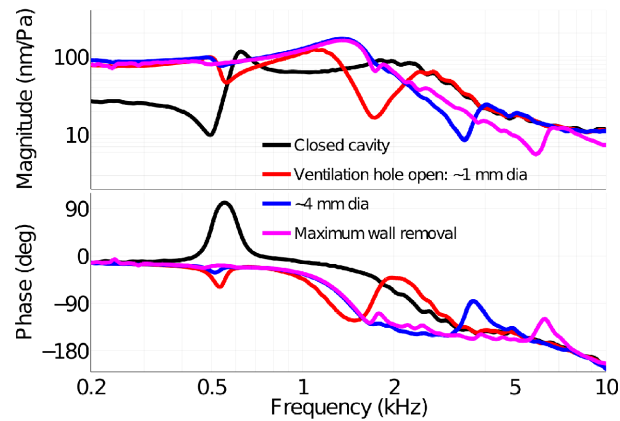


Figure 5.3: Closed and open-cavity umbo displacement responses, normalized by sound pressure, for various sizes of the cavity-wall opening in gerbil E. In this ear the pars flaccida was flat.

The effect of the size of the opening on the low-frequency (297 Hz) displacement magnitude is shown in Figure 5.4. In all ears except the right ear of gerbil G the magnitude with the smallest opening (1 mm in diameter) is from 2.1 to 3.5 times the closed-cavity magnitude. The displacement magnitude with the smallest opening in the right ear of gerbil G is only 1.3 times the closed-cavity value. In most cases, enlarging the opening further does not influence the responses much, the magnitude difference between the largest and smallest hole being less than 5% (0.4 dB). In three ears this difference is from 15 to 30% (1.2 to 2.3 dB). Data from ears with

flat and retracted pars flaccida are indicated by different symbols and it is seen that the patterns are the same.

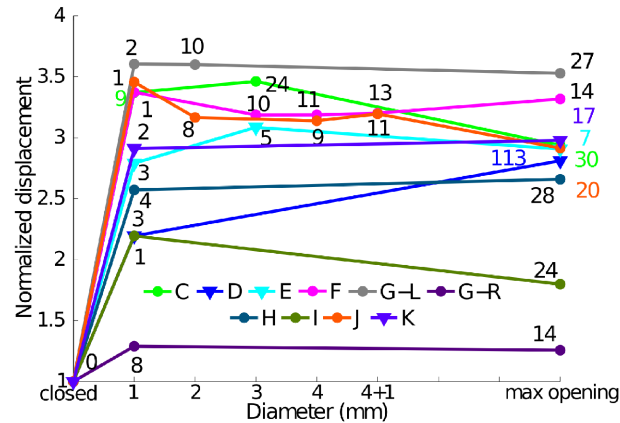


Figure 5.4: Effect of the size of the hole in the cavity wall on the low-frequency displacement magnitude of the umbo. The horizontal axis gives the hole diameter. The vertical axis gives the open-cavity umbo displacement magnitude, normalized by the closed-cavity response, at 297 Hz. Labels on the curves show the time difference to the initial closed-cavity measurement in minutes. Data from ears with a flat pars flaccida are indicated by triangles.

In Figure 5.2 (with a retracted pars flaccida) opening the middle-ear cavity causes a shift in the apparent middle-ear resonance frequency (reflected in both the magnitude and phase curves) from about 1650 Hz to 700 Hz and increases the resonance peak magnitude from 120 to 335 nm/Pa. In Figure 5.3 (with a flat pars flaccida) maximal opening of the cavity shifts the apparent middle-ear resonance from about 1600 Hz, in the closed-cavity condition, down to about 1350 Hz, and increases the resonance peak magnitude from 90 to 170 nm/Pa. In Figure 5.2 the middle-ear resonance frequency with a maximum-possible opening appears to be at 950 Hz, but with a hole 1 mm in diameter it appears to be at 700 Hz. This point can be seen more clearly in Figure 5.3, where the middle-ear resonance frequency with a maximum-possible opening appears to be at 1350 Hz, while with a hole 1 mm in diameter it appears to be at 1100 Hz.

Table 5.1: Effects of maximal opening of the middle-ear cavity on umbo displacements for three ears with flat pars flaccida, compared with one ear from Rosowski et al. (1997, 1999).

	Gerbil D		Gerbil E		Gerbil K		Rosowski et al. (1997, 1999)	
	Closed	Open	Closed	Open	Closed	Open	Closed	Open
Low-frequency magnitudes (nm/Pa)	40	120	26	76	65	190	55	160
Frequency of the minimum of the pars-flaccida contribution (Hz)	720	800	490	490	870	920	350	400
Resonance frequency (kHz)	1.8	1.4	1.6	1.4	1.8	1.1	2.1	0.9
Magnitudes at resonance (nm/Pa)	85	200	90	170	126	250	110	205

Our observations in ears with a maximally opened middle-ear cavity and a flat pars flaccida (gerbils D, E and K) are summarized in Table 5.1 along with data from Rosowski et al. (1997, 1999). (The velocity data of Rosowski et al. have been converted to displacements.) The open-cavity umbo magnitudes reported by Rosowski et al. for low frequencies and at the resonance peak are within the ranges of the values observed in this study. After opening the cavity, in all flat-pars-flaccida ears the frequency of the minimum of the pars-flaccida contribution either remained the same or shifted slightly higher (about 50 Hz) in frequency. We verified the independence of this frequency shift from drying effects by recording the displacement with the ventilation tube in its place, recording after removing the ventilation tube and then again after replacing it, and observing that the frequency shift was reversible. All ears in this study, and also the ear from Rosowski et al., show a shift of the resonance to lower frequencies and an increase in the resonance peak magnitude.

At higher frequencies the pars flaccida has little effect and the umbo responses of ears with either flat or retracted pars flaccida share similar features. As shown in Figure 5.2, an antiresonance emerges at about 2.4 kHz due to the addition of a 1 mm hole in the cavity wall. (In all ears, for a hole of 1 mm in diameter the antiresonance was observed to be between 1.7 and 2.6 kHz.) The increases in the diameter from 1 mm to 4 mm, and then the addition of another hole of 1 mm in diameter, cause the antiresonance in this ear to be at about 2.4, 2.6, 3.6 and 4.3 kHz respectively, and when the cavity wall was opened as much as possible the antiresonance was pushed beyond 7 kHz. A progressive shift of the antiresonance due to progressively enlarging the opening is also seen in Figure 5.3 for a flat pars flaccida. (In order to reduce possible temporal effects, the results in Figure 5.3 were recorded with only two intermediate stages between the closed condition and the maximum possible opening. The time between the initial and final stages was reduced from 20 min for Figure 5.2 to 7 min for Figure 5.3.)

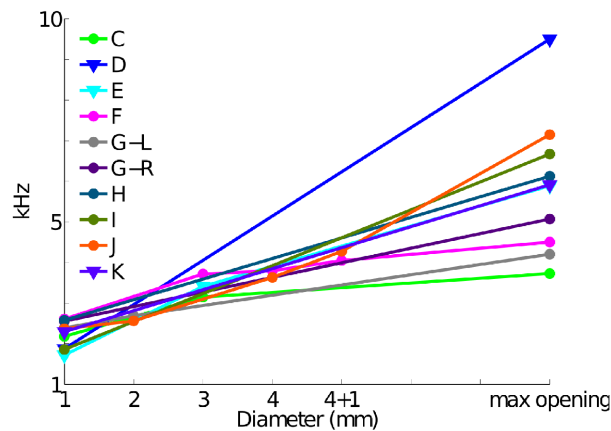


Figure 5.5: Frequency of the notch due to the acoustical effect of the opening in the cavity wall, as a function of cavity-wall hole size, for recordings made at the umbo. Data from ears with a flat pars flaccida are indicated by triangles.

Antiresonance frequencies as a function of hole size are shown for ten ears in Figure 5.5. Leaving the ventilation hole open (1 mm in diameter) caused antiresonances between 1.7 and 2.6 kHz, and enlarging the opening always caused the antiresonance to be shifted to higher

frequencies. The frequency of the antiresonance with maximal opening was quite variable, ranging from 3.7 to 9.5 kHz. Different surgical constraints (e.g., body size and weight, fixation angle of the head in the positioning device under the microscope, extent of removal of soft tissues, and position and angle of the coupler and of the dental cement used for fixing it) resulted in different sizes of opening for different animals. Data from ears with flat and retracted pars flaccida are indicated by different symbols and again it is seen that the patterns are the same. Unlike the low-frequency magnitude, which is not affected much by the extent of opening, the notch moves to higher frequencies as the opening gets bigger.

5.3.2 Pars-flaccida vibrations

We obtained reliable open-cavity pars-flaccida measurements in only one of the three animals that had a flat pars flaccida. The effect of opening the middle-ear cavity on the pars-flaccida response in that ear is illustrated in Figure 5.6. The data were collected when the cavity wall had been removed as much as possible. Opening the middle-ear cavity caused an increase in the low-frequency magnitude and a shift of the pars-flaccida resonance to a lower frequency. Above this frequency the open-cavity response approached the closed-cavity response except in the region of the antiresonance at about 6 kHz that is due to the opening of the cavity. The pars-flaccida resonance in this ear shifted from about 610 to about 490 Hz. The magnitudes at 200 Hz and at the resonance almost doubled (from 0.8 to 1.6 $\mu\text{m}/\text{Pa}$ and from 5.5 to 11.6 $\mu\text{m}/\text{Pa}$ respectively) but the ratio stayed approximately the same. In ears with a retracted pars flaccida, opening the middle-ear cavity did not change the resonance frequency of the pars flaccida, but did cause increases of 4 to 10 dB in the low-frequency displacement magnitude, comparable to the increases in the ear with a flat pars flaccida.

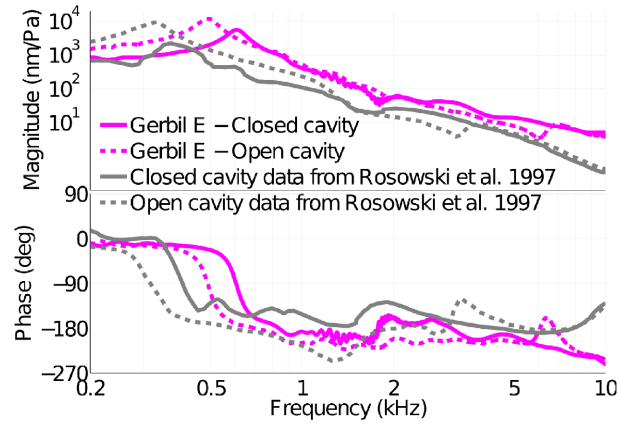


Figure 5.6: Closed-cavity and open-cavity pars-flaccida displacement responses, normalized by sound pressure, in gerbil E (magenta curves). In this ear the pars flaccida was flat and the open-cavity data were collected when the cavity wall had been removed as much as possible. For comparison, closed-cavity and open-cavity displacements of the pars flaccida of Rosowski et al. (1997), with a 1.2 mm hole in diameter in the cavity wall, are also shown (grey curves).

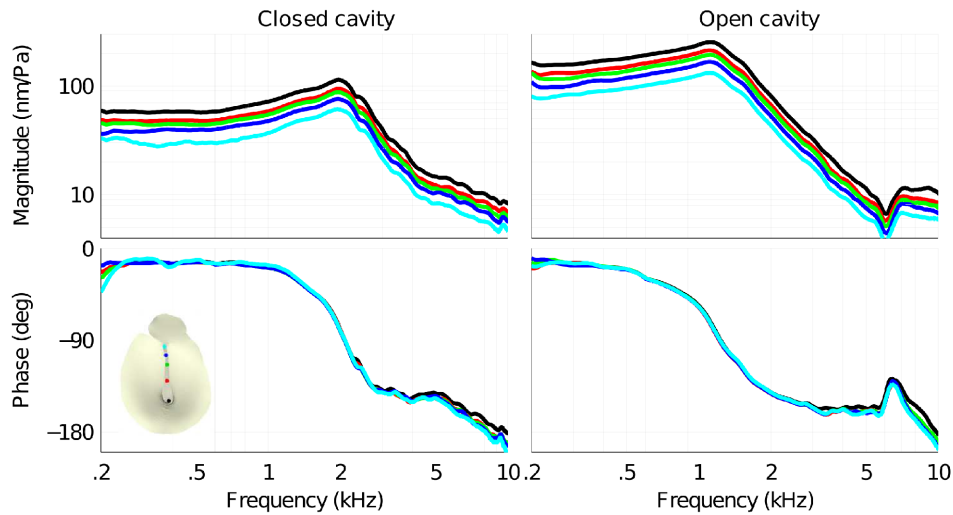


Figure 5.7: Manubrial displacement responses with closed cavity and maximally open cavity, normalized by sound pressure, in gerbil H. Response of each point along the manubrium is shown in the colour of the corresponding location in the TM-schema inset.

5.3.3 Manubrial vibrations

Typical results for vibrations along the manubrium are provided in Figure 5.7. The responses were recorded with the maximum possible removal of the cavity wall, and the antiresonance due to the opening is located at about 6 kHz. Comparison of the panels on the left (closed cavity) and

on the right (open cavity) demonstrates that opening of the middle-ear cavity affects the responses of all of the manubrial points in the same way. The closed-cavity low-frequency magnitudes for points from the short process of the malleus to the umbo vary from 30 to 57 nm/Pa in this ear, a ratio of 1.9; the open-cavity magnitudes vary from 80 to 155 nm/Pa, larger but still with a ratio of 1.9. At the resonance the magnitudes from the short process to the umbo, which were from 62 to 113 nm/Pa (a ratio of 1.8) for the closed cavity, became 131 to 253 nm/Pa (a ratio of 1.9) when the cavity was opened. Across all ears, in the closed-cavity condition the umbo-to-short-process displacement magnitude ratios were between 1.60 and 1.90 at low frequencies and between 1.64 and 1.86 at resonance. When the cavity was opened the umbo-to-short-process magnitude ratios changed by less than 8% at low frequencies and by less than 11% at resonance in all ears. As described in Chapter 4, in the closed-cavity condition, the umbo starts to have a different phase than the other manubrial points for frequencies as low as 5 kHz. After opening the cavity, the same behaviour is present in Figure 5.7 but due to the interference with the opening feature it is less noticeable between 5 and 7 kHz. The phase difference reaches about 14° at 10 kHz.

Figure 5.8 shows how opening the middle-ear cavity affects the vibration modes of the manubrium. In this figure the displacements of the points on the manubrium, normalized by the displacement of the lateral process of the malleus, are drawn for four frequencies and for seven equally spaced time instants within each cycle. This figure shows that the manubrium behaves similarly in the open-cavity and closed-cavity conditions. The displacements at the lowest frequencies (400 and 1600 Hz) are typical for an almost rigid body (say a rod) that rotates in a plane about a nearly fixed point. (In reality the manubrium vibrates in 3-D space – in the plane of the figure and in two planes perpendicular to this plane – but our 1-D observation does not

capture the displacements in the planes perpendicular to the plane of the figure. This ‘point of rotation’ is the point where the instantaneous 3-D axis of rotation crosses the plane of the figure.) Note that at 1600 Hz, the temporal order of appearance is different in the closed-cavity and open-cavity results. This is because of the shift in the middle-ear resonance after opening the cavity, which caused a significant phase change. At this frequency the phases of manubrium points are about -45° with an open cavity (Figure 5.7) and about -125° with a closed cavity (Figure 4.5). The point of rotation remains almost unchanged after opening the cavity. At 8600 and 9500 Hz, closed and open-cavity measurements show varying points of rotation and similar non-straight lines. As pointed out in Chapter 4 for the closed-cavity condition, these characteristics can be attributed to flexing in the region of the umbo, changes in the 3-D rigid-body vibration mode of the malleus, or both.

5.3.4 Pars-tensa vibrations

Generally the changes in the pars-tensa response when the middle-ear cavity is opened are similar to the changes that occur in the umbo response. These changes include the low-frequency magnitude increase, the shift of the main resonance to lower frequencies, and the appearance of an antiresonance. However, unlike the main resonance, the break-up of the pars-tensa vibration pattern still happens at about the same frequency as with a closed cavity.

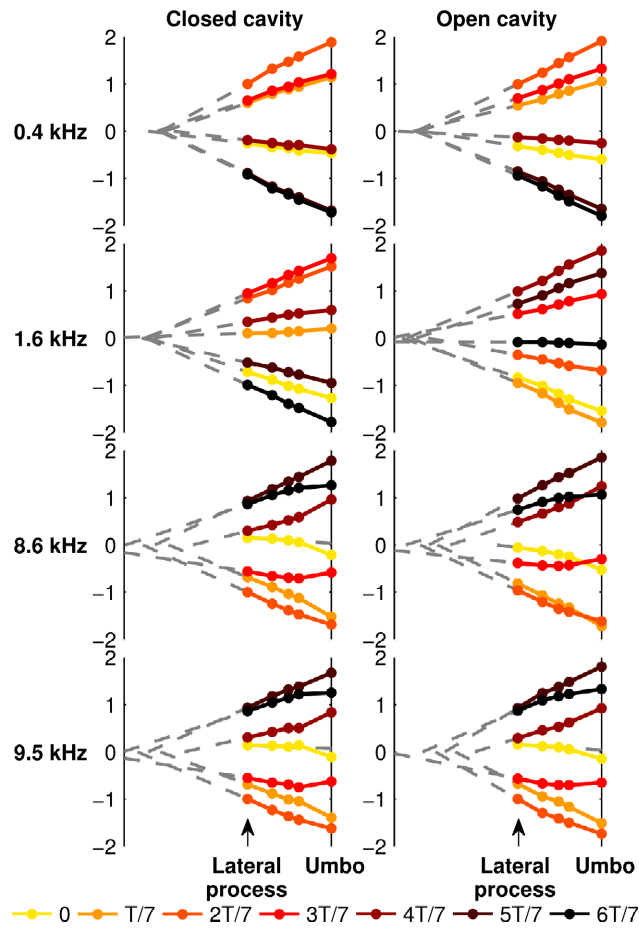


Figure 5.8: Sinusoidal motion of the manubrium at seven time instants (multiples of $T/7$) throughout the cycle in gerbil H at frequencies of 400, 1600, 8600 and 9500 Hz, with closed cavity (left) and open cavity (right).

Since the high-frequency pars-tensa response shapes are very complicated, and differences between open-cavity and closed-cavity measurements at any specific point may involve a combination of cavity and temporal effects, a detailed analysis of response features is very difficult. However, by a close point-to-point comparison between the two conditions, as shown in Figure 5.9, one can appreciate that, although the detailed shapes of the curves change somewhat, opening of the middle-ear cavity does not shift high-frequency response features to lower frequencies, as is the case with the shift of the main resonance. In this figure, each arrow follows the shift of a feature from the closed-cavity response (upper panel) to the maximally open

response (lower panel). The arrows have the same colour as the responses that they track. As an example, the grey arrow tracks a feature in the responses recorded at a point just anterior to the manubrium; this feature shifted upward by about 300 Hz. The time intervals between measuring at one point on the pars tensa in the closed-cavity condition and measuring at same point in the open-cavity condition were between 25 to 75 minutes (average: 50 minutes). The small (100–300 Hz) frequency-dependent and location-dependent shifts toward higher frequencies that are seen in Figure 5.9 may be related to drying effects. The shifts look more prominent than in previous figures because of the expanded frequency scale in this figure.

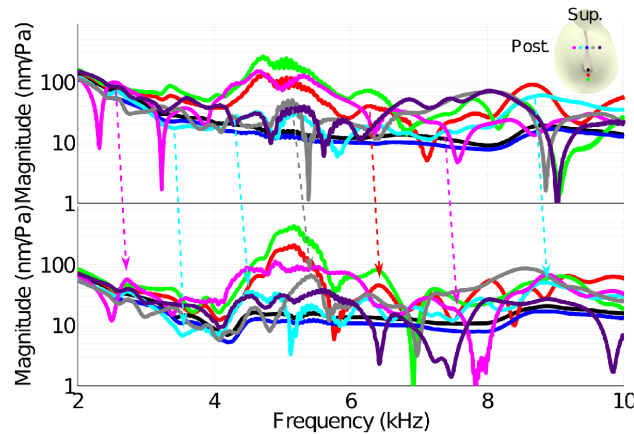


Figure 5.9: Pars-tensa displacement responses with closed cavity (top) and maximally open cavity (bottom), normalized by sound pressure, in the left ear of gerbil *G.* Each coloured arrow shows how a feature in the response at a specific location on the pars tensa changed after opening the middle-ear cavity. Each arrow has the same colour as the responses that it tracks. Each curve colour represents a pars-tensa point as marked in the TM-schema inset.

5.3.5 Estimated ideal open-cavity responses

5.3.5.1 Validation of the method

In this section we validate the method using frequency responses in which the ideal open-cavity responses are known. First, we synthesize a frequency-response function H_{po} that is designed to be similar to an umbo response when an opening exists in the cavity wall. The synthesis is done by combining 6 pairs of complex-conjugate poles and 5 pairs of complex-conjugate zeroes

(shown in Table 5.2) using Equation 4. The synthesized frequency response has the same frequency resolution as the present experimental data.

Table 5.2: Parameters used for synthesizing the frequency responses plotted in Figure 5.10. See Equations 1 & 4 for notations.

g	10^9				
Ideal open-cavity poles	$(3 \pm 13.7j) \times 10^3$	$(6 \pm 32.1j) \times 10^3$	$(7 \pm 30.1j) \times 10^3$	$(50 \pm 27j) \times 10^3$	$(3 \pm 6j) \times 10^3$
Ideal open-cavity zeroes	$(2 \pm 15j) \times 10^3$	$(8 \pm 32j) \times 10^3$	$(9 \pm 30j) \times 10^3$	$(10 \pm 25j) \times 10^3$	
p_a, \bar{p}_a	$(1.2 \pm 12j) \times 10^3$				
z_a, \bar{z}_a	$(0.4 \pm 11j) \times 10^3$				

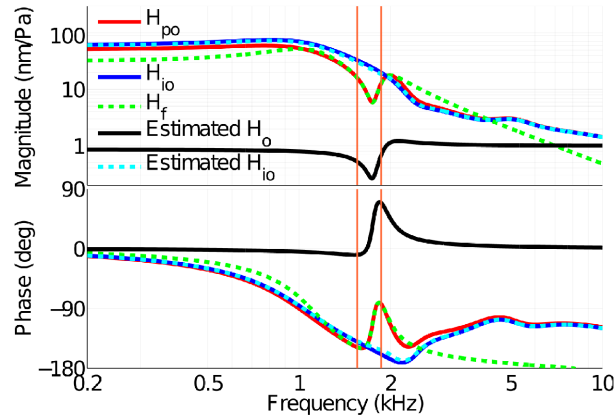


Figure 5.10: Estimation of the ideal open-cavity response H_{io} of a frequency response synthesized from poles and zeroes as described in the text, using the parameters in Table 5.2.

Figure 5.10 shows the synthesized H_{po} in red. The ideal open-cavity response H_{io} (blue) is synthesized by ignoring the known complex-conjugate pairs of poles and zeroes p_a, \bar{p}_a and z_a, \bar{z}_a that form the opening feature in the response. The method described in Section 5.2.2 was applied to the synthesized H_{po} (red) in order to estimate the ideal open-cavity response. A curve H_f was fitted to the H_{po} using only the data in a narrow frequency range around the notch,

indicated by the two vertical orange lines. H_f is shown in green and was plotted over the entire frequency range. H_f is used to define the poles and zeros within the fitting range, and the deviations from H_{po} at higher and lower frequencies are irrelevant to this analysis. The black curve is the estimated H_o obtained from H_f by keeping only the poles and zeroes that are close to the frequency range over which the fitting was done. As can be seen in this figure, the estimated ideal open-cavity response H_{io} (cyan) is essentially the same as the expected response (blue).

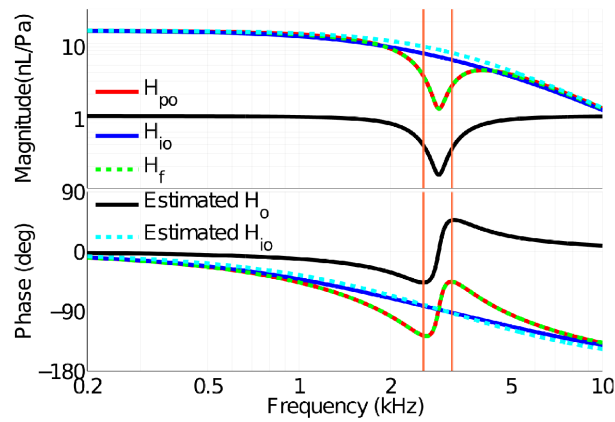


Figure 5.11: Estimation of the ideal open-cavity response H_{io} of a gerbil middle-ear circuit model (blue) suggested by Teoh et al. (1997). With a hole the circuit produces H_{po} (red). An RFP frequency response H_f (green) is fitted to the measured response in the frequency range indicated by the two parallel orange lines. The estimated H_o (solid black) was used to estimate H_{io} (cyan).

Next we evaluate our method using a circuit model suggested by (Teoh et al., 1997) for the gerbil middle-ear based on their admittance measurements. The red line in Figure 5.11 shows the response of their circuit model with an immobilized pars-flaccida and an opening in the cavity wall (their switch positions B and 3), with the parameters for their B8 right ear. We have expressed the circuit response as acoustic receptance (volume displacement/sound pressure), comparable to our normalized vibration displacement measurements. By short-circuiting the cavity and the opening in the cavity wall (their switch positions B and 2) the ideal open-cavity response is obtained (blue). To apply the method suggested in Section 5.2.2, a curve (green) was

fitted to the response in the frequency range shown by the two vertical orange lines and the ideal open-cavity response (cyan) was estimated. The estimation shows a maximum error of less than 2 dB in magnitude and 6° in phase.

5.3.5.2 Umbo response

Figure 5.12 illustrates the application of our method for correcting for the effect of opening the middle-ear cavity, in this case for the umbo response of gerbil J with the smallest opening in the cavity wall (in red and the same as Figure 5.2). The centre frequency of the opening feature is at 2.4 kHz. The green line shows H_f (Equation 6), plotted over the entire frequency range but obtained from the fit over the narrow frequency range shown by two parallel vertical orange lines (2.27 to 2.5 kHz). Figure 5.13 depicts the poles and zeroes of H_f . The poles and zeroes shown in green are the ones that are used in constructing H_o and are marked in Figure 5.12 as well. The other poles and zeroes, shown in red in Figure 5.13, are far from the frequency range over which the fitting was performed. The blue curve shows the ideal open-cavity response H_{io} estimated using Equation 1.

In Equation 6, the complex-conjugate zeroes are mainly responsible for providing the sharp minimum. As designed, the magnitude of H_o (black curve in Figure 5.12) tends to one and its phase tends to zero at both low and high frequencies. If only the complex-conjugate zeroes were included in the definition of H_o , the high-frequency part of the magnitude of H_o would grow with frequency (see the dashed line in Figure 5.12). The complex-conjugate poles (p_a, \bar{p}_a) are responsible for making the high-frequency magnitude approach a value of one and for making both the low-frequency phase and the high-frequency phase approach zero.

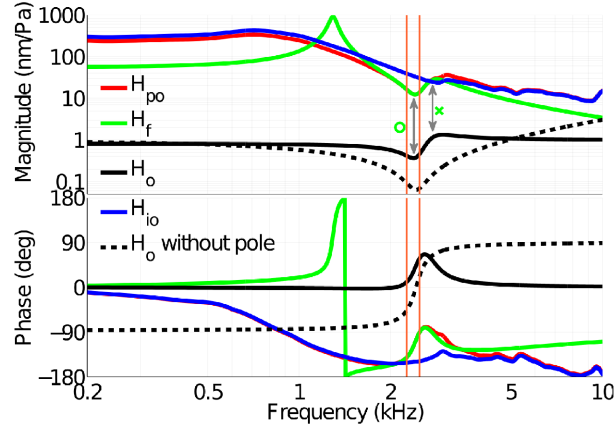


Figure 5.12: Estimation of the ideal open-cavity umbo response H_{io} (blue) based on the measurement with the smallest size of cavity-wall opening H_{po} (red) in gerbil J. An RFP frequency response H_f (green) is fitted to the measured response in the frequency range indicated by the two parallel orange lines. From this fitted frequency response, the complex conjugate pair of zeroes z_a, \bar{z}_a at the central frequency of the opening feature (marked with an arrow and \circ) and the complex conjugate pair of poles p_a, \bar{p}_a at a slightly higher frequency (marked with an arrow and \times) were taken to form H_o (solid black). The dashed black line is what would result if H_o included only the complex conjugate pair of zeroes.

Figure 5.14 shows the p_a and z_a calculated for the umbo responses with a 1 mm opening in the cavity wall, for all ears. This figure shows only the poles and zeroes with positive frequencies; their negative-frequency counterparts (complex conjugates \bar{p}_a, \bar{z}_a) can be imagined by mirroring the figure around the real axis (see Figure 5.13). The imaginary parts of the complex values of the zeroes (1.7 to 2.6 kHz) are very similar to the antiresonance frequencies shown in Figure 5.5. In that figure, the frequency of an antiresonance was taken to be the frequency at which the notch has its minimum. The differences between the antiresonance frequencies estimated using the two methods are less than 2%. The real parts of the complex values are related to the damping of the system. The real parts of the zeroes from all ears are located within a rather narrow band of about 0.1 kHz. This shows that the ears exhibited similar damping characteristics at frequencies in the vicinity of the antiresonance.

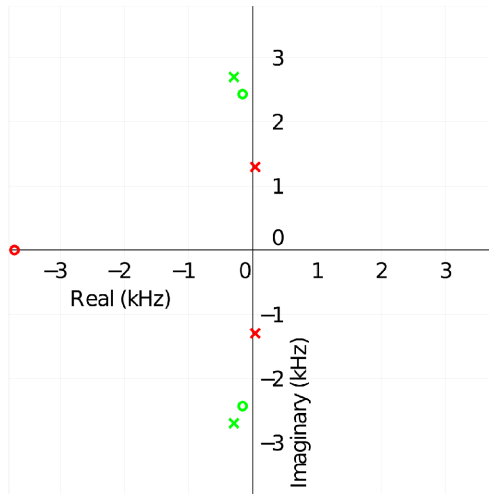


Figure 5.13: Pole-zero diagram of the fitted RFP frequency response H_f of Figure 5.12. Each \circ corresponds to a zero and each \times corresponds to a pole. The poles and zeroes shown in green are the ones used in the definition of H_o , while the ones shown in red are excluded.

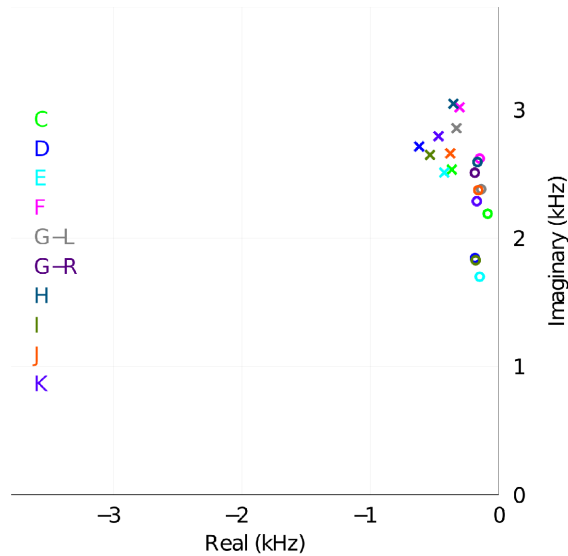


Figure 5.14: Pole-zero diagram of the positive-frequency complex poles (p_a) and zeroes (z_a) for the first size of opening (1 mm) in the cavity wall for all ears. Each \circ corresponds to a zero and each \times corresponds to a pole.

5.3.5.3 Sensitivity to the fitting range

To assess the effects of the frequency range over which the fitting is done, in Figure 5.15 we have applied the method to the same data as presented in Figure 5.12 but now with 5 different fitting frequency ranges, with widths of 155 to 1250 Hz (20 to 160 FFT lines), centred at the frequency of the opening feature. Each frequency range is indicated by a pair of vertical lines of the same colour, the narrowest range being shown in red. The estimated ideal open-cavity responses are shown in the same colours as their respective frequency ranges. Except for the narrowest frequency range (red), the estimated responses are very similar. At mid and high frequencies, the umbo response displays irregularities that have bandwidths of a few hundred Hertz, magnitude changes of a few decibels and phase changes of a few tens of degrees, as discussed in Chapter 4. The second and third frequency ranges (green and blue lines) do not include major irregularities. Between these two ranges, the maximum difference is 0.48 dB and the average difference is 0.04 dB over the entire frequency spectrum. For the first three ranges $Q > 99\%$ but as the frequency range expands it includes more of the irregularities in the umbo frequency response so the quality of the fit decreases ($Q = 97.9\%$ and 94.4% for the two widest ranges, magenta and grey respectively) and the estimated ideal open-cavity responses become slightly different: the maximum differences between the frequency responses for the second range and those for the two widest ranges, magenta and grey, are 1.24 and 2.85 dB respectively, and the average differences are 0.11 and 0.31 dB respectively.

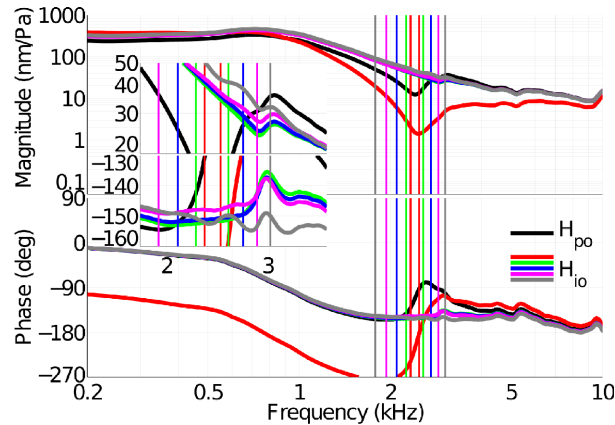


Figure 5.15: Effect of the range of fitting on the estimation of the ideal open-cavity H_{io} and opening H_o frequency responses. The measured response in gerbil J with partially open cavity H_{po} (1 mm hole) is shown in black. The estimated ideal open-cavity response H_{io} based on the narrowest range (155 Hz, indicated by two parallel vertical red lines) is shown in red. The results for four other ranges (up to 1250 Hz, each indicated by two parallel vertical lines of the same colour) are also shown. The estimated ideal open-cavity response H_{io} corresponding to each range is shown in the same colour as the pair of vertical lines. The insets show a zoomed-in view of the responses in the frequency range of 1.8 to 3.8 kHz.

5.3.5.4 Effect of enlarging the opening

The ideal open-cavity responses estimated from measurements in the same ear with different sizes of opening should theoretically be the same. Figure 5.16 explores this hypothesis by applying the method on the umbo measurements of ear F with five sizes of opening, from 1 mm diameter to the maximal opening in the cavity wall. The solid curves represent the measured responses and the dashed curves represent the estimated ideal open-cavity responses. At frequencies below the middle-ear resonance, the estimated ideal open-cavity response based on the smallest opening (red dashed curve) shows differences from the others of up to about 4 dB. At higher frequencies, the estimated ideal open-cavity responses obtained for different opening sizes are within 2 dB, with the greatest differences occurring at mid-frequencies. Part of the differences seen between ideal open-cavity estimates based on different opening sizes might be due to drying effects.

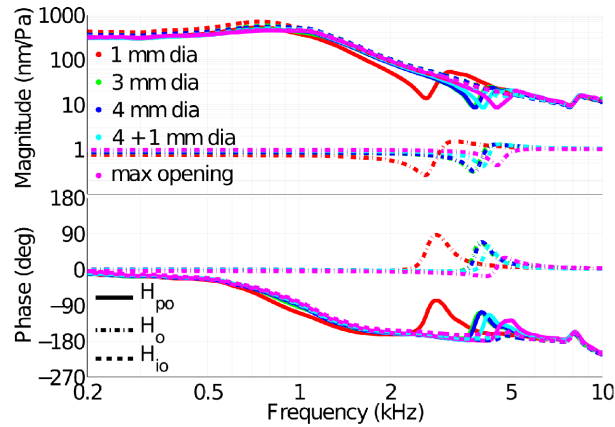


Figure 5.16: Effect of the size of opening on the estimated ideal open-cavity frequency response H_{io} in gerbil F. All responses corresponding to each opening size are shown in the same colour. The measured H_{po} and estimated H_{io} responses are indicated by solid and dashed lines respectively. H_o responses are shown with dash-dotted lines.

Figure 5.17 illustrates an example of the application of the method to the more complex responses resulting from an ear with a flat pars flaccida. The measured displacements (solid curves) in this figure are identical to those presented in Figure 5.3. Compared with the estimated ideal open-cavity responses calculated for ears in which the pars flaccida was retracted, bigger magnitude differences can be seen here at low frequencies: at frequencies below the middle-ear resonance the ideal open-cavity responses estimated based on the smallest opening (red dashed curve) differ by up to 5 dB from those based on the larger openings. At higher frequencies the differences are similar to those for ears with a retracted pars-flaccida (maximum 2 dB at mid-frequencies).

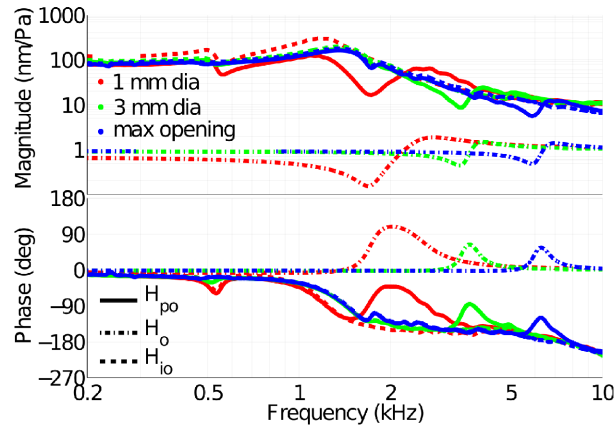


Figure 5.17: Estimation of ideal open-cavity response H_{io} in an ear with a flat pars flaccida (gerbil E) and different sizes of the opening.

5.3.5.5 Manubrium response

In Section 5.3.3 we presented responses with a partially open cavity at different positions of the manubrium and pointed out that from 5 to 7 kHz the opening feature interferes with the responses. To remove the effects of the cavity opening on the data shown in Figure 5.7 (gerbil H), the method described in Section 5.2.2 was applied and all manubrial responses were corrected with the same H_o , obtained by fitting to the response at the middle of the manubrium (green curve in Figure 5.7) in the range of 5.6 to 6.6 kHz. The results in Figure 5.18 are similar for the different manubrial points, except that a phase difference between the umbo and the rest of the manubrium starts to become evident above 5 kHz, as in the closed-cavity case.

5.3.5.6 Pars-tensa response

In Figure 5.19 the responses measured with a maximal cavity opening (solid curves) and the estimated ideal open-cavity responses (dashed curves) are presented for two points on the pars tensa and for a reference point on the manubrium, for gerbil H. As can be seen in Figure 5.19, and as discussed in Section 5.2.2, a plethora of features in the pars-tensa responses makes the direct identification of the notch from those responses very difficult if not impossible, so the same mid-manubrium-based H_o used in the previous section was applied to correct the pars-tensa

responses. The ideal open-cavity estimates exhibit response patterns that differ from the measured data by up to about 4.8 dB and 30° in the frequency of 5.5 to 8.8 kHz, the neighbourhood of the notch. These differences are much bigger than the changes seen when varying the frequency range of fitting (as discussed in Section 5.3.5.3). They presumably reflect the actual effects on the pars tensa due to the antiresonance at 6 kHz that results from the opening in the cavity wall.

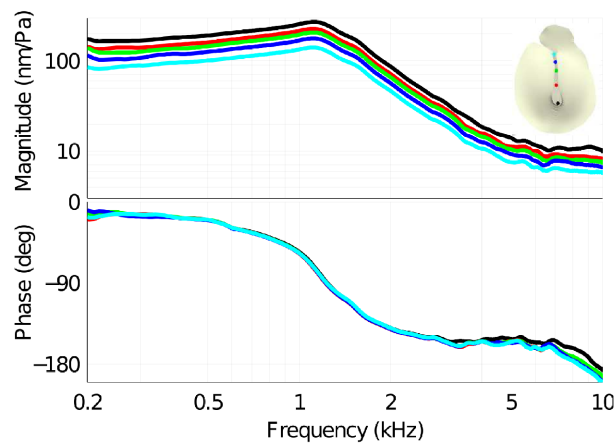


Figure 5.18: Estimated ideal open-cavity manubrial response H_{io} in gerbil H , corresponding to measurements shown in Figure 6, using an H_o identified from the mid-manubrium response.

5.4 Discussion

5.4.1 Effects of opening the middle-ear cavity on manubrium and TM vibrations

Measurements on the manubrium, pars tensa and pars flaccida with an open cavity showed increases in the low-frequency magnitudes and also shifted the middle-ear and pars-flaccida resonance frequencies to lower frequencies. These shifts happen because of the reduction in the stiffness of the system at low frequencies due to the opening of the cavity (cf. model of Ravicz et al., 1992).

In impedance measurements, Ravicz et al. (1992) observed an antiresonance peak at about 2 to 3 kHz in different ears with a hole of about 1 mm in diameter, similar to our range of 1.7 to 2.6 kHz. In admittance measurements, Teoh et al. (1997) observed an antiresonance at about 3 kHz with a hole of about 1.2 mm in diameter. Rosowski et al. (1997, 1999), also with a 1.2 mm hole, reported a hole antiresonance at about 3.1 kHz in LDV measurements. The frequencies of the antiresonance with holes of about 1.2 mm in diameter (Teoh et al., 1997; Rosowski et al., 1997, 1999) was somewhat higher than the highest antiresonance frequency shown in Figure 5.5 for a hole of 1 mm in diameter, which is consistent with the increase that we observe in the antiresonance frequency when the opening is progressively enlarged. Ravicz et al. (1992) and Teoh et al. (1997) reported a frequency of 6 kHz for the antiresonance with maximal opening, which is within our range of 3.7 to 9.5 kHz. No previous measurements for the intermediate openings are available.

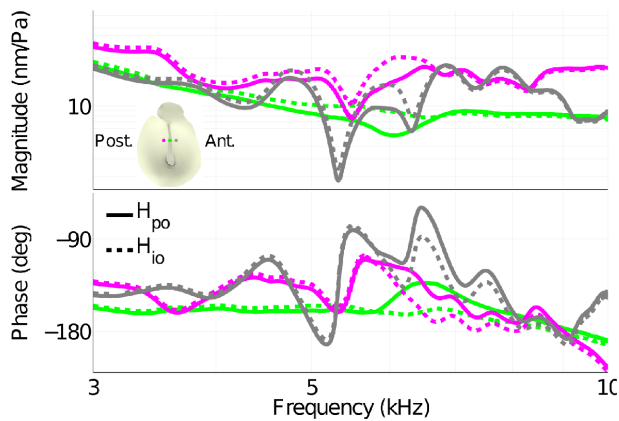


Figure 5.19: Estimated ideal open-cavity pars-tensa responses H_{io} in gerbil H , using an H_o identified from the mid-manubrium response.

The pars-flaccida vibration data reported by Rosowski et al. (1997, Figure 6A) are also included in Figure 5.6 and show the same trends of a low-frequency increase, a shift in the resonance frequency and a lack of change at higher frequencies except for the antiresonance (in their case at about 3.2 kHz).

In the present study we have demonstrated that, in ears with a flat pars flaccida, when the middle-ear cavity is progressively opened the minimum corresponding to the pars-flaccida contribution to the umbo response becomes progressively shallower. We have also demonstrated that the main increase in the low-frequency response magnitude happens upon making the smallest (1-mm) hole in the cavity wall, and that further progressive enlarging of the opening has little or no effect on the low-frequency magnitude. The latter observation is particularly important for modelling and experimental studies that are concerned with static or low-frequency behaviour of the system. In this case two ears (from an experiment and a model or from two experiments) with open cavities can be safely compared independent of the extent of the openings. For instance, static or low-frequency results from a model without a cavity can be safely compared with experimental results from an ear with a very small hole in its cavity wall.

In experimental data not reported here, we have observed that, when the main resonance frequency is shifted to a higher frequency because of drying, the break-up frequency is also shifted to a higher frequency. In contrast, opening of the cavity shifts the main resonance frequency to lower frequencies but does not shift the breakup frequency, nor the response features above this frequency, to lower frequencies. Consistent with this observation, Ishihara (1989) reported that the break-up frequency of the human TM ‘was not affected much’ by the volume of the middle-ear cavity.

The opening also causes the addition of an antiresonance to the response (Teoh et al., 1997). In contrast to the almost constant low-frequency magnitude for different hole sizes, progressive enlarging of the cavity-wall opening progressively shifts the related antiresonance to higher frequencies. We have shown (Section 5.3.1) for different sizes of opening how the resulting antiresonance interferes with the frequency-response shape. For example, the maximum related

to the middle-ear resonance appears at a different frequency with different sizes of opening. This is presumably because the frequency-response curve is deflected downward in the vicinity of the antiresonance (e.g. at 2.4 and 1.8 kHz in Figures 5.2 and 5.3 respectively) so the main middle-ear resonance frequency appears to be located at a lower frequency (700 instead of 950 Hz and 1100 instead of 1350 Hz in Figures 5.2 and 5.3 respectively). When the opening is large enough (diameters of 4 mm and more), the hole antiresonance moves far beyond the region of the maximum of the magnitude and its effect on this region becomes very small. In this case the maximum has a higher magnitude than when the hole is smaller.

The different effects of different opening sizes can cause errors of interpretation when the results of one experiment are compared with those of another experiment with a different size of opening. Elimination of such artefacts may be especially important for the pars-tensa: because of the complexity of its responses, more features can be obscured in the frequency neighbourhood of the antiresonance. The ideal open-cavity condition is also important for validating mathematical models of a simplified system (without the cavity) as a step toward making a comprehensive model of the middle-ear which also includes the cavity.

5.4.2 Estimation of ideal open-cavity responses

The notch caused by opening the cavity obscures pars-tensa and manubrium responses in its frequency neighbourhood. To avoid this problem, either the notch should be at a frequency beyond the frequency range of interest or it should be corrected for. Moving the notch out of the frequency range of interest is not always possible, especially when responses at higher frequencies are of interest. We have presented here a method for correcting for the opening feature by estimating ideal open-cavity responses based on measurements collected with partial opening in the cavity. In this method a frequency response is fitted to the experimental response

in a frequency range that includes the opening feature. The frequency response corresponding to the opening feature is then constructed and utilized to estimate the ideal open-cavity response.

We have experimented with a variety of continuous-time and discrete-time methods to estimate the transfer function of the opening feature. For continuous-time transfer-function estimation, in addition to the RFP method described here, we tried the prediction-error minimization (PEM) approach with parameter initialization using either output-error (OE) or state-space algorithms, followed by nonlinear least-squares search-based updates to minimize a weighted prediction error norm. For discrete-time transfer-function estimation, we tried autoregressive with exogenous input (ARX), instrumental variable (IV), OE and state-space methods. In discrete-time form we also experimented with PEM based on the OE algorithm and nonlinear least-squares search-based updates. Details about all these non-RFP methods can be found in Ljung (1999) and all of them are available in the MATLAB System Identification Toolbox. With other continuous-time transfer-function methods the quality of the fit was always much inferior ($10\% < Q < 66\%$) to RFP ($Q > 94\%$). With some of the discrete-time methods (especially OE and the discrete-time OE-based PEM) we have reached the same quality of fit as with RFP. However, because our method is intended for continuous-time frequency responses the identified discrete-time transfer function would need to be converted to continuous-time form. Discrete-to-continuous conversion with the zero-pole matching method (Franklin, 1990) is not always possible if there are identified poles or zeroes at the origin. If other conversion methods are used, the control on poles and zeroes in the conversion process is lost and, for example, an additional zero may be present in the converted continuous-time form, or the model order may be changed. We did not try, however, to perform the complete process in the discrete-time domain instead of the continuous-time domain.

We have validated our RFP-based method against a synthesized frequency response and against a frequency response calculated using a middle-ear circuit model, and have studied the robustness of the method in handling different opening sizes various frequency ranges for the fitting and also. The analysis showed that the method should not be used with fitting ranges of less than about 155 Hz. If the range is too narrow the required complex-conjugate pair of poles (at a slightly higher frequency than the centre frequency of the opening feature) is not captured correctly and therefore a correct response shape does not form. The method was found to be robust for wider fitting frequency ranges even in the presence of other response features within the selected fitting range.

5.4.3 Implications of ideal open-cavity responses

Although the ideal open-cavity responses estimated based on different sizes of opening are very similar, they do show some differences (Section 5.3.5.4). At low frequencies, estimates based on the smallest opening size exhibit larger magnitudes than the ones based on other opening sizes. These differences are larger in ears with a flat pars flaccida (Figure 5.17) than in ears with a retracted pars flaccida (Figure 5.16). The differences are probably due to a residual influence of the cavity on the low-frequency acoustical coupling between the pars tensa and the pars flaccida. This coupling is more pronounced with the smallest opening and in ears with a flat pars flaccida, as seen in Section 5.3.1. If it is desired to avoid this low-frequency artefact, the opening in the cavity wall should be made at least about 4 mm in diameter before attempting to estimate ideal open-cavity responses.

The method was applied to pars-tensa responses measured in ears with partial cavity opening. The method corrects the responses in the opening-feature frequency neighbourhood. We have demonstrated that, compared with the measured responses with partial cavity opening, in the

ideal open-cavity responses both the frequencies and excursions of the local minima and maxima are different.

The estimated ideal open-cavity results also have practical value because they are better suited than the directly measured data for comparison with results from middle-ear finite-element models with no cavity. Such models are a valuable intermediate step in refining methods and parameters to be used later in more complete models.

5.5 Acknowledgements

The authors would like to thank Ms. Shruti Nambiar and Ms. Zinan He for their contributions to the development of the surgical and measurement techniques; Dr. Jim Gourdon for advice on the anaesthesia procedure; and Dr. Dan Citra for his help dealing with the animals. This work was supported in part by the Canadian Institutes of Health Research, the Fonds de recherche en santé du Québec, the Natural Sciences and Engineering Research Council (Canada), the Montréal Children's Hospital Research Institute, the McGill University Health Centre Research Institute and the Research Fund of Flanders (Belgium).

6 Finite-element modelling of the response of the gerbil middle ear to sound

Submitted to the *Journal of the Association for Research in Otolaryngology*,
2014 May.

Preface

In Chapters 4 and 5 we presented our experimental vibration measurements on the tympanic membrane of the gerbil. This chapter presents a finite-element model of the gerbil middle ear. The presented model is then validated against the experimental observations described in Chapters 4 and 5. In Chapter 5 a theoretical method was presented to estimate vibration responses of the tympanic membrane when no middle-ear cavity is present, based on responses measured with a partial opening in the cavity wall. In the model-validation process, these ideal open-cavity estimates are used to facilitate comparison with the experimental results.

Abstract

A finite-element model of the gerbil middle ear is presented in this study. Responses from the model, using a set of baseline parameters based primarily on *a priori* estimates from the literature, were validated against our multi-point vibrometry measurements and against measurements from other groups. This was done by investigating the similarity of certain features in the experimental responses with corresponding ones in the model responses, as opposed to simply computing frequency-by-frequency differences between experimental and model responses. The umbo response of the model is within the range of variability seen in the experimental data in terms of the low-frequency magnitude and phase, the main resonance frequency and magnitude, and the roll-off slope and the irregularities in the response above the resonance frequency, but is somewhat high for frequencies above the resonance frequency. At low frequencies the ossicular axis of rotation of the model appears to correspond to the anatomical axis but the behaviour is more complex at high frequencies. The behaviour of the pars tensa in the model is similar to what is observed experimentally in terms of magnitudes, phases, the break-up frequency of the spatial vibration pattern, and the bandwidths of the high-frequency response features. A sensitivity analysis showed that the parameters that have the strongest effects on the model results are the Young's modulus, thickness and density of the pars tensa; the Young's modulus of the stapedial annular ligament; the Young's modulus and density of the malleus; and the Poisson's ratios of the incudomalleolar and incudostapedial joints. The large effects of the Poisson's ratios suggest that more sophisticated models of the joints would be beneficial.

6.1 Introduction

Models of the middle ear have proven to be important for understanding its function and for predicting its response to pathological changes, diagnostic tests and treatment methods, and they are indispensable for developing surgical simulators. Different approaches to modelling the middle ear were recently reviewed by Funnell et al. (2012, 2013). In finite-element (FE) models that are based on the detailed anatomical and biomechanical properties of the middle-ear structures, the model parameters are fundamentally connected to the physiological characteristics of the system. With increasing accessibility of FE preprocessing programmes and solvers, this method has been increasingly applied in modelling of the middle ear. Most middle-ear FE models have been developed for the human middle ear, starting with Wada et al. (1992), but higher-quality experimental data are available for validating the models that have been developed for other species, including cat (e.g., Funnell & Laszlo, 1978; Ladak & Funnell, 1996; Tuck-Lee et al., 2008), rabbit (Aernouts et al., 2010) and rat (Hesabgar et al., 2010; Ghadarghadar et al., 2013). Gerbils are widely used in auditory research and therefore a wealth of knowledge is available concerning their auditory system (see Chapter 4 for some references). The middle ear of this species has been the subject of a number of FE studies. Funnell et al. (1999, 2000) presented some preliminary model results for low-frequencies and the model was later refined by Elkhouri et al. (2006). Material characterization was done using FE modelling in conjunction with pressurization by Decraemer et al. (2010) for the pars flaccida, and in conjunction with indentation data by Aernouts and Dirckx (2011, 2012) for the pars flaccida and pars tensa respectively. Decraemer et al. (2011b) used FE modelling to study the effects of tympanic-membrane (TM) geometrical asymmetry on ossicle-motion asymmetry in response to positive and negative static pressures. Maftoon et al. (2011) presented some preliminary

modelling results on the response of the gerbil middle ear at audio frequencies. The latter study is extended by the present work.

In this study simulated responses are compared with our multi-point vibrometry measurements (Chapters 4 and 5) and with measurements from other groups. This was done by investigating the similarity of certain features in the experimental responses with corresponding ones in the model responses, as opposed to simply computing frequency-by-frequency differences between experimental and model responses. Our model does not include the tympanic cavity. We have previously proposed a method for estimating ideal open-cavity responses from measurements with partial openings in the cavity wall (Chapter 5). In this paper we use that method to compare our no-cavity modelling results with experimental results. The results of the simulations are compared with the experimental measurements in the frequency domain and, as in our experimental studies, we focus on the frequency range between 0.2 and 10 kHz.

6.2 Materials and methods

6.2.1 Geometry, model components and mesh

The FE model used in this study is shown in Figure 6.1. The 3D geometry of the model is a refinement of the one used by Decraemer et al. (2011b) and is based on segmentation of a microCT dataset, supplemented by histological images. The posterior incudal ligament was based on the orthogonal-plane fluorescence optical sectioning (OPFOS) data of Buytaert et al. (2011). The model includes the pars tensa, pars flaccida, malleus, incus, stapes, posterior incudal ligament, stapedial annular ligament, incudomalleal joint and incudostapedial joint, as well as a representation of the cochlear load. In-house FE preprocessing software¹, Fie, Tr3 and Fad, were used to perform image segmentation and surface triangulation and to prepare surface meshes for

¹ <http://audilab.bme.mcgill.ca/AudiLab/sw/>

volume mesh generation using the open-source software Gmsh (Geuzaine & Remacle, 2009). The FE solver was Code_Aster² version 11.3, which is also open-source. Simulations were done on the supercomputer Guillimin of McGill University. Guillimin is a cluster of Intel Westmere EP Xeon X5650 and Intel Sandy Bridge EP E5-2670 processors running under CentOS 6 Linux distribution. The baseline study was performed using one processor and 8 GB of RAM. Sensitivity analyses were typically done using 6 processors, each using 20 GB of RAM, in a Code_Aster parametric-study session. This launched 6 instances of the simulation in parallel. Each simulation for one set of parameters takes about an hour.

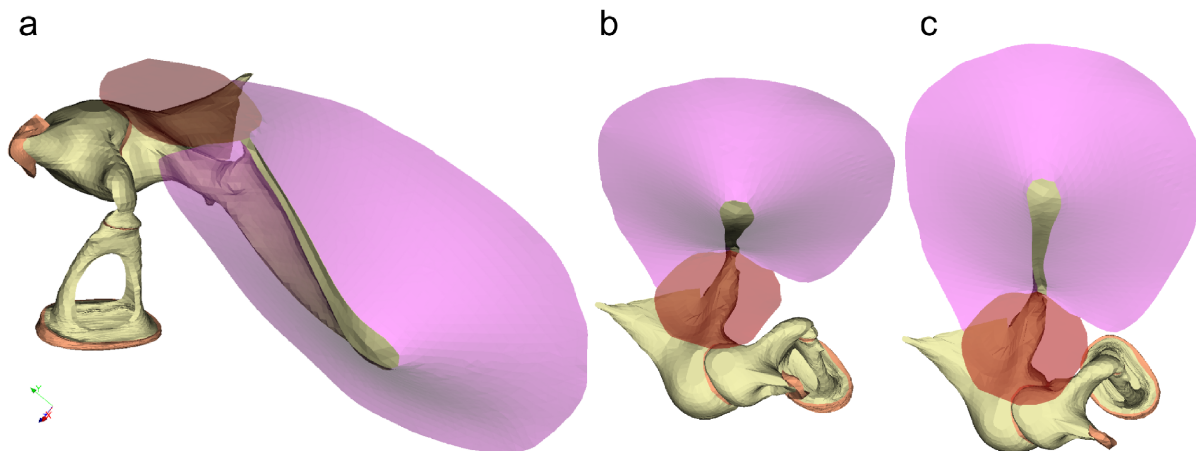


Figure 6.1: Reconstructed 3D model of gerbil middle ear used in finite-element analysis. (a) A posterolateral view of all components of the model; (b) and (c) two views of the tympanic membrane as seen from extreme angles through the ear canal in our experimental measurements (Chapters 4 and 5). The TM is shown as semi-transparent.

The TM was modelled using seven-node second-order *TRIA7 COQUE_3D* shell elements. In this element type, each node possesses three translational and three rotational degrees of freedom, except for the centre node which possesses only three rotational degrees of freedom. Kuypers et al. (2005) reported thicknesses along four lines across the pars tensa in the gerbil. An interpolation algorithm (which will be described elsewhere) has been developed to reconstruct a

² <http://code-aster.org/>

thickness map for the entire pars-tensa surface from their measurements. The thickness distribution of the pars flaccida in Kuypers et al. (2005) data is irregular. For simplicity, we used a constant thickness of 23.5 μm (their reported mean) for the pars flaccida in our model.

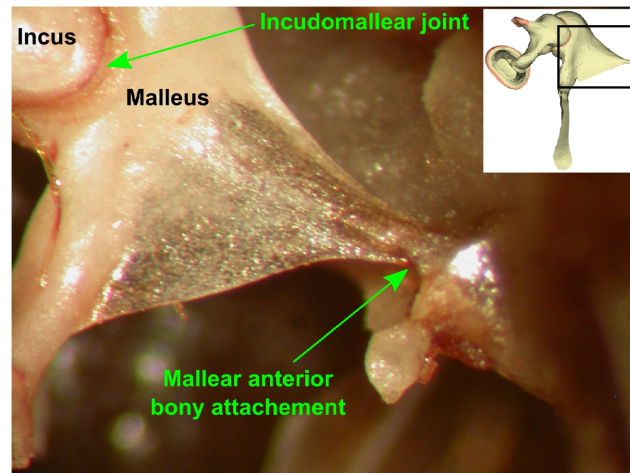


Figure 6.2: Anterior mallear bony attachment in gerbil ear. The inset in the top right corner shows a view of the model in the orientation as seen in the photograph. The black frame in the inset shows the frame of the image. Unlike the case in human, the anterior process of the malleus is long and is attached directly to the bony cavity wall by a thin bony attachment (Rosowski et al., 1999).

Ten-node second-order *TETRA10* 3D tetrahedral solid elements were used to model the ossicular chain. Each node of this element type possesses three translational degrees of freedom and no rotational degrees of freedom. In order to ensure correct coupling between the shell elements of the TM and the 3D solid elements of the malleus, the pars tensa was continued over the lateral surface of the manubrium and nodes were shared between the two structures³. As described by Rosowski et al. (1999), in the gerbil the malleus is connected to the cavity anteriorly by a bony attachment (Figure 6.2)⁴.

3 In the previous gerbil model from our group (Elkhouri et al., 2006), based on magnetic-resonance-microscopy images, the inferior part of the manubrium was narrower than it should have been.

4 Instead of this bony attachment, Elkhouri et al. (2006) used a ligament to connect the malleus to the cavity wall.

The ossicular ligaments and joints were modelled using ten-node second-order *TETRA10* *3D_INCO* tetrahedral incompressible solid elements with a 3-field (displacement, pressure and volumetric strain) mixed formulation. Like the elements used for the ossicles, these elements have only translational degrees of freedom. The posterior incudal ligament surrounds the posterior end of the short process of the incus, as seen in the histological image shown in Figure 6.3 and as reported by Buytaert et al. (2011) using OPFOS⁵. For simplicity, the joints were assumed to be elastic solids and details of the synovial fluid, cartilage and joint capsule were not modelled.

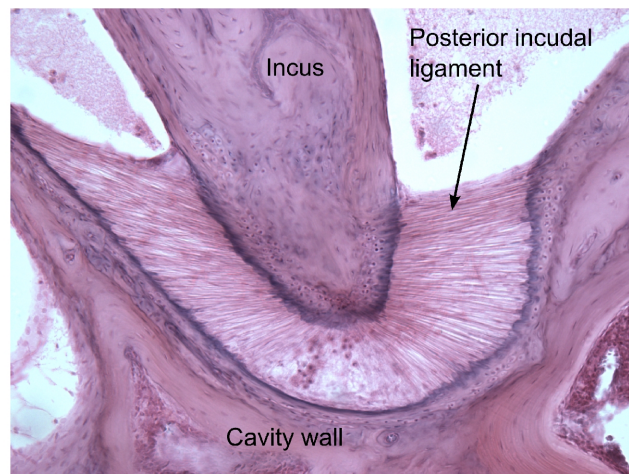


Figure 6.3: Histology of posterior incudal ligament in right ear of gerbil (courtesy of Clarinda Northrop). The posterior incudal ligament in the gerbil surrounds the posterior end of the short process of the incus.

The cochlear load was modelled using four dashpots parallel to the piston-motion direction and connected to the stapes footplate (two at the ends of the long axis and two at the ends of the short axis).

⁵ In the model by Elkhouri et al. (2006) this ligament was considered to be composed of two bundles.

6.2.2 Boundary conditions

The pars tensa was considered to be fully clamped around its periphery (i.e., all of the six degrees of freedom were set to zero). The pars flaccida was considered to be simply supported around its periphery (i.e., the 3 translational degrees of freedom were set to zero but the rotational degrees of freedom were not), as suggested by Gea et al. (2009). It shared nodes (and all of the 6 degrees of freedom of shell elements) with the pars tensa at their interface. For the ligaments and the anterior malleolar bony attachment, all three degrees of freedom were set to zero for the nodes where they would be attached to the cavity wall, which was not explicitly included in the model⁶.

6.2.3 Calculation of frequency responses

6.2.3.1 Procedure

Frequency responses were calculated following the procedure suggested by Funnell et al. (1987), by applying a unit-step sound pressure of 1 Pa on the TM surface and performing transient FE analyses. The direct implicit time-integration scheme of Newmark (1959) was employed. The two parameters β and γ of this method were set to 0.25 and 0.5 respectively, to provide an unconditionally stable solution. Simulations were continued for 50 ms after the onset of the unit-step sound-pressure function. Frequency responses were obtained by differentiating the step responses and then computing the fast Fourier transforms of the resulting impulse responses. Since the main purpose of this paper is to validate the model results against the multi-point experimental data of Chapters 4 and 5, we chose to greatly reduce the computation time by not computing frequency responses for all of the ~84,000 nodes in the model. Instead, we processed

⁶ In the model of Elkhouri et al. (2006) the stapedial annular ligament was modelled by shell elements and the rotational degrees of freedom of its nodes were fixed by mistake. That boundary condition allowed only piston-like motion of the stapes.

only nodes corresponding to where we made experimental measurements: a row of nodes along the manubrium, a row of nodes on the pars tensa on a line perpendicular to the manubrium midway along its length, and a node at the centre of the pars flaccida. To permit comparison with stapes data in the literature, we also processed a node at the centre of the stapes footplate.

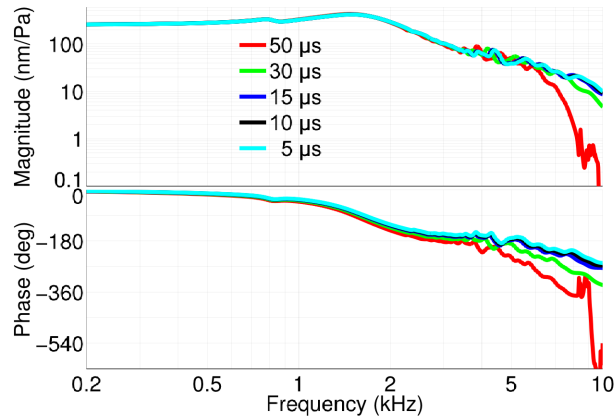


Figure 6.4: Effect of size of time step on simulated umbo response. When the time step is fine enough its effect on the responses becomes negligible. All of these time steps have negligible effects for frequencies below 2 kHz. At higher frequencies, large time steps significantly affect responses. A time step of 10 ms (black) has been selected for analyses in the current study.

6.2.3.2 Time dependence

An increase of 50% in the time span of the simulation (from 50 to 75 ms) changed the responses by less than 0.03 dB, so the time span of 50 ms was used in order to reduce computation time. The selected time span provides a frequency resolution of 12 Hz. The effect of the time step on the responses is demonstrated in Figure 6.4, where umbo responses with time steps of 50, 30, 15, 10 and 5 μ s are shown. When the time step is fine enough its effect on the responses becomes negligible. This range of time steps causes negligible effects for frequencies below 2 kHz. At 9 kHz, comparing with the smallest time step (5 μ s), the four larger time steps (from the biggest to smallest) resulted in maximal magnitude changes of 30, 6, 2 and 0.8 nm/Pa and phase errors of 374, 73, 22 and 12°, respectively. As a trade-off between accuracy and length of computation time, we chose a time step of 10 μ s for our simulations.

6.2.3.3 Mesh dependence

The original mesh that resulted from image segmentation, surface triangulation and volume mesh generation contained about 3300 triangular elements and 46200 tetrahedral elements. We used Code_Aster's Homard utility (Nicolas & Fouquet, 2013) to refine the mesh by dividing each triangle into four coplanar triangles. This increased the number of triangular elements by a factor of four and the number of tetrahedral elements by a factor of eight. The refined mesh resulted in only a 0.2 dB increase in the umbo magnitude at the lowest frequency (200 Hz) and at the resonance. It caused a decrease of only 24 Hz in the resonance frequency, no difference in the break-up frequency of the pars tensa (to within our frequency resolution of 12 Hz), and no visible changes in the frequency-response shapes. Based on these results, we chose to perform this study with the original mesh.

6.2.3.4 Effect of viewing angle

The simulations provide 3-D displacement vectors. Unless otherwise specified, all results from the model are presented in terms of the vector components parallel to the direction of the laser beam in our experiments (Chapters 4 and 5). Panels b and c in Figure 6.1 show the range of viewing directions that we had in different experimental animals. Because the viewing directions in most measurements were close to that of panel b, the model results in this paper are presented for this view. Changing the viewing angle to that of panel c, a change of about 20°, causes a difference of about 3 dB in the umbo response and less than 7 dB in the pars-tensa responses except at very sharp minima, and causes negligible changes in the frequencies of response features.

6.2.4 Baseline material properties

6.2.4.1 Stiffness

Due to the small displacements occurring in the middle ear in response to the sound pressure, all materials in the model were assumed to be linearly elastic. All soft tissues were modelled as nearly incompressible, with a baseline Poisson's ratio of 0.49 (Funnell & Laszlo, 1982).

6.2.4.1.1 Pars tensa

The stiffness of the pars tensa has large effects on middle-ear responses and a number of experimental studies have been dedicated to measuring it in different species, including one study in gerbil (Aernouts & Dirckx, 2012). To justify the value that we have chosen for our simulations, we situate it with respect to values in the literature.

Békésy (1960) estimated the bending stiffness of the pars tensa to be 20 MPa by applying a static force at the end of a cantilevered flap. Kirikae (1960) estimated a Young's modulus of 40 MPa by vibrating (at 890 Hz) a strip of pars tensa weighted at one end. Decraemer et al. (1980) estimated a Young's modulus of 23 MPa at higher strains from uniaxial tensile testing of human pars-tensa strips. Cheng et al. (2007) performed uniaxial tensile measurements on human pars-tensa strips and reported a Young's modulus value of 22 MPa at higher strains, consistent with that of Decraemer et al. (1980). Gaihede et al. (2007) applied static pressure in the ear canal *in vivo* and measured volume changes due to TM deformation. To calculate the Young's modulus they assumed that the TM is a flat circular membrane; this simplistic model resulted in Young's modulus estimates of 10.3 and 6.9 MPa for their young and old human subjects, respectively. Huang et al. (2008) performed static indentation measurements on small human pars-tensa samples and used FE modelling to obtain the Young's modulus after relaxation. They calculated values of 17.4 to 19.0 MPa (in-plane) and 0.6 MPa (through-thickness). Daphalapurkar et al.

(2009) removed the epidermal layer⁷ of the pars tensa and then applied the same approach as Huang et al. They calculated higher values of the Young's modulus: 25.7 to 37.8 MPa (in-plane) and 2 to 15 MPa (through-thickness). It is not clear why the through-thickness Young's modulus of the pars tensa is so variable in these two studies. Luo et al. (2009), doing uniaxial tensile testing on pars-tensa strips with a 'miniature split Hopkinson tension bar', obtained Young's moduli of 45.2 to 58.9 MPa for the radial direction and 34.1 to 56.8 MPa for the circumferential direction at strain rates of 300 to 2000 s⁻¹. In a series of studies, Aernouts et al. (2010, 2012) and Aernouts and Dirckx (2012) used *in situ* indentation measurements and fitting with an isotropic single-layer FE model to obtain Young's moduli of the pars tensa in the rabbit, human and gerbil. Aernouts et al. (2010) obtained quasi-static Young's moduli of 30.4 MPa for the rabbit pars tensa if the Poisson's ratio in the model was 0.3 to 0.4 and 26.4 MPa if the material was considered to be nearly incompressible (Poisson's ratio near 0.5). Aernouts et al. (2012) obtained values of 2.1 to 4.4 MPa at 0.2 Hz for the human pars tensa. Aernouts and Dirckx (2012) estimated the Young's modulus to be between 71 and 106 MPa at 0.2 Hz and between 79 and 118 MPa at 8.2 Hz for the gerbil pars tensa. Their results for rabbit were comparable to those from other groups but their values were high for gerbil and low for human. Hesabgar et al. (2010) performed *in situ* indentation measurements and Ghadarghadar et al. (2013) performed *in situ* pressurization measurements, in both cases on the rat pars tensa. Single-layer FE model fitting was used in both studies to estimate the Young's modulus, resulting in values of 21.7 and 22.8 MPa respectively. These values do not seem to be consistent with the suggestion by Aernouts et al. (2012) that the discrepancy between their gerbil and human Young's modulus values were due to "better high-frequency hearing of gerbil", since the rat also has good high-frequency hearing.

7 Note that their Figure 3, also used by Vollandi et al. (2011), neglects the subepidermal and submucosal connective-tissue layers that lie lateral and medial to the radial and circular fibre layers (Lim, 1970).

As seen above, experimental estimates for the Young's modulus of the pars tensa have been very diverse. As summarized in a recent review by Vollandri et al. (2011), values of the Young's parameter that have been used in middle-ear models are also very diverse⁸. However, in most linearly elastic isotropic models Young's moduli of 20 to 40 MPa were used. Some authors used orthotropic models for the pars tensa and assigned different Young's moduli in the radial and circumferential directions (e.g., Sun et al., 2002). Some studies have used hyperelastic (e.g., Aernouts et al., 2010) or visco-hyperelastic (Motallebzadeh et al., 2013) constitutive equations for the pars tensa.

All of the above studies considered the pars tensa as a single layer of homogeneous material. Rabbitt and Holmes (1986) used an asymptotic analytical analysis and modelled the pars tensa as a ground substance and two sets of locally orthogonal fibres. They concluded that the pars tensa has strong anisotropy dictated by the local density of fibres and that the Young's modulus may vary by over one order of magnitude from one point to another. Fay et al. (2005) considered the multilayer nature of the pars tensa in estimating its Young's modulus. In the human they estimated the Young's modulus to be from 100 to 300 MPa. In the cat, they reported a wider range, 30 to 400 MPa. The fact that their estimates are high is to be expected since they apply to the thickness of just the fibrous layers of the TM. Later Fay et al. (2006) used Young moduli of 100 and 80 MPa for the radial and circumferential fibre layers, respectively. Tuck-Lee et al.

8 The very high value of 20 GPa reported in Table 3 of Vollandri et al. (2011) was a typographical error (GPa rather than MPa) in the original paper by Gentil et al. (2005) (personal communication with Gentil). The very low value of 1.5 MPa used by Lesser & Williams (1988) was for a 2D model. The very low values used by Funnell & Laszlo (1978) and Funnell (2001) for E_c were intended to be extreme examples of anisotropy, not realistic estimates. The very low values used by Ferrazzini (2003) were for a pars-tensa model that was overly thick and was not smooth.

(2008) used a high Young's modulus (100 MPa) for both the radial and circumferential fibres and a low Young's modulus (1 MPa) for the ground substance in a multilayer model.

For simplicity, and because the quantitative distribution of the layer thicknesses and the difference between the radial and circumferential Young's moduli are not well known, we modelled the pars tensa as a single layer of isotropic material. In this study we chose a Young's modulus of 10 MPa for the pars tensa. It is not far out of the range of the measured values that have been reported, and with this value the model gives results that are in the range of our experimental data collected in gerbils *in vivo* (Chapter 5). The fact that our selected value is on the low side is consistent with the finding that the collagen fibres are less dense in gerbil than in human (Chole & Kodama, 1989). The choice of parameter will be discussed again later.

6.2.4.1.2 Pars flaccida

The pars flaccida is a continuation of the external ear canal skin (Lim, 1968b) that spans Rivinus' incisure. Agache et al. (1980) estimated the Young's modulus of the human forearm skin *in vivo* to be 0.42 MPa in their younger subjects and 0.85 MPa in subjects more than 30 years old. Recently, Geerligs et al. (2011) estimated the Young's moduli of the human epidermis and stratum *corneum* to be between 1 and 2 MPa using *in vitro* indentation measurements on abdominal skin.

At a low frequency (200 Hz) we measured a displacement magnitude of 1.5 $\mu\text{m}/\text{Pa}$ (Chapter 5, gerbil E) near the centre of the pars flaccida. Assuming that the pars flaccida is a circular disk subjected to a uniform static pressure (Timoshenko & Woinowsky-Krieger, 1959, p. 57, Eq. 68) with a radius of 0.7 mm and a constant thickness of 23.5 μm , with a Poisson's ratio of 0.49 and simply supported all around its periphery, then a centre deformation of 1.5 $\mu\text{m}/\text{Pa}$ leads to a Young's modulus of 6.4 MPa. If the circular disk is considered to be fully clamped all around its

periphery, a Young's modulus of 1.7 MPa is obtained (ibid, p. 55, Eq. e). Gea et al. (2009) demonstrated that the boundary of the pars flaccida can be considered to be simply supported at the bony edge but it is neither simply supported nor fully clamped at its interface with the pars tensa.

Based on the Young's modulus measurements on the skin and on the simplistic analysis of a circular plate, we assumed a Young's modulus of 2 MPa, a round number with which the model gives results that are in the range of experimental data, as seen in the Results. With an open middle-ear cavity, the pars flaccida is an almost independent structure whose parameters have little effect on the responses of the rest of the system.

6.2.4.1.3 Other structures

Fumagalli (1949) reported that the posterior incudal ligament is composed of highly organized collagen fibres in various species. In the absence of experimental data, we assumed that the Young's modulus of the ligament is equal to that of the pars tensa, which is partly composed of highly organized collagen fibres.

We assumed the Young's modulus of the stapedial annular ligament to be 10 kPa, as estimated by Lynch et al. (1982) in the cat. A recent measurement by Gan et al. (2011) in human temporal bones reported a shear modulus of 3.6 kPa for the smallest measured shear stress. Using this value and assuming an incompressible material, the Young's modulus of the stapedial annular ligament would be 10.8 kPa, close to the value estimated by Lynch et al.

Zhang and Gan (2011) performed uniaxial tension and compression tests on the human incudostapedial joint in the piston direction of the stapes. Fitting a straight line to the portion of their average experimental tension curve with displacements below 0.03 mm (in their Figure 4b), and using dimensions given by them (length L and mean length a and width b), we calculated a

Young's modulus of 0.27 MPa. We used this value in our model for the Young's moduli of both incudomalleolar and incudostapedial joints.

The ossicles were modelled with a Poisson's ratio of 0.3 (Elkhouri et al., 2006). Recently, Soons et al. (2010) reported a Young's modulus of 16 ± 3 GPa for the rabbit incus and malleus. We used their average value (16 GPa) for the Young's moduli of all three ossicles.

6.2.4.2 Mass

For all soft tissues, a density of 1100 kg/m^3 was chosen as being in the middle of the possible range between the density of water (1000 kg/m^3) and that of undehydrated collagen (1200 kg/m^3) (Funnell & Laszlo, 1982).

Sim et al. (2007) reported mean density values for the malleus and incus in human temporal bones as 2390 and 2150 kg/m^3 respectively. Cohen et al. (1992) reported masses for the malleus and incus in gerbils. Nummela (1995) provided the masses for the malleus and incus, close to the ones reported by Cohen et al., and also the mass of the stapes. Using volumes from their 3D models of the gerbil ossicles, and mass values from Nummela (1995), Buytaert et al. (2011) reported average densities of 1740 kg/m^3 for the malleus and incus and 1370 kg/m^3 for the stapes. In the present work, based on volumes calculated from our model and the mass data reported by Nummela (1995), we calculated densities of 1918 , 1855 and 1565 kg/m^3 for the malleus, incus and stapes, respectively.

6.2.4.3 Damping

Rayleigh damping was used for all model components. The Rayleigh damping matrix is given by $\alpha M + \beta K$, where M is the mass matrix and K is the stiffness matrix. The damping parameters α and β are the least well known parameters of the middle ear. We assumed a stiffness-proportional

damping (i.e., $\alpha=0$) for all middle-ear structures and divided the soft tissues into ones with highly organized collagen fibres (the pars tensa (Lim, 1968a) and posterior incudal ligament (Fumagalli, 1949)) and ones with abundant elastic fibres (the pars flaccida (Lim, 1968b) and the stapedial annular ligament, incudomalleal joint and incudostapedial joint (e.g., Davies, 1948; Harty, 1953)). In a series of simulations we varied the damping parameters, with the other material properties fixed at their baseline values, and compared model results with responses that we measured in gerbil ears in terms of the magnitude of the umbo response at low frequencies and at the resonance peak, the break-up frequency, and the bandwidth of the high-frequency features in the pars-tensa responses. Based on these comparisons, we used a damping parameter β of 2×10^{-6} s for the structures with highly organized collagen fibres and 3×10^{-5} s for the structures with abundant elastic fibres. We assumed that the ossicles have a damping parameter of 2×10^{-7} s, one order of magnitude less than that of the pars tensa. In the Results section we explore how changing the damping parameters of each structure affects the responses.

6.2.4.4 Cochlear load

Measurements in the gerbil ear (Overstreet & Ruggero, 2002; Decraemer et al., 2007; de La Rochefoucauld et al., 2008; Ravicz et al., 2008) suggest that the cochlear load is purely resistive over most of the frequency range of the present analysis (0.2 to 10 kHz) An average cochlear input impedance of about 4×10^{10} Pa-s/m³ for frequencies less than 30 kHz was derived by de La Rochefoucauld et al. (2008, Figure 9) using a stapes footplate area of 0.62 mm². From these values we have calculated a viscous damping coefficient of 15.4×10^{-3} N-s/m³. In our simulations we uniformly distributed this value to the four dashpots that are attached to the stapes footplate to represent the cochlear load.

6.2.5 Sensitivity analysis

After establishing the baseline model using the material properties specified in Section 6.2.4, we performed a one-variable-at-a-time sensitivity analysis. We increased and decreased each material parameter by 10% of its baseline value while keeping all other parameters at their baseline values. (Because the Poisson's ratio cannot be greater than 0.5, for the nearly incompressible soft tissues we decreased it but did not increase it.)

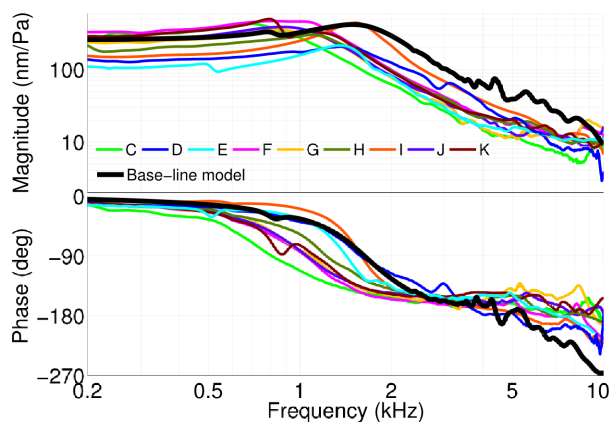


Figure 6.5: Simulated umbo response, and responses from measurements in 9 gerbil ears with partial openings in the cavity wall (Chapter 5). Following the method proposed in that paper, the experimental responses in this figure are estimated ideal open-cavity responses; that is, although they were measured with a partial opening in the middle-ear cavity wall, they have been adjusted so they appear as though they were measured with no cavity wall.

6.3 Results

6.3.1 Umbo and pars-flaccida responses

In our experimental measurements (Chapters 4 and 5) and in earlier studies (e.g., Lee & Rosowski, 2001; Rosowski & Lee, 2002) it was observed that the vibrations of the pars flaccida affect responses measured at the umbo. In this section we present these responses together. Recall that for all experimental results from Chapter 5 the estimated ideal open-cavity frequency responses are shown.

6.3.1.1 Low frequencies

Figure 6.5 shows the ideal open-cavity umbo responses in 9 experimental ears from Chapter 5, as well as the umbo response from the model. The magnitude of the experimental umbo responses at the lowest frequency was between 110 and 330 nm/Pa, compared with 260 nm/Pa for the model. The model response is on the high side of the variability seen in the experimental responses. Similar to the experimental responses, the umbo in the model moves with a phase of zero at the lowest frequency.

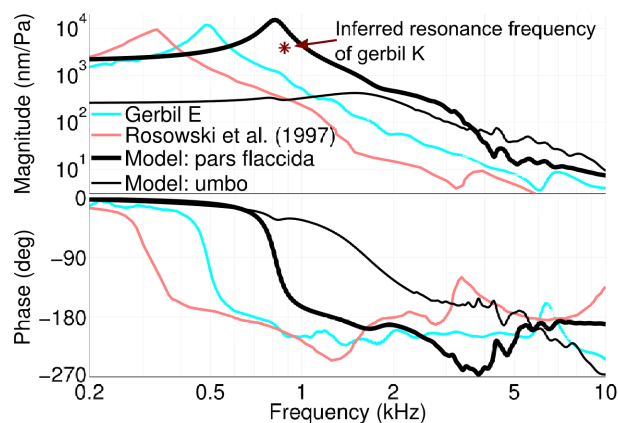


Figure 6.6: Simulated and experimental pars-flaccida responses and a simulated umbo response. Thick black: simulated pars-flaccida response. Thin black: simulated umbo response. Pink: experimental pars-flaccida response in a gerbil ear reported by Rosowski et al. (1997). Cyan: experimental pars-flaccida response in the ear of gerbil E of Chapter 5. Asterisk: frequency of the pars-flaccida resonance inferred from the umbo response in gerbil K of Chapter 5.

Figure 6.6 shows simulated responses at the centre of the pars flaccida, as well as the response at the umbo (the same curve as shown in Figure 6.5). In our experimental measurements in gerbil ears we often observed that the pars flaccida is retracted into the middle-ear cavity. Figure 6.6 shows the experimental open-cavity pars-flaccida responses for ear E from Chapter 5, the only ear in which we could measure the response of a naturally flat pars flaccida, as well as the one ear from Rosowski et al. (1997). At the lowest frequency the centre of the pars flaccida in the

model has a phase of zero and a magnitude of $2.2 \mu\text{m}/\text{Pa}$. The experimental ears show phases of nearly zero and magnitudes of $1.5 \mu\text{m}/\text{Pa}$ (Chapter 5) and $2.5 \mu\text{m}/\text{Pa}$ (Rosowski et al.) at low frequencies.

Similar to experimental observations (Figure 4.3), the umbo and pars flaccida of the model move almost in phase with each other up to about 700 Hz, as seen in Figure 6.6. The model pars flaccida shows a resonance at about 820 Hz. Between about 700 and 950 Hz, the umbo response from the model shows a feature that includes a shallow maximum (at 780 Hz) followed by a shallow minimum (at 880 Hz) in the magnitude, and a local minimum (at 840 Hz) in the phase. The correspondence of this feature in the umbo response to the resonance of the pars flaccida was discussed in Chapter 4. In Figure 6.5 only ears E and K had a naturally flat pars flaccida; in all the other ears the pars flaccida was retracted into the middle-ear cavity. The umbo responses in these two ears show the pars-flaccida feature in both magnitude and phase. The shallow maximum and shallow minimum are 60 and 135 Hz apart and the ratios of their magnitudes are 1.3 and 1.8 in gerbils E and K, respectively. The shallow maximum and shallow minimum in the model umbo result are 100 Hz apart and the ratio of their magnitudes is 1.1.

The magnitude of the simulated response at the centre of the pars-flaccida at resonance (800 Hz) is $15 \mu\text{m}/\text{Pa}$. The pars-flaccida responses in the two experimental ears (Figure 6.6) show resonances at 350 and 500 Hz with magnitudes of 9.5 and $11.6 \mu\text{m}/\text{Pa}$. We were not able to record the pars-flaccida response in gerbil K but the resonance frequency of the pars flaccida inferred from the umbo response is at about 900 Hz as indicated in Figure 6.6 by an asterisk. The pars-flaccida response in the model shows a full width at half maximum of 210 Hz. This value (a measure of damping) was observed to be between 110 and 230 Hz in the experimental measurements.

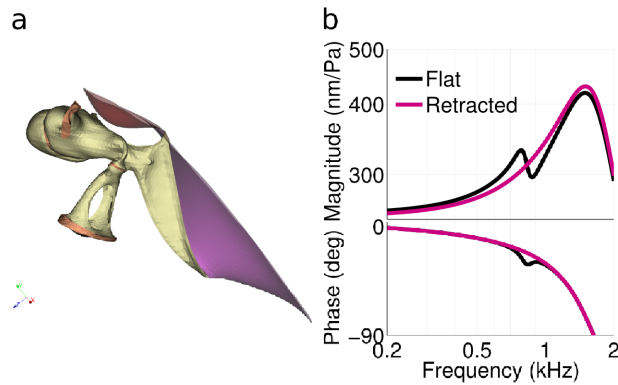


Figure 6.7: (a) 3D model of gerbil middle ear with retracted pars flaccida. (b) Simulated umbo responses with flat and retracted pars flaccida. In our experimental measurements in gerbil ears we often observed that the pars flaccida is retracted into the middle-ear cavity. To replicate this experimental condition in the model, we applied a static pressure of 100 Pa to the lateral side of the pars flaccida.

The possible causes of the retraction of the pars flaccida into the middle-ear cavity were discussed in Chapter 4. To replicate this experimental condition in the model, we applied a static pressure of 100 Pa to the lateral side of the pars flaccida. As Figure 6.7a shows, this static pressured deformed the original flat pars flaccida to an inverted dome-like shape, similar to what we observed experimentally. Figure 6.7b shows that retraction of the pars flaccida removes the pars-flaccida feature from both magnitude and phase of the simulated umbo response.

6.3.1.2 Mid and high frequencies

Similar to experimental observations (e.g., Figure 4.3), the displacement magnitude at the centre of the pars-flaccida remains higher than that of the umbo up to about 3.5 kHz (Figure 6.6). At higher frequencies we observed experimentally that the pars-flaccida magnitude was at the level of or as much as 7.5 dB lower than that of the umbo. A similar pattern is observed in the model result, with the pars-flaccida magnitude going to as much as 10 dB below that of the umbo.

The simulated umbo response in Figure 6.5 shows a rather broad resonance with a peak of 420 nm/Pa at 1.5 kHz. In the umbo responses of all experimental ears in Figure 6.5, the

resonance frequencies are between 940 Hz and 1.6 kHz and the magnitudes at the resonance are between 210 and 460 nm/Pa. The ratio of the umbo magnitude at the resonance to that at low frequencies is between 1.2 and 2.9 in these experimental ears, compared with 1.6 for the model.

In experimental ideal open-cavity responses, the width of the resonance (in terms of the full width at half maximum of the umbo velocity response) is between 1.0 and 2.2 kHz. This quantity is 1.8 kHz in the model response. As for the experimental ears, the umbo response for the model shows a roll off with substantial irregularities. For both measurements and model, the irregularities have bandwidths of a few hundred hertz, magnitude changes of a few decibels, and phase changes of a few tens of degrees. For frequencies above the resonance frequency, the simulated umbo response is higher than any of the measured responses.

6.3.2 Manubrial response

Figure 6.8 shows the model responses at five points along the manubrium. Similar to experimental observations (Figure 5.18), the magnitude increases from the lateral process to the umbo, and all points along the manubrium move in phase with each other up to about 4.5 kHz, except in a narrow range (50 Hz) at about 3.3 kHz. This pattern in the responses is consistent with a classical rotation of the malleus around a fixed axis of rotation at low frequencies. At the resonance peak, the umbo-to-lateral-process displacement magnitude ratio is 1.40, somewhat smaller than the ratios of 1.47 to 2.00 measured experimentally in the open-cavity condition. If the motions are calculated based on the view shown in Figure 6.1c instead of the one in Figure 6.1b, the umbo-to-lateral-process displacement magnitude ratio will be 1.90, close to the upper limit of the experimental observations.

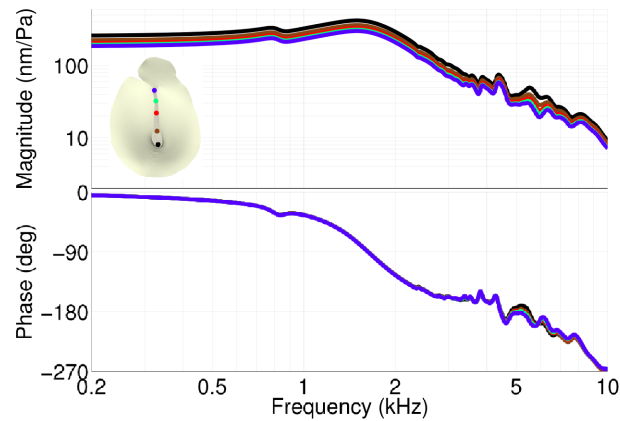


Figure 6.8: Model responses at five locations along the manubrium. Between about 4.5 and 8 kHz, the phases show differences of more than 5° , with a maximum difference of 13° between the umbo and the lateral process at 5.4 kHz.

In Figure 6.8 between about 4.5 and 8 kHz, the phases show differences of more than 5° , with a maximum difference of 13° between the umbo and the lateral process at 5.4 kHz. Above 7 kHz the manubrial points again move in phase with each other (within 5°). Experimentally phase differences were seen above about 5 kHz.

Figure 6.9 shows the simulated displacements of the five manubrial points for four frequencies and for seven equally spaced time instants within each cycle. The locations of the points on the abscissa were determined by projection onto a plane perpendicular to the laser beam. The asterisk in each panel indicates the position of the anatomical axis of rotation, which was assumed to run from the anterior bony attachment of the malleus to the posterior tip of the short process of the incus. At the lowest frequency (200 Hz) the manubrium rotates as a rigid body around a fixed axis of rotation shown by the intersection of the instantaneous lines. This intersection is not exactly at our estimated anatomical axis of rotation but it is close to it. At the resonance peak (1.5 kHz) the manubrium again rotates as a rigid body around an almost fixed axis of rotation, at about the same position as before. The position of the axis of rotation starts to shift at frequencies above 1.8 kHz. At 5.4 and 9.5 kHz the mode of vibration of the manubrium

has clearly changed, with the position of the instantaneous axis of rotation moving throughout the cycle. At 5.4 and 9.5 kHz the lines show slight deflections that might be due to mild bending of the manubrium. Changes in the position of the axis and evidence of manubrial bending were also seen experimentally (Figure 4.6).

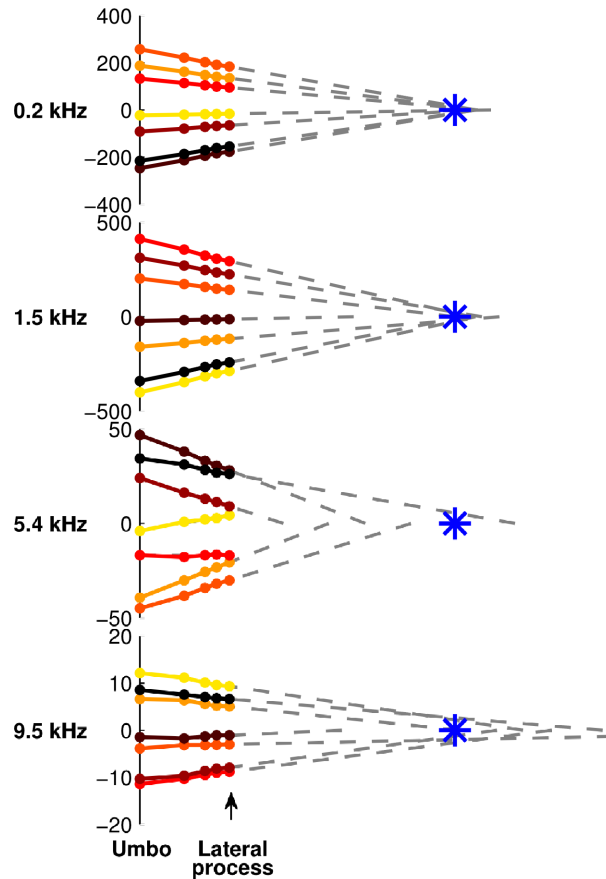


Figure 6.9: The displacements of five points along the manubrium at four frequencies and for seven equally spaced time instants within each cycle. The locations of the points on the line were determined by projection onto a plane perpendicular to the laser beam. We assumed that the anatomical axis of rotation (the position where the axis crosses the figure plane is indicated by an asterisk) runs from the anterior bony attachment of the malleus to the posterior tip of the short process of the incus. At the two higher frequencies, the axis of rotation is not fixed and the lines indicate slight deflection of the lower half of the manubrium.

6.3.3 Pars-tensa response

Figure 6.10 shows model responses for six pars-tensa points and one manubrial point at the level of the middle of the manubrium. All points vibrate in phase for frequencies up to about 2 kHz. At these frequencies the pars-tensa points exhibit a simple motion pattern. Similar to manubrial points, all pars-tensa responses show the pars-flaccida feature. At low frequencies the magnitude at the manubrium is the smallest and, for the same distances from the manubrium, points on the posterior side show larger displacements than the ones on the anterior side. The displacement pattern at low frequencies is similar to the patterns observed in gerbil ears experimentally (Figure 4.9).

At higher frequencies the simple in-phase motion breaks up and each point shows different frequency-dependent magnitudes and phases. We define the break-up frequency as the frequency at which the phase divergence of the points is more than 15° (Chapter 4). The break-up frequency for the model is 2 kHz, which is within the range of 1.8 to 2.8 kHz observed experimentally.

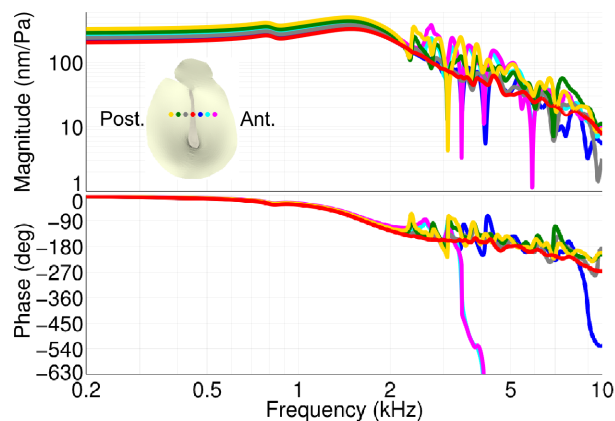


Figure 6.10: Model responses of six pars-tensa points and one manubrial point at the level of the middle of the manubrium. For frequencies above 2 kHz the responses of the pars tensa are much less smooth than that of the manubrium.

The experimental inter-animal variability of the pars-tensa motion is illustrated in Figure 6.11. The variability in this figure is due to differences among animals and to slight differences in the locations of the measurement points. This figure includes the estimated ideal open-cavity responses on the pars tensa about 150 μm posterior to the manubrium in 8 experimental ears. The result from the model at a similar location is also plotted (in grey) in this figure. The curves show complex responses which are all different from one another. The magnitude response from the model is on the high side of the range seen in the experimental responses. Similar to the experimental responses, the pars-tensa responses from the model show features with frequency bandwidths of a few hundred to a few thousand Hertz. As in the experimental responses in Figure 6.11, the phases of some points in the model results in Figure 6.10 show very large phase shifts at some sharp magnitude minima.

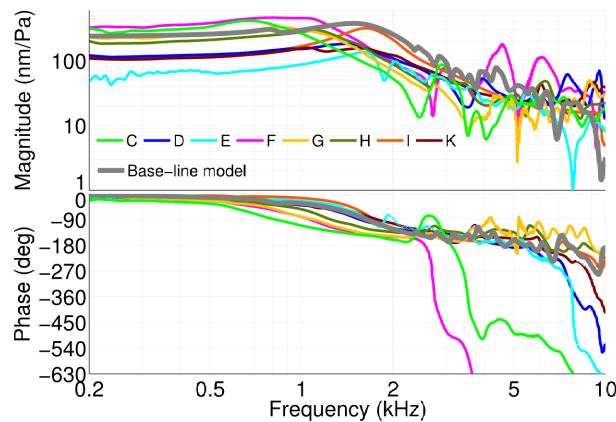


Figure 6.11: Simulated pars-tensa response (grey) at a point posterior to the manubrium at the level of the middle of the manubrium (the grey point in the schematic inset in Figure 6.10), together with responses from measurements in 8 gerbil ears (with partial openings in the cavity wall) at the first bead posterior to the manubrium at the level of the middle of the manubrium (Chapter 5). As in Figure 6.5, the experimental responses in this figure are estimated ideal open-cavity responses.

6.3.4 Stapes response

The ratio of umbo displacement to stapes displacement is often specified in terms of a lever ratio (although Figure 6.9 shows that the lever model with a fixed fulcrum does not hold for frequencies above a few kHz). In order to calculate this ratio in our model, we assumed the anatomical axis to be as described in Section 6.3.2. The lengths of the 3-D lines drawn perpendicular to the anatomical axis from the end point of the central line of the long process of the incus and from the umbo are 1.0 and 3.2 mm, providing a lever ratio of 3.2. Using 2-D calculations, Rosowski et al. (1999) calculated the average anatomical lever ratio in seven gerbil ears to be 3.1, and using their measurements they estimated a lever ratio of 3.5 at low frequencies. The ratio of umbo displacement to stapes displacement in the gerbil measurements of Decraemer et al. (2014) was between 3 and 4 at low frequencies.

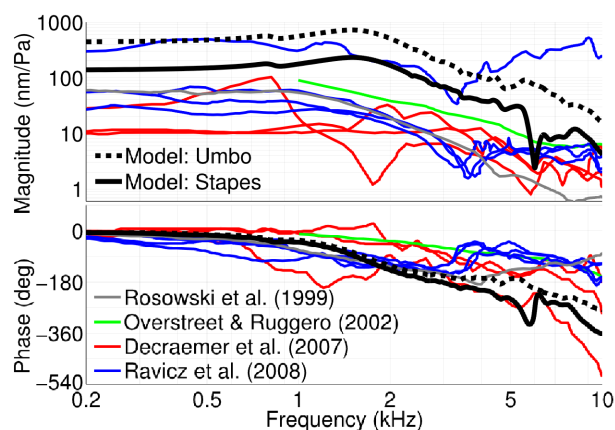


Figure 6.12: Piston component of the stapes footplate displacement from the model (solid black line) and measured experimentally in gerbil ears. Grey: the mean of 6 ears from Rosowski et al. (1999, Figure 4); green: the median of 8 adult ears from Overstreet and Ruggero (2002, Figure 2); red: 3 ears from Decraemer et al. (2007, Figure 6, 10 and 12); blue: 4 ears from Ravicz et al. (2008, Figure 4). Except for the responses from Decraemer et al., the experimental responses were originally presented in terms of velocities but for this figure we have converted them to displacements. The simulated umbo response (in the direction of the normal to the plane passing through the anatomical axis of rotation and the umbo) is also shown (dashed black line).

Figure 6.12 shows the displacement of the centre of the stapes footplate in the direction of piston-like motion (solid black line). (The piston-like direction was taken as the direction normal to the plane passing through the anatomical axis of rotation and the end point of the central line of the long process of the incus.) This figure also shows the umbo displacement in the direction of the normal to the plane passing through the anatomical axis of rotation and the umbo. Dividing the umbo response by the stapes response gives a lever ratio of 3.2 at the lowest frequencies. Above 500 Hz the lever ratio starts to decrease with frequency, going down to 2.3 (-30%) at about 5 kHz. Above this frequency the lever ratio shows drastic changes with frequency.

The stapes and umbo responses in Figure 6.12 have the same phase at low frequencies and show resonances at the same frequency (1.5 kHz). A similar correspondence between the resonance frequencies of the stapes and umbo responses was experimentally observed by Rosowski et al. (1999). The phase of the stapes response starts to depart from that of the umbo at frequencies as low as 300 Hz (where the difference is 2°). At 2 kHz this phase difference becomes 15° and continues to grow with frequency except between 5.8 and 7.8 kHz.

Figure 6.12 also includes stapes displacement responses from four experimental studies in gerbil ears: the mean of 6 ears from Rosowski et al. (1999, Figure 4), shown in grey; the median of 8 adult ears from Overstreet and Ruggero (2002, Figure 2), shown in green; 3 ears from Decraemer et al. (2007, Figures 6, 10 and 12), shown in red; and 4 ears from Ravicz et al. (2008, Figure 4), shown in blue. (Except for the responses from Decraemer et al., the experimental responses were originally presented in terms of velocities but for this figure we have converted them to displacements.) The experimental responses from Decraemer et al. (at about 6 kHz) and from Rosowski et al. and Ravicz et al. (between 3 and 4 kHz) are affected by the antiresonance due to

the acoustic contribution of the hole in the middle-ear cavity wall (cf. Ravicz et al., 1992; Chapter 5), an effect that of course is not present in the model results. The Data of Overstreet and Ruggero do not show this effect, presumably because calculating the median of the responses filters out the effect. The stapes response from the model is on the high side of the variability seen in these experimental responses. The model manubrial and pars tensa magnitude responses are also on the high side of our own experimental data, as indicated by Figures 6.6 and 6.11.

The model stapes response shows minima in both magnitude and phase in the frequency range of 5.5 to 6.5 kHz. The dependence of this and other features on the middle-ear structures and model parameters will be explored in the next section.

6.3.5 Sensitivity analysis

In this section we present model results obtained as the model parameters are varied one at a time by $\pm 10\%$ from their baseline values. In the figures presented in this section, response changes due to changes in the parameters of a particular model structure are consistently shown in the same colour (e.g., red for pars tensa), and each type of parameter is indicated by a unique symbol across all structures (e.g., circle for Young's modulus). These symbols are filled when the parameters are increased by 10% and open when the parameters are decreased by 10%. Recall that Poisson's ratios for nearly incompressible structures are only decreased, not increased.

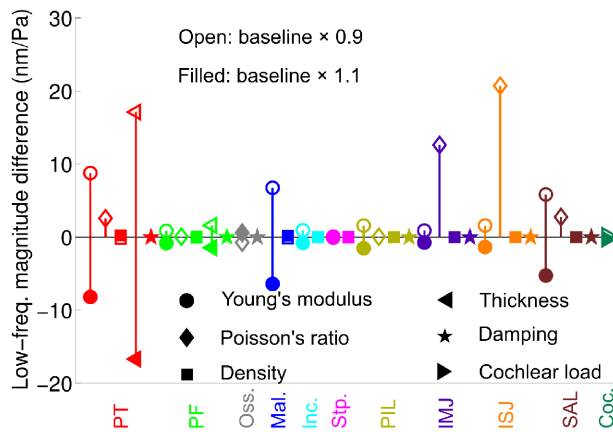


Figure 6.13: Changes in the magnitude of the umbo response at a low frequency (200 Hz) as the parameters of the model were varied $\pm 10\%$. PT: pars tensa, PF: pars flaccida, Oss.: ossicles, Mal.: malleus, Inc.: incus, Stp.: stapes, PIL: posterior incudal ligament, IMJ: incudomalleolar joint, ISJ: incudostapedial joint, SAL: stapedial annular ligament, Coc.: cochlear load. Changes due to the variation in parameters of each of these groups are shown in the same colour. Each parameter is shown by a unique symbol across all structures. The symbols are filled when the parameters were increased by 10% and are open when the parameters were decreased by 10%.

Figure 6.13 shows the changes in the magnitude of the umbo response at a low frequency (200 Hz) as the parameters of the model were varied by $\pm 10\%$. For this amount of variation, the most influential parameters, in decreasing order of importance, are the Poisson's ratio of the incudostapedial joint (which causes an increase of 20 nm/Pa); the thickness and Young's modulus of the pars tensa; the Poisson's ratio of the incudomalleolar joint; and the Young's moduli of the malleus and the stapedial annular ligament. All other parameters have effects of less than 3 nm/Pa (less than 1 dB).

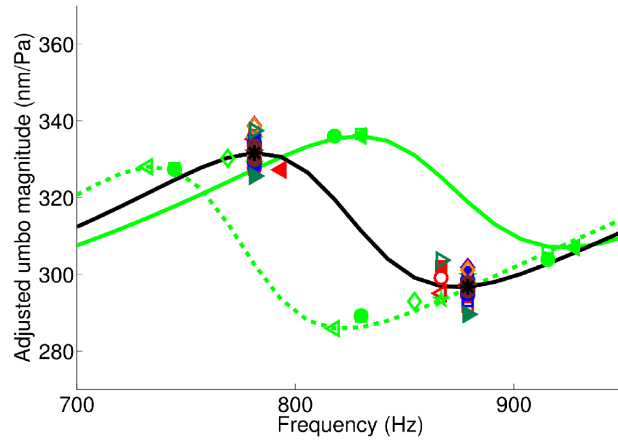


Figure 6.14: Changes in the pars-flaccida feature in the umbo response as the parameters of the model varied $\pm 10\%$. The markers show the magnitude and frequency of the two extrema. For symbols and colours refer to Figure 6.13.

Each curve in Figure 6.14 shows the shallow maximum and shallow minimum in the umbo response due to the pars flaccida, as described in Section 6.3.1. Variations in the model parameters change the frequencies and/or magnitudes of these two extrema. The baseline-related curves and symbols are shown in black and symbols indicate the magnitude and frequency of each extremum. (The symbol types and colours in this figure are the same as in Figure 6.13.) Since variations in parameters also cause changes in the low-frequency magnitude, which in turn affects the magnitudes of the extrema, we subtracted the change in the low-frequency magnitude (in nm/Pa) from the magnitude of each response. In other words, we adjusted the umbo responses so that all of them have the same low-frequency magnitude as the baseline umbo response. The green lines and symbols again indicate pars-flaccida parameters. The solid and dashed green curves show the normalized umbo responses that result when the pars-flaccida thickness is changed by -10% and $+10\%$ respectively. These variations in the thickness parameter cause the biggest changes in the responses. A 10% decrease in the thickness shifted the maximum and minimum 50 and 60 Hz lower, respectively, and decreased their respective magnitudes by 5 and 10 nm/Pa. A 10% increase in the thickness shifted both maximum and

minimum 50 Hz higher and increased their respective magnitudes 5 and 10 nm/Pa. The Young's modulus, density and damping of the pars flaccida are the next most influential parameters. As expected, increasing the Young's modulus or decreasing the density of the pars flaccida shifts the feature to higher frequencies, and increasing the pars-flaccida damping decreases the magnitude difference between the two extrema. We see in the figure that most other parameters do not change the frequencies of the extrema.

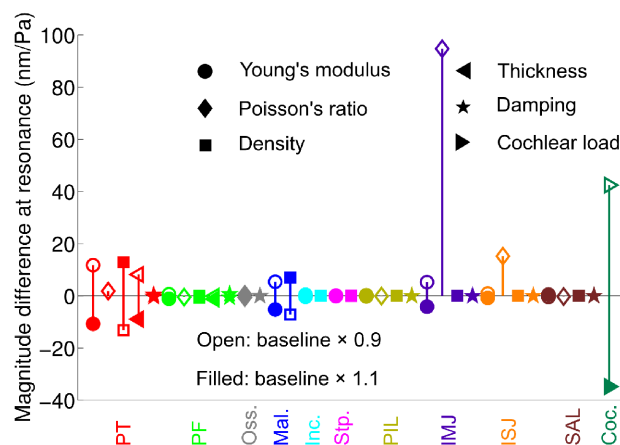


Figure 6.15: Shifts in the middle-ear resonance frequency (seen in the umbo response) as the parameters of the model varied $\pm 10\%$. PT: pars tensa, PF: pars flaccida, Oss.: ossicles, Mal.: malleus, Inc.: incus, Stp.: stapes, PIL: posterior incudal ligament, IMJ: incudomalleal joint, ISJ: incudostapedial joint, SAL: stapedia annular ligament, Coc.: cochlear load. Changes due to the variation in parameters of each of these groups are shown in the same colour. Each parameter is shown by a unique symbol across all structures. The symbols are filled when the parameters were increased by 10% and are open when the parameters were decreased by 10%. The frequency resolution in our analyses is 12 Hz.

Figure 6.15 shows the shifts in the middle-ear resonance frequency (as seen in the umbo response) due to parameter variations. Since the frequency resolution of our analyses is 12 Hz, the frequency shifts that are given are multiples of this number and changes smaller than that are not captured. Decreases of 10% in the Poisson's ratios of the incudomalleal and incudostapedial joints cause shifts of +100 and -50 Hz in the resonance frequency, respectively. This unexpectedly large effect is discussed later. Increasing and decreasing the thickness of the pars

tensa cause frequency shifts of +36 and -24 Hz, respectively. Such an asymmetry is seen for other parameters as well (e.g., the Young's modulus and density of the malleus). The Young's moduli and densities of the pars tensa and the malleus and the Young's modulus of the stapedial annular ligament cause resonance-frequency shifts of up to 24 Hz. As expected, the Young's modulus and density of the pars tensa (and those of the malleus) oppositely affect the resonance frequency. Other parameters have effects of 12 Hz or less.

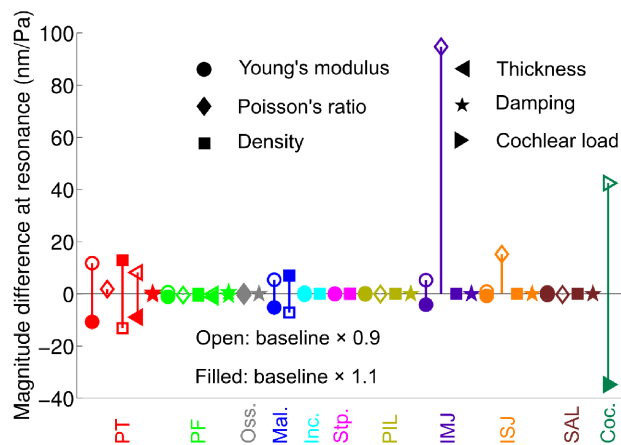


Figure 6.16: Changes in the magnitude of the umbo response at the resonance peak as the parameters of the model varied $\pm 10\%$. PT: pars tensa, PF: pars flaccida, Oss.: ossicles, Mal.: malleus, Inc.: incus, Stp.: stapes, PIL: posterior incudal ligament, IMJ: incudomalleal joint, ISJ: incudostapedial joint, SAL: stapedial annular ligament, Coc.: cochlear load. Changes due to the variation in parameters of each of these groups are shown in the same colour. Each parameter is shown by a unique symbol across all structures. The symbols are filled when the parameters were increased by 10% and are open when the parameters were decreased by 10%.

Effects of parameter variations on the magnitude of the umbo response at the resonance peak are shown in Figure 6.16. A 10% decrease in the Poisson's ratio of the incudomalleal joint again has a large effect: an increase of 95 nm/Pa (~ 2 dB). Increasing and decreasing the cochlear load cause changes of -35 and 42 nm/Pa (-0.7 and 0.8 dB), respectively. Other influential parameters, in decreasing order of importance, are the Poisson's ratio of the incudostapedial joint, density,

Young's modulus and thickness of the pars tensa and density and Young's modulus of the malleus. All other parameters have effects of less than 0.1 dB.

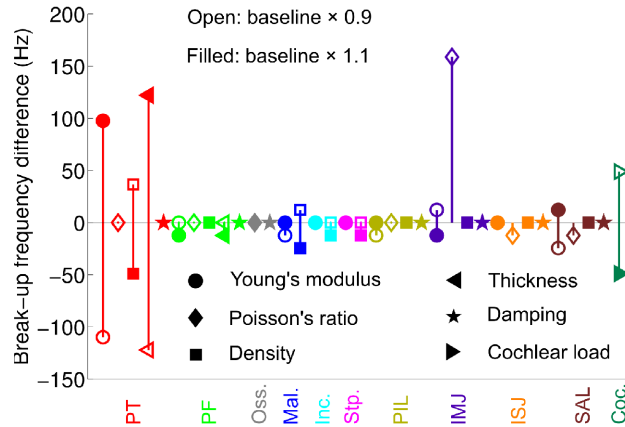


Figure 6.17: Changes in the pars-tensa break-up frequency as the parameters of the model varied $\pm 10\%$. PT: pars tensa, PF: pars flaccida, Oss.: ossicles, Mal.: malleus, Inc.: incus, Stp.: stapes, PIL: posterior incudal ligament, IMJ: incudomalleal joint, ISJ: incudostapedial joint, SAL: stapedial annular ligament, Coc.: cochlear load. Changes due to the variation in parameters of each of these groups are shown in the same colour. Each parameter is shown by a unique symbol across all structures. The symbols are filled when the parameters were increased by 10% and are open when the parameters were decreased by 10%.

The effects of parameter variations on the low-frequency magnitude, resonance frequency and magnitude at the resonance peak of the pars-tensa response are similar to their effects on those features of the umbo response. As Figure 6.17 shows, the break-up frequency of the pars tensa is shifted by +160 Hz when the Poisson's ratio of the incudomalleal joint decreased by 10%. It is shifted by -120, -110, +50 and +40 Hz when the thickness and Young's modulus of the pars tensa, the cochlear load and the density of the pars tensa are decreased, respectively. Increasing these parameters causes opposite effects that are similar but not always the same in size. All other parameters have considerably less effect (less than 24 Hz) on the break-up frequency shift. Above the break up, the high-frequency features in the pars-tensa responses are most strongly influenced by the thickness, Young's modulus and density of the pars tensa, the Poisson's ratio of the incudomalleal joint and the damping of the pars tensa, in decreasing order of importance.

The low-frequency lever ratio increases from 3.19 to 3.57 when the Poisson's ratio of the incudomalleolar joint decreased by 10% (not shown). Variations in each of the other parameters change the low-frequency lever ratio less than 0.05.

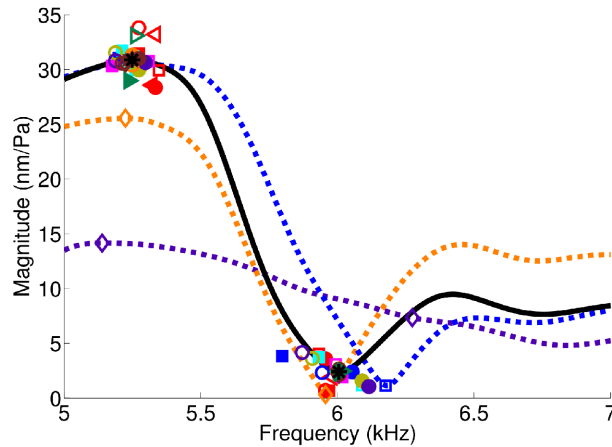


Figure 6.18: Effect of $\pm 10\%$ parameter variations on the magnitude of a high-frequency feature seen in the stapes response in the piston motion direction. Black curve: baseline; violet curve: Poisson's ratio of the incudomalleolar joint decreased by 10%; orange curve: Poisson's ratio of the incudostapedial joint decreased by 10%; blue curve: density of the malleus decreased by 10%. The markers show the magnitude and frequency of the two extrema. For symbols and colours refer to Figures 6.15-6.17.

As mentioned above, the magnitude of the stapes response in Figure 6.11 shows a minimum between 5.5 and 6.5 kHz. Figure 6.18 explores the effects of parameters on the shape of this feature. The symbols and colours in this figure are the same as those used in other figures of this section. The black curve shows the baseline piston-like stapes response and the other curves show responses corresponding to changes in selected parameters. The symbols show the magnitudes and frequencies of the two extrema. A 10% decrease in the Poisson's ratio of the incudomalleolar joint flattens out this feature (violet curve). Among the other parameters, the Young's modulus of the pars tensa causes the greatest change (an increase of 5 nm/Pa, about 1 dB) in the depth of the feature. A 10% decrease in the Poisson's ratio of the incudostapedial

joint decreases the depth of the feature by 3.3 nm/Pa (orange curve). The other parameters do not affect the depth of this feature much.

Unlike other frequency-response features investigated in this paper, the frequencies of the extrema of this feature are very asymmetrically affected by the direction of change of the pars tensa parameters: either increasing or decreasing the Young's modulus, density or thickness of the pars tensa results in changes in the same direction, increasing the frequency of the maximum by 24 to 96 Hz and decreasing the frequency of the minimum by 24 to 72 Hz (red symbols in Figure 6.18). Furthermore, unlike the pars-flaccida feature in the umbo response (Figure 6.14), the frequencies of the maximum and minimum here are affected very differently from one another. As an example, when the density of the malleus is decreased by 10%, the maximum stays at the same frequency but the minimum shifts by +170 Hz (open blue squares, blue curve); when this parameter is increased by 10%, however, the maximum and the minimum shift by -50 and -210 Hz, respectively (filled blue squares).

The parameters having the greatest influence on the frequency of the maximum are, in decreasing order of importance, the density (100 Hz), Young's modulus (85 Hz) and thickness of the pars tensa (85 Hz); the density of the stapes (75 Hz); the Young's moduli of the incudomalleolar joint (60 Hz) and the posterior incudal ligament (60 Hz); the Poisson's ratio of the pars tensa (50 Hz); the density of the malleus (50 Hz); the density of the incus (36 Hz); and the Young's modulus of the stapedial annular ligament (36 Hz). The most influential parameters for the frequency of the minimum are, in order of importance, the density of the malleus (210 Hz); the Young's moduli of the incudomalleolar joint (135 Hz) and posterior incudal ligament (100 Hz); the densities of the incus (85 Hz) and pars tensa (75 Hz); the Young's moduli of the malleus (60 Hz) and pars tensa (50 Hz); and the Poisson's ratio of the incudostapedial joint (50 Hz).

6.4 Discussion

6.4.1 Study approach

6.4.1.1 Baseline model

This study is mainly focused on the TM displacement responses in the frequency domain. We have collected experimental data on TM motions in two preceding studies (Chapters 4 and 5) and those data are used to validate the model. We have concentrated here on the frequency range between 0.2 and 10 kHz, as in our experimental data. There were two reasons for selecting this range in our experimental studies: (1) the noise that we had in our experimental vibration data below 200 Hz; and (2) the complications that standing waves may cause in the ear canal at higher frequencies.

Furthermore, this study does not try to explore the model response in terms of ossicular vibrations in detail: we have presented the displacements of the manubrium along only a single direction and only the piston component of the stapes displacement. Validation of the ossicular motion will require further study, taking into account the 3D ossicular motions that have been reported by Decraemer et al. (2007, 2014) as well as the experimental manubrial motion results presented in Chapters 4 and 5.

6.4.1.2 Sensitivity analysis

The sensitivity analysis in this paper only considers the uncertainty in the material properties. Funnell and Decraemer (1996) showed that the TM shape also has a substantial effect on the responses, and the morphological variability of other components of the middle ear (e.g., Salih et al., 2012) may also cause substantial differences in behaviour.

N model parameters define an N -dimensional space of input parameters. The baseline results are the results of the model at only one point in this N -dimensional space. The one-variable-at-a-time

sensitivity analysis that we performed here provides response variations in the neighbourhood of the baseline point in the N -dimensional space of the parameters. The other points in this space remain unexplored. Furthermore, interactions between parameters, as two or more parameters vary simultaneously, are not investigated in the current study. Systematic exploration of such interactions should be done, and will be computationally extremely demanding.

Because we wanted to rank the parameters in order of importance in the neighbourhood of the baseline, we varied all of them by the same percentage ($\pm 10\%$). However, uncertainties in most of the parameters are much more than 10%. As an example, Soons et al. (2010) reported a variation from the mean Young's modulus of the malleus and incus of about 20% in a number of measurements in rabbits. For most parameters of the middle-ear model, one can expect even more uncertainty, in part because of questions about experimental methods and artefacts. Some of the parameters that did not show significant effects in this study may affect the responses significantly if the variation range is extended. To provide two examples, Figure 6.19 shows the umbo responses with baseline parameters together with those when the damping of the pars tensa is changed from 2×10^{-6} s to 3×10^{-5} s (the damping that we used for the pars flaccida and joints) and when the Young's modulus of the posterior incudal ligament is decreased by 50%. The increased pars-tensa damping shifts the frequency of the middle resonance 60 Hz lower, decreases the umbo magnitude at the resonance peak by about 1 dB, and, most importantly, heavily smooths the high-frequency irregularities. It also changes the phase of the response above 3.5 kHz, with a phase change of 50° at 10 kHz. The decrease in the Young's modulus of the posterior incudal ligament changes the shapes of the high-frequency irregularities in the range of 2.5 to 6 kHz. Figure 6.19 also shows the umbo response when the Young's moduli of the incudomalleal joint is changed from 0.27 MPa to 3 MPa. This value resulted from fitting a

line to the high-stretch part of the experimental curve of (Zhang & Gan, 2011, Figure 4b, 0.16 to 0.2 mm). It changes the magnitudes at the lowest frequency and at the resonance peak by about 0.8 and 1 dB respectively. It also smooths the irregularities in the range of 2.5 to 5.8 kHz but introduces rather distinct peaks in the magnitude and phase at about 5.8 kHz.

6.4.2 Model parameters

The baseline material properties used in the present study are largely based on *a priori* estimates derived from measurements. Although our current model with an isotropic single-layer TM provides acceptable results in the range of experimental observations, the effects of the TM's multiple layers and their presumed orthotropy need to be explored in a future study. The damping parameters are the least well known parameters of the middle ear. In this study we, like many others, have used the Rayleigh damping model, which provides a practical way of dealing with the phenomenon in the middle ear. However, there is no physiological evidence in favour of Rayleigh damping, which is based purely on computational convenience. Other damping models should be explored in subsequent studies.

The Young's modulus of the pars tensa is one the most important parameters of the model. The baseline value that we used here for this parameter is 10 MPa. In previous models from our group, in other species, we frequently considered this parameter to be 20 MPa, as have other groups. Changing the baseline pars-tensa Young's modulus here to 20 MPa changes the low-frequency magnitude from 260 nm/Pa to 200 nm/Pa and causes a 220-Hz increase in the resonance frequency of the middle ear; the magnitude at the resonance peak decreases by 1.8 dB. Thus, this change causes the model to have a resonance at a frequency slightly higher than what we have measured experimentally but the magnitudes at low-frequencies and at the resonance peak stay within the range of experimental observations.

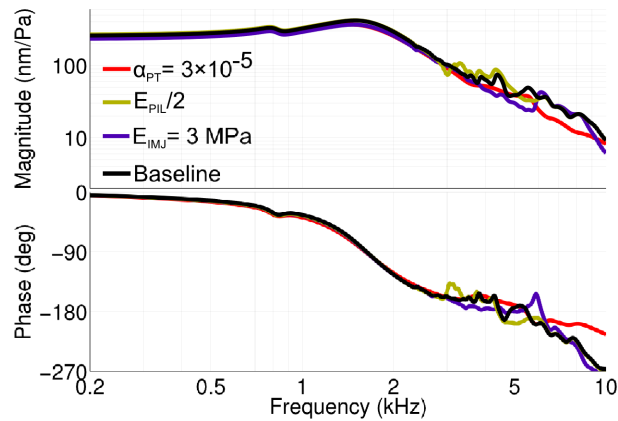


Figure 6.19: Umbo responses with baseline parameters and two examples of extended range of variations. Red: when the damping of the pars tensa is changed to that of the pars flaccida. Gold: when the Young's modulus of the posterior incudal ligament decreased by 50%.

The previous gerbil model from our group (Elkhoury et al., 2006) used a Young's modulus of 60 MPa for the pars tensa. This was based on the value in common between the estimates of Fay et al. (2005) for the posterior section (30-60 MPa) and anterior section (60-90 MPa) of the cat pars tensa. As mentioned earlier (Section 6.2.4.1.1), because the estimates by Fay et al. were not based on the full thickness of the pars tensa, the resulting high Young's moduli are not really relevant to isotropic models that model the entire thickness of the pars tensa in a single layer. With this value for the Young's modulus of the pars tensa, Elkhoury et al. (2006) calculated a static (low-frequency) displacement of 104 nm/Pa at the umbo. If the Young's modulus of the pars tensa is set to 60 MPa in the present model, which is different from theirs in a number of ways, a very similar low-frequency umbo displacement (100 nm/Pa) is obtained. The focus of the study by Elkhoury et al. was low-frequency behaviour and the Young's modulus of 60 MPa for the pars tensa results in acceptable displacements at low frequencies, at the low end of the range of experimental observations (our Figure 6.5). However, the results at higher frequencies are not acceptable; for example, a middle-ear resonance frequency of 2.5 kHz is obtained with the model presented here, which is outside the range of experimental observations.

6.4.3 Model responses

6.4.3.1 *Pars flaccida and umbo*

The pars flaccida in the model shows responses similar to those measured by Rosowski et al. (1997) and by us (Chapter 5). Our sensitivity analysis shows that the resonance of the pars flaccida shifts to lower frequencies as its Young's modulus or thickness decreases. To have a resonance frequency closer to the one from the ear that Rosowski et al. reported, either or both of these two parameters should be decreased. However, this will result in increasing the low-frequency magnitude, which is already in the range of that ear. The model currently has a simplistic treatment of the thickness of the pars flaccida. A model with a variable thickness distribution for the pars flaccida, like what is done for the pars tensa, may provide better results. Since with an open middle-ear cavity the pars flaccida has a very small effect on the motions of the other structures of the middle ear, and because this small effect is limited to a narrow frequency range, we did not try to make the pars-flaccida model more sophisticated.

The model shows that retraction of the pars-flaccida into the middle-ear cavity does indeed remove the pars-flaccida feature from the umbo response, in agreement with our experimental study (Chapter 4).

The umbo response of the model is within the range of variability seen in the experimental data in terms of the low-frequency magnitude and phase; the main resonance frequency and magnitude; and the roll-off slope and the irregularities in the response above the resonance frequency. However, for frequencies above the resonance frequency the simulated umbo response is higher than any of the measured responses. The simulated response matches the resonance magnitude and frequency of gerbil I but has heavier damping in that frequency range,

more like that of the other gerbils. A more sophisticated model of damping may improve the results in this regard.

6.4.3.2 Manubrium

Similar to our experimental observations, the displacement magnitudes along the manubrium increase from the lateral process of the malleus toward the umbo. In our experimental data we saw a phase difference between the umbo and other manubrial points above 5 kHz. The model results show a noticeable phase difference between about 4.5 and 8 kHz only. The time-domain presentation of the manubrium motion (Figure 6.9) shows a rigid-body motion with a fixed axis of rotation at low frequencies. At higher frequencies there is no fixed axis of rotation and slight bending of the lower half of the manubrium appears. These observations should be further investigated in a future study with a particular focus on ossicular motion.

6.4.3.3 Pars tensa

The model provides pars-tensa responses similar to experimental responses. At low frequencies the displacements in the posterior region of the pars tensa are bigger than the ones in the anterior region. The frequency at which the simple low-frequency motion pattern breaks up is determined based on the phase divergence of 15° between pars tensa points. This is the criterion that we chose in our experimental study (Chapter 4). The break-up frequency and the bandwidths of the high-frequency response features in the model responses are in the range of experimental observations.

6.4.3.4 Stapes

The ossicular lever ratio of 3.2 resulting from the simulations is very close to the one calculated using analytical geometry on the reconstructed 3D model and also very close to what Rosowski

et al. (1999) reported based on 2D geometrical measurements. This suggests that the model acts as though it has a rotational axis close to the anatomical axis at low frequencies (up to about 500 Hz).

Between 5.5 and 6.5 kHz, the stapes response of the model shows minima in both magnitude and phase. The sensitivity analysis shows that this feature is very sensitive to the Poisson's ratio of the incudomalleolar joint. In order to make sure that this effect was not caused by having too few elements representing the joint (1434 elements), we refined the mesh of this structure, increasing the number of its elements by a factor of 8. Other than a shift to a slightly higher frequency, no other significant changes happened to this feature after the refinement. The feature is also sensitive to the properties of the pars tensa, ossicles, ligaments and cochlear load. Further explorations will be required to understand what causes this feature. Some of the experimental results presented in Figure 6.12 show similar behaviour in this frequency neighbourhood.

6.4.4 Model sensitivity

The model shows high sensitivity to the Poisson's ratios of the incudomalleolar and incudostapedial joints. In the present work, these synovial joints were modelled as simple elastic materials. The same material model was also used for the ligaments but the responses do not show the same level of sensitivity to the Poisson's ratios of the ligaments. The high sensitivity to the Poisson's ratio of the joints might be because the elements representing the joints are confined in the narrow spaces between the ossicles on either side, which do not easily accommodate incompressible element deformations. This makes the behaviour of the joint models very different near the limit of incompressibility (at a Poisson's ratio of 0.49) compared with its behaviour not so close to that limit (at a Poisson's ratio 10% smaller, 0.44). More sophisticated treatments of the joints may be very beneficial to the quality of the model.

Most features in the model responses do not show significant sensitivity to the parameters of the incus, posterior incudal ligament or stapes. Sensitivity to the malleus stiffness is probably due to the fact that the malleus is attached to the cavity wall at the tip of its anterior process. This very thin bone-to-bone attachment (with no ligament in between) permits rotation of the ossicles because of local deformation of the malleus.

At low frequencies the responses are dominated by the stiffness-related parameters. The thickness and Young's modulus of the pars tensa, the Young's modulus of the malleus and stapedial annular ligament and the Poisson's ratio of the joints have the greatest influence on the magnitude of the umbo displacement at low frequencies. The fact that the low-frequency lever ratio remains almost constant as these parameters are varied by $\pm 10\%$ (except for the change in the Poisson's ratio of the incudomalleal joint) implies that they also have the most influence on the low-frequency stapes displacement.

Damping of the cochlea mainly affects the sharpness of the middle-ear resonance peak. It has very little effect on the damping of high-frequency vibration features in the pars-tensa responses.

6.5 Acknowledgements

This work was supported in part by the Canadian Institutes of Health Research, the Fonds de recherche en santé du Québec, the Natural Sciences and Engineering Research Council (Canada), the Montréal Children's Hospital Research Institute, the McGill University Health Centre Research Institute and the Research Fund of Flanders (Belgium). Computations were made on the supercomputer Guillimin of McGill University, managed by Calcul Québec and Compute Canada; the operation of this supercomputer is funded by the Canada Foundation for Innovation, NanoQuébec, the Réseau de Médecine Génétique Appliquée and the Fonds de recherche du

Québec – Nature et technologies. We thank Clarinda Northrop for providing a collection of gerbil histological slides and Yu Xin Shen for digitizing and cataloguing the collection.

7 Conclusion

7.1 Summary

In this thesis, measurements of vibrations of the gerbil tympanic membrane with closed middle-ear cavity have been presented, as well as the effects of opening the middle ear cavity. To estimate ideal open-cavity responses from vibration measurements made in ears with a partial opening in the cavity wall, a theoretical method has been presented and validated. A finite-element model of the gerbil middle ear has been developed and it was shown that this model can reproduce key aspects of experimental observations. The knowledge obtained in this study and the finite-element model that embodies this knowledge can serve as the basis for further studies aimed at better tools for hearing screening, diagnosis and treatment.

7.2 Original contributions

1. Vibrations of the gerbil tympanic membrane were studied *in vivo*. The major findings are:
 - a) The magnitude minimum in the low-frequency displacement magnitude of the manubrium and pars tensa, due to the pars flaccida, was shown to become gradually less distinct with a greater degree of retraction of the pars flaccida.
 - b) Our multiple-point manubrial and pars-tensa measurements allowed us to observe that the broad resonance in the range of 1.6 to 2 kHz occurs at all points.
 - c) Our multiple-point measurements along the manubrium revealed that the manubrium rotates as rigid body around a fixed axis of rotation at low frequencies. Above 5 kHz

- the axis of rotation is not fixed and evidence of a slight bending of the manubrium is seen.
- d) Our multiple-point measurements revealed that the simple low-frequency vibration pattern of the pars tensa breaks up at between 1.8 and 2.8 kHz.
2. The effects of progressive opening of the middle-ear cavity on the vibrations of the tympanic membrane were studied. It was found that:
- a) The main increase in the low-frequency response magnitude happens upon making the smallest hole in the cavity wall, and further progressive enlarging of the opening has little or no effect on the low-frequency magnitude.
- b) Opening the cavity has little or no effect on either the mode of vibration of the manubrium or the breakup frequency of the pars tensa.
- c) When the opening is gradually widened the antiresonance frequency moves gradually to higher frequencies. The opening cannot be made big enough to move the antiresonance out of the frequency range of interest due to surgical limitations.
3. A method was developed to estimate the ideal open-cavity responses from vibration measurements made in ears with a partial opening in the cavity wall.
- a) The method has been validated against a synthesized frequency response and against a frequency response calculated using a middle-ear circuit model.
- b) The robustness of the method in handling different opening sizes and various frequency ranges for the fitting have been studied.

- c) The utility of the method to correct manubrial and pars-tensa responses has been shown.
4. A finite-element model of the gerbil middle ear was developed.
- a) Responses from the model were validated against our multiple-point vibrometry measurements on the pars tensa, pars flaccida and along the manubrium. The piston component of the stapes response from the model was compared with experimental data from the literature. The validation was done by investigating the similarity of certain features in the experimental responses with corresponding ones in the model responses, as opposed to simply calculating frequency-by-frequency differences between experimental and model responses.
 - b) With a set of baseline material parameters largely based on *a priori* estimates derived from measurements in the literature, this model reproduces key features of experimental observations.
 - c) A sensitivity analysis ranked the parameters in order of the importance of their effects on the response features.

7.3 Significance

As described in Chapter 1, the main motivation for performing the research presented in this thesis was the need for improved screening and diagnosis of hearing disorders in infants. The new or improved screening and diagnostic methods should be able to distinguish between conductive and sensorineural hearing loss. Tympanometry can be used to help in identifying conductive hearing loss but the response of the newborn ear to this test is not well understood. Tympanometry uses small-amplitude sound pressures (probe tones) to measure input admittance

or reflectance in the presence of large static pressures. A quantitative model of tympanometry is required. The multiple-point vibration-measurement data required for validation of such a model cannot be acquired in living human ears. Access to newborn temporal bones is extremely limited, and even if they are available they are affected by *post mortem* effects. In this thesis, a methodology for obtaining multiple-point vibration data from living gerbil ears was developed and baseline data at ambient pressure were obtained. The developed method can be used in human temporal bones, whether adult or newborn. The validated gerbil finite-element model will guide development of a finite-element model of the human ear for ambient pressure.

The experimental work, Chapters 4 and 5, established the groundwork for performing pressurized multiple-point vibration measurements in gerbil ears in the future, and the validated model presented in Chapter 6 will be the basis for developing a model of the gerbil ear under large static pressures. These pressurized experimental and modelling gerbil studies will subsequently guide work aimed at developing the first quantitative model of tympanometry in human newborns.

7.4 Future work

This work established the scientific ground for using the gerbil middle-ear finite-element model as a guide for developing a finite-element model for the human middle ear. This study should therefore be extended for both gerbil and human middle ears.

7.4.1 Future gerbil studies

To obtain a more complete view of tympanic-membrane vibrations, measurements at more points are required. The multiple-point measurements presented in this thesis have been extended to more points closer to the tympanic annulus in a preliminary study by He (2012). That method needs to be pursued. The number of measurement points can also be greatly increased by applying a reflective coating on the tympanic membrane (e.g., Dirckx & Decraemer, 1997). Making measurements at more points requires that the measurement time for each point be reduced, possibly by automation.

In another attempt to have motion data at more points, we have performed holographic measurements in gerbil ears in collaboration with Dr. Rosowski's team at Harvard University. These measurements give valuable high-spatial-resolution information about the motion of the entire tympanic membrane. However, in holographic measurements the frequency resolution is much lower than that of the multiple-point measurements presented in this thesis. Furthermore, the quality of the collected holographic data is poor in some areas of the tympanic membrane. We have developed an image-processing-based algorithm to deal with this problem. This algorithm needs to be further validated and then applied to the holographic data collected in gerbils. The improved holographic-measurement data could then be compared with the multiple-point measurements reported here.

The measurements here were done with a single viewing direction. 3-D motion measurements, like ones that have been done on the ossicles (e.g., Decraemer et al., 2014), are required to provide a complete view of tympanic-membrane motion at each measurement point and a better basis for validating the model results.

Because the main purpose of the modelling in this thesis was to validate the model results against the unidirectional multi-point experimental data, no 3-D model results were presented in this thesis. A related limitation is that we have processed model data only at nodes that correspond to where we made experimental measurements. This greatly reduced the computation time. A future study should compute frequency responses for all of the $\sim 84,000$ nodes in the model and report the 3-D motions in the gerbil middle ear. This will allow validation of the complete 3-D ossicular motion with the recent experimental data of Decraemer et al. (2007, 2014). A post-processing tool needs to be developed to allow visualization of the ossicular deformations that occur as part of a complex frequency-dependent mixture of deformations and rigid-body motions.

In the model developed in this thesis, for simplicity, the incudomalleolar and incudostapedial joints were assumed to be elastic solids and details of the synovial fluid, cartilage and joint capsule were not modelled. The model shows high sensitivity to the Poisson's ratios of the joints. This might be because the elements representing the joints are confined in the narrow spaces between the ossicles on either side, which do not easily accommodate incompressible element deformations. This makes the behaviour of the joint models very different near the limit of incompressibility compared with its behaviour not very far from that limit. More sophisticated treatments of the joints may be very beneficial to the quality of the model.

In Chapter 6 we discussed how our sensitivity analysis explored the near neighbourhood ($\pm 10\%$) of only one point (the baseline point) in the N -dimensional parameter space, and other points in this space remained unexplored. Additionally, interactions between parameters were not investigated. A future study should systematically explore other points beyond the neighbourhood explored here and the interactions between parameters.

For computational convenience, in this work the Rayleigh damping model was used. Although the Rayleigh model provides a practical way of dealing with damping, there is no physiological evidence in its favour. The use of this damping model might be the reason for having rather high magnitudes above the resonance frequency in the umbo responses. Other damping models, like the ones used by Zhang & Gan (2010) and Aernouts et al. (2012), should be explored in subsequent studies.

The model presented in this thesis, with an isotropic single-layer representation of the pars tensa, provides acceptable results in the range of experimental observations. However, the effects of the multiple layers and their presumed orthotropy (Chapter 2) may need to be explored to get even closer to the physiology. This may become more important when the model results are compared with experimental results that have higher spatial resolution.

As described above, tympanometry can be used to help in identifying conductive hearing loss. The experimental and modelling work presented in this thesis can serve as the basis for collecting the required experimental data and developing such models. The experiments presented in this thesis should be extended to pressurized measurements, that is, applying static pressures to the tympanic membrane and measuring its vibration. As a first attempt in this direction, in another study in our lab, Shapiro (2014) performed preliminary *post mortem* multiple-point measurements on the pressurized gerbil tympanic membrane. This work should be extended to more points and to *in vivo* measurements. The pressurization introduces nonlinearities into the problem so the model developed in this study should be extended to nonlinear regimes of motion as in our lab's static newborn human models (Qi et al., 2006, 2008). The nonlinear viscoelastic behaviour of the soft tissues can be modelled using the approaches developed in our lab by Charlebois et al. (2013) and Motallebzadeh et al. (2013).

The measurements and modelling in this thesis were limited to 10 kHz. A future study can try to extend this range to 20 kHz, to cover the entire human hearing range, or to extend it to 60 kHz to cover the gerbil hearing range. Because the sound pressure field is not uniform in these extended frequency ranges, point-wise pressure measurements should be done using a fibre-optic miniature microphone (Olson, 1998) or a better future solution. The model would then need an exact definition of the sound-pressure distribution over the TM. Alternatively, the ear canal and middle-ear cavity could be added to the model, as done for the human ear, for example, by Gan et al. (2004). After these additions, the experiments presented in Chapter 5, regarding progressive opening of the cavity wall, could be used to validate the model's predictions. This more complete model might provide some insight into how the method suggested for estimating ideal open-cavity responses could be improved.

7.4.2 Application to the human middle ear

In this study we were able to collect multiple-point experimental vibration data in living ears. This provided good data with which we could validate the model for the gerbil middle ear. It is not possible to collect such data in humans. We established a set of physiologically acceptable parameter values that enable the model to reproduce key features of the experimental observations. This study also established a modelling methodology, such as appropriate element formulations, damping model, time-integration scheme and time steps. A human middle-ear model needs to be developed based on the parameters and the modelling methodology established in this work.

References

- Aernouts, J., Aerts, J. R. M., & Dirckx, J. J. J. (2012). Mechanical properties of human tympanic membrane in the quasi-static regime from in situ point indentation measurements. *Hearing Research*, *290*(1–2), 45–54.
- Aernouts, J., & Dirckx, J. J. J. (2011). Elastic characterization of the gerbil pars flaccida from in situ inflation experiments. *Biomechanics and Modeling in Mechanobiology*, *10*(5), 727–741.
- Aernouts, J., & Dirckx, J. J. J. (2012). Static versus dynamic gerbil tympanic membrane elasticity: derivation of the complex modulus. *Biomechanics and Modeling in Mechanobiology*, *11*(6), 829–840.
- Aernouts, J., Soons, J. A. M., & Dirckx, J. J. J. (2010). Quantification of tympanic membrane elasticity parameters from in situ point indentation measurements: Validation and preliminary study. *Hearing Research*, *263*(1–2), 177–182.
- Agache, P. G., Monneur, C., Leveque, J. L., & Rigal, J. D. (1980). Mechanical properties and Young's modulus of human skin in vivo. *Archives of Dermatological Research*, *269*(3), 221–232.
- Aibara, R., Welsh, J. T., Puria, S., & Goode, R. L. (2001). Human middle-ear sound transfer function and cochlear input impedance. *Hearing Research*, *152*(1–2), 100–109.
- Akache, F., Funnell, W. R. J., & Daniel, S. J. (2007). An experimental study of tympanic membrane and manubrium vibrations in rats. *Audiology and Neurotology*, *12*(1), 49–58.
- Akinpelu, O. V., Peleva, E., Funnell, W. R. J., & Daniel, S. J. (2014). Otoacoustic emissions in newborn hearing screening: A systematic review of the effects of different protocols on test outcomes. *International Journal of Pediatric Otorhinolaryngology*, *78*(5), 711–717.
- Alm, P., Bloom, G., Hellström, S., Stenfors, L., & Widemar, L. (1983). Middle ear effusion

- caused by mechanical stimulation of the external auditory canal: an experimental study in the rat. *Acta Oto-Laryngologica*, 96(1-2), 91–98.
- Aziz, P. M., Sorensen, H. V., & Van Der Spiegel, J. (2002). An overview of sigma-delta converters. *Signal Processing Magazine, IEEE*, 13(1), 61–84.
- Von Bally, G. (1977). Holographic analysis of tympanic membrane vibrations in human temporal bone preparations using a double pulsed ruby laser system. In E. Marom, A. A. Friesem, & E. Wiener-Avneer (Eds.), *Applications of Holography and Optical Data Processing* (pp. 593–602). Pergamon. Retrieved from <http://www.sciencedirect.com/science/article/pii/B978008021625650066X>
- Von Bally, G. (1979). Holography in Otology. In G. von Bally (Ed.), *Holography in Medicine and Biology*, Springer Series in Optical Sciences (pp. 183–197). Springer Berlin Heidelberg. Retrieved from http://link.springer.com/chapter/10.1007/978-3-540-38961-3_26
- Von Bally, G. (1982). Otosopic Investigations by Holographic Interferometry: A Fiber Endoscopic Approach Using a Pulsed Ruby Laser System. In G. von Bally & P. D. P. Greguss (Eds.), *Optics in Biomedical Sciences*, Springer Series in Optical Sciences (pp. 110–114). Springer Berlin Heidelberg. Retrieved from http://link.springer.com/chapter/10.1007/978-3-540-39455-6_23
- Von Bally, G., & Baumeister, S. (1979). Otologische Untersuchungen mittels holographischer Interferometrie. *Archives of oto-rhino-laryngology*, 223(2-4), 181–183.
- Békésy, G. V. (1960). *Experiments in hearing* (Vol. 8). McGraw-Hill New York. Retrieved from http://asadl.org/books/01_03_11_experiments
- Von Békésy, G. (1960). *Experiments in hearing*. McGraw-Hill New York.
- Bergevin, C., & Olson, E. S. (2014). External and middle ear sound pressure distribution and acoustic coupling to the tympanic membrane. *The Journal of the Acoustical Society of America*, 135(3), 1294–1312.
- Bigelow, D. C., Swanson, P. B., & Saunders, J. C. (1996). The effect of tympanic membrane

- perforation size on umbo velocity in the rat. *The Laryngoscope*, 106(1), 71–76.
- Borg, E. (1968). A quantitative study of the effect of the acoustic stapedius reflex on sound transmission through the middle ear of man. *Acta oto-laryngologica*, 66(1-6), 461–472.
- Borg, E., & Zakrisson, J.-E. (1975). The Activity of the Stapedius Muscle in Man During Vocalization. *Acta Oto-laryngologica*, 79(3-6), 325–333.
- Bryant, W. S. (1890). Observations on the topography of normal human tympanum. *Archives of Otolaryngology*, XIX(4), 217–231.
- Buunen, T. J. F., & Vlaming, M. S. M. G. (1981). Laser--Doppler velocity meter applied to tympanic membrane vibrations in cat. *The Journal of the Acoustical Society of America*, 69(3), 744–750.
- Buytaert, J. A. N., Salih, W. H. M., Dierick, M., Jacobs, P., & Dirckx, J. J. J. (2011). Realistic 3D Computer Model of the Gerbil Middle Ear, Featuring Accurate Morphology of Bone and Soft Tissue Structures. *Journal of the Association for Research in Otolaryngology*, 12(6), 681–696.
- Carmel, P. W., & Starr, A. (1963). Acoustic and Nonacoustic Factors Modifying Middle-Ear Muscle Activity in Waking Cats. *Journal of Neurophysiology*, 26(4), 598–616.
- Castracane, J., Conerty, M., Cacace, A. T., Gardner, G. M., Miller, M. B., & Parnes, S. M. (1993). Advanced ESPI-based medical instruments for otolaryngology (Vol. 1893, pp. 33–42). Retrieved from <http://dx.doi.org/10.1117/12.146356>
- Chang, E. W., Cheng, J. T., Röösl, C., Kobler, J. B., Rosowski, J. J., & Yun, S. H. (2013). Simultaneous 3D imaging of sound-induced motions of the tympanic membrane and middle ear ossicles. *Hearing Research*, 304, 49–56.
- Charlebois, M., Motallebzadeh, H., & Funnell, W. R. J. (2013). Visco-hyperelastic law for finite deformations: a frequency analysis. *Biomechanics and Modeling in Mechanobiology*, 12(4), 705–715.
- Chen, C.-T. (2010). Signals and systems: A fresh look. Retrieved August 21, 2013, from <http://www.ece.sunysb.edu/~ctchen/media/freshlook.pdf>

- Cheng, J. T., Aarnisalo, A. A., Harrington, E., Hernandez-Montes, M. S., Furlong, C., Merchant, S. N., & Rosowski, J. J. (2010). Motion of the surface of the human tympanic membrane measured with stroboscopic holography. *Hearing Research*, 263(1-2), 66–77.
- Cheng, T., Dai, C., & Gan, R. Z. (2007). Viscoelastic Properties of Human Tympanic Membrane. *Annals of Biomedical Engineering*, 35(2), 305–314.
- Chole, R. A., & Kodama, K. (1989). Comparative histology of the tympanic membrane and its relationship to cholesteatoma. *The Annals of otology, rhinology, and laryngology*, 98(10), 761–766.
- Cohen, Y. E., Bacon, C. K., & Saunders, J. C. (1992). Middle ear development III: Morphometric changes in the conducting apparatus of the Mongolian gerbil. *Hearing Research*, 62(2), 187–193.
- Cohen, Y. E., Doan, D. E., Rubin, D. M., & Saunders, J. C. (1993). Middle-ear development. V: Development of umbo sensitivity in the gerbil. *American Journal of Otolaryngology*, 14(3), 191–198.
- Conerty, M. D., Castracane, J., Cacace, A. T., Parnes, S. M., Gardner, G. M., & Miller, M. B. (1995). Preliminary results of real-time in-vitro electronic speckle pattern interferometry (ESPI) measurements in otolaryngology (Vol. 2395, pp. 124–134). Retrieved from <http://dx.doi.org/10.1117/12.209093>
- Dai, C., Cheng, T., Wood, M. W., & Gan, R. Z. (2007). Fixation and detachment of superior and anterior malleolar ligaments in human middle ear: Experiment and modeling. *Hearing research*, 230(1-2), 24–33.
- Dancer, A. L., Franke, R. B., Smigielski, P., Albe, F., & Fagot, H. (1975). Holographic interferometry applied to the investigation of tympanic-membrane displacements in guinea pig ears subjected to acoustic impulses. *The Journal of the Acoustical Society of America*, 58(1), 223–228.
- Daniel, S. J., Funnell, W. R. J., Zeitouni, A. G., Schloss, M. D., & Rappaport, J. (2001). Clinical Applications of a Finite-Element Model of the Human Middle Ear. *Journal of*

- Otolaryngology*, 30(6), 340.
- Daphalapurkar, N. P., Dai, C., Gan, R. Z., & Lu, H. (2009). Characterization of the linearly viscoelastic behavior of human tympanic membrane by nanoindentation. *Journal of the Mechanical Behavior of Biomedical Materials*, 2(1), 82–92.
- Davies, D. V. (1948). A Note on the Articulations of the Auditory Ossicles and Related Structures. *The Journal of Laryngology & Otology*, 62(08), 533–536.
- Decraemer, W. F., Dirckx, J. J. J., & Funnell, W. R. J. (2003). Three-Dimensional Modelling of the Middle-Ear Ossicular Chain Using a Commercial High-Resolution X-Ray CT Scanner. *Journal of the Association for Research in Otolaryngology*, 4(2), 250–263.
- Decraemer, W. F., Dirckx, J. J. J., Maftoon, N., & Funnell, W. R. (2010). Simulating large deformations of the gerbil pars flaccida to determine its material properties. *33rd Midwinter Research Meeting., Association for research in otolaryngology*. Presented at the 33rd Midwinter Research Meeting, Association for research in otolaryngology, Anaheim, USA. Retrieved from http://www.aro.org/archives/2010/2010_48_1287521996.html
- Decraemer, W. F., & Funnell, W. R. J. (2008). Anatomical and mechanical properties of the tympanic membrane. *Chronic otitis media: Pathogenesis-oriented therapeutic management*, 51.
- Decraemer, W. F., Khanna, S. M., & Funnell, W. R. (1989). Interferometric measurement of the amplitude and phase of tympanic membrane vibrations in cat. *Hearing research*, 38(1-2), 1–17.
- Decraemer, W. F., Khanna, S. M., & Funnell, W. R. (1991). Malleus vibration mode changes with frequency. *Hearing research*, 54(2), 305–318.
- Decraemer, W. F., Khanna, S. M., & Funnell, W. R. J. (1994a). A method for determining three-dimensional vibration in the ear. *Hearing research*, 77(1-2), 19–37.
- Decraemer, W. F., Khanna, S. M., & Funnell, W. R. J. (1994b). Bending of the manubrium in cat under normal sound stimulation. *Proc Opt Imaging Tech Biomed*, 2329, 74–84.

- Decraemer, W. F., Khanna, S. M., & Funnell, W. R. J. (1999). Vibrations at a fine grid of points on the cat tympanic membrane measured with a heterodyne interferometer. *EOS/SPIE International Symposia on Industrial Lasers and Inspection, Conference on Biomedical Laser and Metrology and Applications*.
- Decraemer, W. F., de La Rochefoucauld, O., & Olson, E. S. (2011a). Measurement of the Three-Dimensional Vibration Motion of the Ossicular Chain in the Living Gerbil. In C. A. Shera & E. S. Olson (Eds.), *Proceedings of the 11th International Mechanics of Hearing Workshop* (Vol. 1403, pp. 528–533). Presented at the What fire is in mine ears: Progress in auditory biomechanics. Retrieved from <http://link.aip.org/link/?APC/1403/528/1>
- Decraemer, W. F., Maes, M. A., & Vanhuysse, V. J. (1980). An elastic stress-strain relation for soft biological tissues based on a structural model. *Journal of Biomechanics*, *13*(6), 463–468.
- Decraemer, W. F., Maftoon, N., Dirckx, J. J. J., & Funnell, W. R. J. (2011b). The effects of the asymmetric shape of the tympanic membrane on the asymmetry of ossicular displacements for positive and negative static pressures. *34th ARO MidWinter Meeting*. Retrieved from http://www.aro.org/archives/2011/2011_52_1305771725.html
- Decraemer, W. F., Rochefoucauld, O. de L., Dong, W., Khanna, S. M., Dirckx, J. J. J., & Olson, E. S. (2007). Scala vestibuli pressure and three-dimensional stapes velocity measured in direct succession in gerbil. *The Journal of the Acoustical Society of America*, *121*(5), 2774–2791.
- Decraemer, W. F., Rochefoucauld, O. de L., Funnell, W. R. J., & Olson, E. S. (2014). Three-Dimensional Vibration of the Malleus and Incus in the Living Gerbil. *Journal of the Association for Research in Otolaryngology*, 1–28.
- Dirckx, J. J., Decraemer, W., von Unge, M., & Larsson, C. (1997). Measurement and modeling of boundary shape and surface deformation of the Mongolian gerbil pars flaccida. *Hearing Research*, *111*(1-2), 153–164.
- Dirckx, J. J. J., & Decraemer, W. F. (1997). Coating techniques in optical interferometric metrology. *Applied Optics*, *36*(13), 2776–2782.

- Dirckx, J. J. J., & Decraemer, W. F. (2001). Effect of middle ear components on eardrum quasi-static deformation. *Hearing Research*, 157(1-2), 124–137.
- Dirckx, J. J. J., Decraemer, W. F., von Unge, M., & Larsson, C. (1998). Volume displacement of the gerbil eardrum pars flaccida as a function of middle ear pressure. *Hearing research*, 118(1-2), 35–46.
- Djupesland, G. (1965). Electromyography of the tympanic muscles in man. *International Journal of Audiology*, 4(1), 34–41.
- Doyle, W. J., Alper, C. M., & Seroky, J. T. (1999). Trans-mucosal inert gas exchange constants for the monkey middle ear. *Auris Nasus Larynx*, 26(1), 5–12.
- Doyle, W. J., Seroky, J. T., & Alper, C. M. (1995). Gas Exchange Across the Middle Ear Mucosa in Monkeys: Estimation of Exchange Rate. *Arch Otolaryngol Head Neck Surg*, 121(8), 887–892.
- Elkhouri, N., Liu, H., & Funnell, W. R. (2006). Low-frequency finite-element modeling of the gerbil middle ear. *JARO-Journal of the Association for Research in Otolaryngology*, 7(4), 399–411.
- Ellaham, N. (2008). *An experimental study of middle-ear vibrations in gerbils* (Master of Engineering thesis). Montréal, Canada: McGill University.
- Ellaham, N. N., Akache, F., Funnell, W. R., & Daniel, S. J. (2007). Experimental study of the effects of drying on middle-ear vibrations in the gerbil. *30th Ann Conf Can Med Biol Eng Soc*. Presented at the 30th Ann Conf Can Med Biol Eng Soc, Toronto.
- Emgård, P., & Hellström, S. (1997). An animal model for external otitis. *European Archives of Oto-rhino-laryngology*, 254(3), 115–119.
- Eriksson, P., Mattsson, C., & Hellstrom, S. (2003). First forty-eight hours of developing otitis media: An experimental study. *Annals of Otology Rhinology and Laryngology*, 112(6), 558–566.
- Fay, J. P., Puria, S., & Steele, C. R. (2006). The discordant eardrum. *Proceedings of the National Academy of Sciences*, 103(52), 19743–19748.

- Fay, J., Puria, S., Decraemer, W. F., & Steele, C. (2005). Three approaches for estimating the elastic modulus of the tympanic membrane. *Journal of Biomechanics*, 38(9), 1807–1815.
- Ferrazzini, M. (2003). *Virtual middle ear: a dynamic mathematical model based on the finite element method*. ETH Zürich. Retrieved from <http://cds.cern.ch/record/894552>
- Ferreira, A., Gentil, F., & Tavares, J. M. R. S. (2012). Segmentation algorithms for ear image data towards biomechanical studies. *Computer methods in biomechanics and biomedical engineering*.
- Ferris, P., & Prendergast, P. J. (2000). Middle-ear dynamics before and after ossicular replacement. *Journal of Biomechanics*, 33(5), 581–590.
- Flisberg, K., Ingelstedt, S., & Örtengren, U. (1963). On middle ear pressure. *Acta Oto-Laryngologica*, 56(S182), 43–56.
- Formenti, D., & Richardson, M. (2002). Parameter estimation from frequency response measurements using rational fraction polynomials (twenty years of progress). *Proceedings of the 20th International Modal Analysis Conference, Orlando, Florida*. Retrieved from <http://systemplus.co.jp/support/data/techpaper/mescope/tech/39.pdf>
- Forsythe, G. E. (1957). Generation and use of orthogonal polynomials for data-fitting with a digital computer. *Journal of the Society for Industrial & Applied Mathematics*, 5(2), 74–88.
- Franklin, G. F. (1990). *Digital control of dynamic systems* (2nd ed.). Reading, Mass: Addison-Wesley Pub. Co.
- Fritze, W., Kreitlow, H., & Winter, D. (1979). On Holographic-Interferometric Investigations of the Membrana Tympani (Living Man). In D. P. G. von Bally (Ed.), *Holography in Medicine and Biology*, Springer Series in Optical Sciences (pp. 206–211). Springer Berlin Heidelberg. Retrieved from http://link.springer.com/chapter/10.1007/978-3-540-38961-3_28
- Fulghum, R. S., & Marrow, H. G. (1996). Experimental otitis media with *Moraxella* (Branhamella) catarrhalis. *The Annals of Otolaryngology, Rhinology, and Laryngology*, 105(3),

234–241.

- Fumagalli, Z. (1949). *Ricerche morfologiche sull'apparato di trasmissione del suono. Sound-conducting apparatus: a study of morphology*. Milano: Istituto per la diffusione di opere scientifiche.
- Funnell, W. R., Decraemer, W. F., & Khanna, S. M. (1987). On the damped frequency response of a finite-element model of the cat eardrum. *The Journal of the Acoustical Society of America*, *81*, 1851.
- Funnell, W. R., Heng Siah, T., McKee, M. D., Daniel, S. J., & Decraemer, W. F. (2005). On the Coupling Between the Incus and the Stapes in the Cat. *JARO: Journal of the Association for Research in Otolaryngology*, *6*(1), 9–18.
- Funnell, W. R. J. (1983). On the undamped natural frequencies and mode shapes of a finite-element model of the cat eardrum. *The Journal of the Acoustical Society of America*, *73*, 1657.
- Funnell, W. R. J. (2001). High-frequency time-domain behaviour of a finite-element model of the eardrum. Presented at the 24th Midwinter Research Meeting of the Association for Research in Otolaryngology, St. Petersburg Beach, FL. Retrieved from <http://audilab.bme.mcgill.ca/AudiLab/research.html>
- Funnell, W. R. J., & Decraemer, W. F. (1996). On the incorporation of moiré shape measurements in finite-element models of the cat eardrum. *The Journal of the Acoustical Society of America*, *100*(2), 925–932.
- Funnell, W. R. J., Decraemer, W. F., Von Unge, M., & Dirckx, J. J. J. (1999). Finite-element modelling of the gerbil eardrum and middle ear. *22nd ARO MidWinter Meeting*. Retrieved from <http://www.aro.org/archives/1999/799.html>
- Funnell, W. R. J., Decraemer, W. F., Von Unge, M., & Dirckx, J. J. J. (2000). Finite-element modelling of the gerbil eardrum and middle ear. *23rd ARO MidWinter Meeting*. Retrieved from <http://www.aro.org/archives/1999/799.html>
- Funnell, W. R. J., Khanna, S. M., & Decraemer, W. F. (1992). On the degree of rigidity of the

- manubrium in a finite-element model of the cat eardrum. *The Journal of the Acoustical Society of America*, 91(4), 2082–2090.
- Funnell, W. R. J., & Laszlo, C. A. (1982). A critical review of experimental observations on eardrum structure and function. *ORL*, 44(4), 181–205.
- Funnell, W. R. J., Maftoon, N., & Decraemer, W. F. (2012). Mechanics and modelling for the middle ear. Retrieved March 3, 2013, from <http://audilab.bme.mcgill.ca/~funnell/AudiLab/mammie/mammie.pdf>
- Funnell, W. R. J., Maftoon, N., & Decraemer, W. F. (2013). Modeling of Middle-Ear Mechanics. In S. Puria, R. R. Fay, & A. N. Popper (Eds.), *The Middle Ear - Science, Otolaryngology, and Technology*.
- Funnell, W. R., & Laszlo, C. A. (1978). Modeling of the cat eardrum as a thin shell using the finite-element method. *The Journal of the Acoustical Society of America*, 63, 1461.
- Furlong, C., Rosowski, J. J., Hulli, N., & Ravicz, M. E. (2009). Preliminary Analyses of Tympanic-Membrane Motion from Holographic Measurements. *Strain*, 45(3), 301–309.
- Gaihede, M., Liao, D., & Gregersen, H. (2007). In vivo areal modulus of elasticity estimation of the human tympanic membrane system: modelling of middle ear mechanical function in normal young and aged ears. *Physics in medicine and biology*, 52(3), 803–814.
- Gan, R. Z., Cheng, T., Dai, C., Yang, F., & Wood, M. W. (2009). Finite element modeling of sound transmission with perforations of tympanic membrane. *The Journal of the Acoustical Society of America*, 126, 243.
- Gan, R. Z., Feng, B., & Sun, Q. (2004). Three-Dimensional Finite Element Modeling of Human Ear for Sound Transmission. *Annals of Biomedical Engineering*, 32(6), 847–859.
- Gan, R. Z., Reeves, B. P., & Wang, X. (2007). Modeling of sound transmission from ear canal to cochlea. *Annals of biomedical engineering*, 35(12), 2180–2195.
- Gan, R. Z., Sun, Q., Dyer Jr, R. K., Chang, K. H., & Dormer, K. J. (2002). Three-dimensional modeling of middle ear biomechanics and its applications. *Otology & Neurotology*, 23(3), 271.

- Gan, R. Z., Sun, Q., Feng, B., & Wood, M. W. (2006). Acoustic-structural coupled finite element analysis for sound transmission in human ear—Pressure distributions. *Medical engineering & physics*, 28(5), 395–404.
- Gan, R. Z., & Wang, X. (2007). Multifield coupled finite element analysis for sound transmission in otitis media with effusion. *The Journal of the Acoustical Society of America*, 122, 3527.
- Gan, R. Z., Yang, F., Zhang, X., & Nakmali, D. (2011). Mechanical Properties of Stapedial Annular Ligament. *Medical engineering & physics*, 33(3), 330–339.
- Gea, S. L. R., Decraemer, W. F., Funnell, R. W. J., Dirckx, J. J. J., & Maier, H. (2009). Tympanic Membrane Boundary Deformations Derived from Static Displacements Observed with Computerized Tomography in Human and Gerbil. *Journal of the Association for Research in Otolaryngology*, 11(1), 1–17.
- Geerligs, M., van Breemen, L., Peters, G., Ackermans, P., Baaijens, F., & Oomens, C. (2011). In vitro indentation to determine the mechanical properties of epidermis. *Journal of Biomechanics*, 44(6), 1176–1181.
- Gentil, F., Jorge, R. N., Ferreira, A. J. M., Parente, M. P. L., Moreira, M., & Almeida, E. (2005). Biomechanical study of middle ear. *Proc. COMPLAS VIII* (Vol. 2, pp. 785–788). Retrieved from <http://congress.cimne.upc.es/complas05/admin/Files/FilePaper/p313.pdf>
- Geuzaine, C., & Remacle, J.-F. (2009). Gmsh: A 3-D finite element mesh generator with built-in pre- and post-processing facilities. *International Journal for Numerical Methods in Engineering*, 79(11), 1309–1331.
- Ghadarghadar, N., Agrawal, S. K., Samani, A., & Ladak, H. M. (2013). Estimation of the quasi-static Young's modulus of the eardrum using a pressurization technique. *Computer Methods and Programs in Biomedicine*, 110(3), 231–239.
- Guilford, F. R., & Anson, B. J. (1967). Osseous fixation of the malleus. *Transactions - American Academy of Ophthalmology and Otolaryngology. American Academy of Ophthalmology and Otolaryngology*, 71(3), 398–407.

- Guinan, J. J., & Peake, W. T. (1967). Middle-ear characteristics of anesthetized cats. *The Journal of the Acoustical Society of America*, 41(5), 1237–1261.
- Gulya, A. J., & Schuknech, H. F. (1994). *Anatomy of the Temporal Bone with Surgical Implications, Second Edition*. Taylor & Francis.
- Gutiérrez Acuña, C. (2003). Rational Fraction Polynomial Method. MATLAB Central File Exchange. Retrieved from <http://www.mathworks.com/matlabcentral/fileexchange/3805-rational-fraction-polynomial-method>
- Hartwein, J. H. J., & Rauchfuss, A. (1987). The development of the ossicular ligaments in the human middle ear. *Archives of oto-rhino-laryngology*, 244(1), 23–25.
- Harty, M. (1953). Elastic Tissue in the Middle-Ear Cavity. *The Journal of Laryngology & Otology*, 67(12), 723–729.
- Hellström, S., Goldie, P., Salén, B., & Stenfors, L.-E. (1985). Mechanisms in middle ear effusion production caused by irritation of the external auditory canal. *American Journal of Otolaryngology*, 6(3), 220–222.
- Hernandez-Montes, M. S., Mendoza Santoyo, F., Perez Lopez, C., Munoz Solis, S., & Esquivel, J. (2011). Digital holographic interferometry applied to the study of tympanic membrane displacements. *Optics and Lasers in Engineering*.
- Hesabgar, S. M., Marshall, H., Agrawal, S. K., Samani, A., & Ladak, H. M. (2010). Measuring the quasi-static Young's modulus of the eardrum using an indentation technique. *Hearing Research*, 263(1–2), 168–176.
- He, Z. (2012). *Vibration measurements on the widely exposed gerbil eardrum*. McGill University.
- Hiraide, F., & Eriksson, H. (1978). The effects of the vacuum on vascular permeability of the middle ear. *Acta Oto-Laryngologica*, 85(1-6), 10–16.
- Hiraide, F., & Paparella, M. M. (1972). Vascular Changes in Middle Ear Effusions. *Archives of Otolaryngology—Head & Neck Surgery*, 96(1), 45–51.
- Huang, G., Gan, R. Z., Lu, H., & Daphalapurkar, N. P. (2008). A Method for Measuring Linearly

- Viscoelastic Properties of Human Tympanic Membrane Using Nanoindentation. *Journal of Biomechanical Engineering*, 130(1), 014501–014501.
- Huang, G. T., Rosowski, J. J., Flandermeyer, D. T., Iii, T. J. L., & Peake, W. T. (1997). The middle ear of a lion: Comparison of structure and function to domestic cat. *The Journal of the Acoustical Society of America*, 101(3), 1532–1549.
- Huber, A., Koike, T., Wada, H., Nandapalan, V., & Fisch, U. (2003). Fixation of the anterior malleolar ligament: diagnosis and consequences for hearing results in stapes surgery. *ANNALS OF OTOTOLOGY RHINOLOGY AND LARYNGOLOGY*, 112(4), 348–355.
- Hutchings, M. (1987). The gerbil as an animal model of otitis media with effusion. *Journal of Physiology (London)*, 396, 175.
- Irvine, D. R. F. (1976). Effects of reflex middle-ear muscle contractions on cochlear responses to bone-conducted sound. *International Journal of Audiology*, 15(5), 433–444.
- Ishihara, M. (1989). Experimental study of vibration analysis in middle ear models by holographic interferometry. Effects of the cross-sectioned area of aditus on the vibration of tympanic membrane. *Nihon Jibiinkoka Gakkai Kaiho*, 92(5), 726–735.
- Joint Committee on Infant Hearing. (2007). Year 2007 Position Statement: Principles and Guidelines for Early Hearing Detection and Intervention Programs. *Pediatrics*, 120(4), 898–921.
- Joint Committee on Infant Hearing, American Academy of Audiology, American Academy of Pediatrics, American Speech-Language-Hearing Association, & Directors of Speech and Hearing Programs in State Health and Welfare Agencies. (2000). Year 2000 Position Statement: Principles and Guidelines for Early Hearing Detection and Intervention Programs. *Pediatrics*, 106(4), 798–817.
- Kawase, T., Shibata, S., Katori, Y., Ohtsuka, A., Murakami, G., & Fujimiya, M. (2012). Elastic fiber-mediated entheses in the human middle ear. *Journal of Anatomy*, 221(4), 331–340.
- Kelly, D. J., Prendergast, P. J., & Blayney, A. W. (2003). The effect of prosthesis design on vibration of the reconstructed ossicular chain: a comparative finite element analysis of

- four prostheses. *Otology & Neurotology*, 24(1), 11.
- Kelly, L. G. (1967). *Handbook of numerical methods and applications*. Addison-Wesley Pub. Co.
- Khaleghi, M., Lu, W., Dobrev, I., Cheng, J. T., Furlong, C., & Rosowski, J. J. (2013). Digital holographic measurements of shape and three-dimensional sound-induced displacements of tympanic membrane. *Optical Engineering*, 52(10), 101916–101916.
- Khanna, S. M., & Tonndorf, J. (1972). Tympanic Membrane Vibrations in Cats Studied by Time-Averaged Holography. *The Journal of the Acoustical Society of America*, 51, 1904.
- Kim, N., Homma, K., & Puria, S. (2011). Inertial Bone Conduction: Symmetric and Anti-Symmetric Components. *Journal of the Association for Research in Otolaryngology*, 12(3), 261–279.
- Kirikae, I. (1960). *The structure and function of the middle ear*. Tokyo: University of Tokyo Press.
- Kobayashi, M. (1955). The articulations of the auditory ossicles and their ligaments of various species of mammalian animals. *Hiroshima J Med Sci*, 4, 319–349.
- Kohllöffel, L. U. E. (1984). Notes on the comparative mechanics of hearing. III. On Shrapnell's membrane. *Hearing Research*, 13(1), 83–88.
- Koike, T., Wada, H., & Kobayashi, T. (2002). Modeling of the human middle ear using the finite-element method. *The Journal of the Acoustical Society of America*, 111, 1306.
- Konrédsson, K. S., Ivarsson, A., & Bank, G. (1987). Computerized Laser Doppler Interferometric Scanning of the Vibrating Tympanic Membrane. *Scandinavian Audiology*, 16(3), 159–166.
- Kuhl, P., Williams, K., Lacerda, F., Stevens, K., & Lindblom, B. (1992). Linguistic experience alters phonetic perception in infants by 6 months of age. *Science*, 255(5044), 606–608.
- Kuypers, L. C., Dirckx, J. J. J., Decraemer, W. F., & Timmermans, J.-P. (2005). Thickness of the gerbil tympanic membrane measured with confocal microscopy. *Hearing Research*, 209(1–2), 42–52.
- Ladak, H. M., & Funnell, W. R. (1996). Finite-element modeling of the normal and surgically

- repaired cat middle ear. *The Journal of the Acoustical Society of America*, 100, 933.
- Ladak, H. M., Funnell, W. R., Decraemer, W. F., & Dirckx, J. J. (2006). A geometrically nonlinear finite-element model of the cat eardrum. *The Journal of the Acoustical Society of America*, 119, 2859.
- De La Rochefoucauld, O., Decraemer, W. F., Khanna, S. M., & Olson, E. S. (2008). Simultaneous measurements of ossicular velocity and intracochlear pressure leading to the cochlear input impedance in gerbil. *JARO - Journal of the Association for Research in Otolaryngology*, 9(2), 161–177.
- De La Rochefoucauld, O., Kachroo, P., & Olson, E. S. (2010). Ossicular motion related to middle ear transmission delay in gerbil. *Hearing Research*, 270(1-2), 158–172.
- De La Rochefoucauld, O., & Olson, E. S. (2010). A sum of simple and complex motions on the eardrum and manubrium in gerbil. *Hearing Research*, 263(1-2), 9–15.
- Larsson, C., Dirckx, J. J. J., Bagger-Sjöbäck, D., & von Unge, M. (2005). Pars flaccida displacement pattern in otitis media with effusion in the gerbil. *Otology & Neurotology*, 26(3), 337.
- Lay, D. M. (1972). The anatomy, physiology, functional significance and evolution of specialized hearing organs of gerbilline rodents. *Journal of morphology*, 138(1), 41–120.
- Lee, C.-F., Chen, J.-H., Chou, Y.-F., Hsu, L.-P., Chen, P.-R., & Liu, T.-C. (2007). Optimal Graft Thickness for Different Sizes of Tympanic Membrane Perforation in Cartilage Myringoplasty: A Finite Element Analysis. *The Laryngoscope*, 117(4), 725–730.
- Lee, C.-F., Hsu, L.-P., Chen, P.-R., Chou, Y.-F., Chen, J.-H., & Liu, T.-C. (2006). Biomechanical Modeling and Design Optimization of Cartilage Myringoplasty Using Finite Element Analysis. *Audiology and Neurotology*, 11(6), 380–388.
- Lee, C. Y., & Rosowski, J. J. (2001). Effects of middle-ear static pressure on pars tensa and pars flaccida of gerbil ears. *Hearing research*, 153(1-2), 146–163.
- Lesser, T. H. J., & Williams, K. R. (1988). The tympanic membrane in cross section: a finite element analysis. *The Journal of Laryngology and Otology*, 102(03), 209–214.

- Lesser, T. h. j., Williams, K. r., & Blayney, A. w. (1991). Mechanics and materials in middle ear reconstruction. *Clinical Otolaryngology & Allied Sciences*, *16*(1), 29–32.
- Lim, D. J. (1968a). Tympanic Membrane: Electron microscopic observation part I: pars tensa. *Acta oto-laryngologica*, *66*(1-6), 181–198.
- Lim, D. J. (1968b). Tympanic Membrane Part II.: Pars Flaccida. *Acta oto-laryngologica*, *66*(1-6), 515–532.
- Lim, D. J. (1970). Human tympanic membrane: an ultrastructural observation. *Acta oto-laryngologica*, *70*(3), 176–186.
- Ljung, L. (1999). *System identification: theory for the user*. Prentice-Hall information and system sciences series (2nd ed.). Upper Saddle River, NJ: Prentice Hall PTR.
- Løkberg, O. J., Høgmoen, K., & Gundersen, T. (1980). Vibration Measurement of the Human Tympanic Membrane-In Vivo. *Acta Oto-Laryngologica*, *89*(1-2), 37–42.
- Løkberg, O. J., Høgmoen, K., & Gundersen, T. (1979). Use of ESPI to Measure the Vibration of the Human Eardrum in vivo and Other Biological Movements. In D. P. G. von Bally (Ed.), *Holography in Medicine and Biology*, Springer Series in Optical Sciences (pp. 212–217). Springer Berlin Heidelberg. Retrieved from http://link.springer.com/chapter/10.1007/978-3-540-38961-3_29
- Luo, H., Dai, C., Lu, H., & Gan, R. Z. (2009). Measurement of Young's Modulus of Human Tympanic Membrane at High Strain Rates. *Journal of Biomechanical Engineering*, *131*(6), 064501–064501.
- Lynch, T. J., III, Peake, W. T., & Rosowski, J. J. (1994). Measurements of the acoustic input impedance of cat ears: 10 Hz to 20 kHz. *The Journal of the Acoustical Society of America*, *96*(4), 2184–2209.
- Lynch, T. J. I., Nedzelnitsky, V., & Peake, W. T. (1982). Input impedance of the cochlea in cat. *The Journal of the Acoustical Society of America*, *72*(1), 108–130.
- Maeta, M. (1991). [Effects of the perforation of the tympanic membrane on its vibration--with special reference to an experimental study by holographic interferometry]. *Nihon*

- Jibiinkoka Gakkai Kaiho*, 94(2), 231–240.
- Maftoon, N., Nambiar, S., Funnell, W. R. J., Decraemer, W. F., & Daniel, S. J. (2011). Experimental and modelling study of gerbil tympanic-membrane vibrations. *34th ARO MidWinter Meeting*. Retrieved from http://www.aro.org/archives/2011/2011_46_1305771725.html
- Maia, N. M. M., & Ewins, D. J. (1989). A new approach for the modal identification of lightly damped structures. *Mechanical Systems and Signal Processing*, 3(2), 173–193.
- Manley, G. A. (1972a). The middle ear of the Tokay Gecko. *Journal of comparative physiology*, 81(3), 239–250.
- Manley, G. A. (1972b). Frequency response of the middle ear of geckos. *Journal of comparative physiology*, 81(3), 251–258.
- Manley, G. A., & Johnstone, B. M. (1974). Middle-ear function in the guinea pig. *The Journal of the Acoustical Society of America*, 56(2), 571–576.
- Meruane, V. (2013). Model updating using antiresonant frequencies identified from transmissibility functions. *Journal of Sound and Vibration*, 332(4), 807–820.
- Mikhael, C. (2005). *Finite-element Modelling of the Human Middle Ear*. McGill University.
- Mikhael, C. S., Funnell, W. R. J., & Bance, M. (2004). Middle-ear finite-element modelling with realistic geometry and a priori material-property estimates. *28th Ann Conf Can Med Biol Eng Soc* (pp. 126–129). Retrieved from http:// earmuff.biomed.mcgill.ca/AudiLab/pubs/mikhael_funnell_bance_2004.pdf
- Møller, A. R. (1965). An experimental study of the acoustic impedance of the middle ear and its transmission properties. *Acta oto-laryngologica*, 60(1-6), 129–149.
- Motallebzadeh, H., Charlebois, M., & Funnell, W. R. J. (2013). A non-linear viscoelastic model for the tympanic membrane. *The Journal of the Acoustical Society of America*, 134(6), 4427–4434.
- Nambiar, S. (2010). *An experimental study of middle-ear vibrations in gerbils* (Master of Engineering thesis). Montréal, Canada: McGill University. Retrieved from

http://digitool.library.mcgill.ca/R/-?func=dbin-jump-full&object_id=86940¤t_base=GEN01

- Nandapalan, V., Pollak, A., Langner, A., & Fisch, U. (2002). The anterior and superior malleal ligaments in otosclerosis: a histopathologic observation. *Otology & neurotology: official publication of the American Otological Society, American Neurotology Society [and] European Academy of Otology and Neurotology*, 23(6), 854–861.
- Newmark, N. M. (1959). A Method of Computation for Structural Dynamics. *Journal of the Engineering Mechanics Division*, 85(7), 67–94.
- Nicolas, G., & Fouquet, T. (2013). Adaptive mesh refinement for conformal hexahedral meshes. *Finite Elements in Analysis and Design*, 67, 1–12.
- Nummela, S. (1995). Scaling of the mammalian middle ear. *Hearing Research*, 85(1-2), 18–30.
- Ohashi, M., Ide, S., Kimitsuki, T., Komune, S., & Suganuma, T. (2006). Three-dimensional regular arrangement of the annular ligament of the rat stapediovestibular joint. *Hearing Research*, 213(1–2), 11–16.
- Okano, K. (1990). [Influence of liquid volume in the middle ear on tympanic membrane vibration (experimental study by holographic interferometry)]. *Nihon Jibiinkoka Gakkai Kaiho*, 93(11), 1847–1855.
- Olson, E. S. (1998). Observing middle and inner ear mechanics with novel intracochlear pressure sensors. *The Journal of the Acoustical Society of America*, 103(6), 3445.
- Overstreet, E. H. I., & Ruggero, M. A. (2002). Development of wide-band middle ear transmission in the Mongolian gerbil. *The Journal of the Acoustical Society of America*, 111, 261.
- Pang, X. D., & Guinan, J. J. J. (1997). Effects of stapedius-muscle contractions on the masking of auditory-nerve responses. *The Journal of the Acoustical Society of America*, 102(6), 3576–3586.
- Paradise, J. L. (1999). Universal Newborn Hearing Screening: Should We Leap Before We Look? *Pediatrics*, 103(3), 670–672.

- Prendergast, P. J., Ferris, P., Rice, H. J., & Blayney, A. W. (1999). Vibro-Acoustic Modelling of the Outer and Middle Ear Using the Finite-Element Method. *Audiology and Neuro-Otology*, 4(3-4), 185–191.
- Qi, L., Funnell, W. R., & Daniel, S. J. (2008). A nonlinear finite-element model of the newborn middle ear. *The Journal of the Acoustical Society of America*, 124, 337.
- Qi, L., Liu, H., Lutfy, J., Funnell, W. R., & Daniel, S. J. (2006). A nonlinear finite-element model of the newborn ear canal. *The Journal of the Acoustical Society of America*, 120, 3789.
- Qin, Z., Wood, M., & Rosowski, J. J. (2010). Measurement of conductive hearing loss in mice. *Hearing Research*, 263(1–2), 93–103.
- Rabbitt, R. D., & Holmes, M. H. (1986). A fibrous dynamic continuum model of the tympanic membrane. *The Journal of the Acoustical Society of America*, 80(6), 1716–1728.
- Ravicz, M. E., Cooper, N. P., & Rosowski, J. J. (2008). Gerbil middle-ear sound transmission from 100 Hz to 60 kHz. *The Journal of the Acoustical Society of America*, 124, 363.
- Ravicz, M. E., Olson, E. S., & Rosowski, J. J. (2007). Sound pressure distribution and power flow within the gerbil ear canal from 100 Hz to 80 kHz. *The Journal of the Acoustical Society of America*, 122(4), 2154–2173.
- Ravicz, M. E., & Rosowski, J. J. (1997). Sound-power collection by the auditory periphery of the Mongolian gerbil *Meriones unguiculatus*: III. Effect of variations in middle-ear volume. *The Journal of the Acoustical Society of America*, 101, 2135.
- Ravicz, M. E., Rosowski, J. J., & Voigt, H. F. (1992). Sound-power collection by the auditory periphery of the Mongolian gerbil *Meriones unguiculatus*. I: Middle-ear input impedance. *The Journal of the Acoustical Society of America*, 92(1), 157–177.
- Ravicz, M. E., Rosowski, J. J., & Voigt, H. F. (1996). Sound-power collection by the auditory periphery of the mongolian gerbil *Meriones unguiculatus*. II. External-ear radiation impedance and power collection. *The Journal of the Acoustical Society of America*, 99, 3044.
- Richardson, M. H., & Formenti, D. L. (1982). Parameter estimation from frequency response

- measurements using rational fraction polynomials. *Proceedings of the 1st International Modal Analysis Conference* (Vol. 1, pp. 167–186). Retrieved from <http://systemplus.co.jp/support/data/techpaper/mescope/tech/07.pdf>
- Rolain, Y., Pintelon, R., Xu, K. Q., & Vold, H. (1995). Best conditioned parametric identification of transfer function models in the frequency domain. *IEEE Transactions on Automatic Control*, 40(11), 1954–1960.
- Rosowski, J. J. (2010). External and middle ear function. In P. A. Fuchs (Ed.), *Oxford Handbook of Auditory Science: The Ear*. Oxford University Press. Retrieved from <http://www.oxfordhandbooks.com/view/10.1093/oxfordhb/9780199233397.001.0001/oxfordhb-9780199233397-e-03>
- Rosowski, J. J., Cheng, J. T., Merchant, S. N., Harrington, E., & Furlong, C. (2011). New Data on the Motion of the Normal and Reconstructed Tympanic Membrane. [Miscellaneous Article]. *Otology & Neurotology December 2011*, 32(9), 1559–1567.
- Rosowski, J. J., Cheng, J. T., Ravicz, M. E., Hulli, N., Hernandez-Montes, M., Harrington, E., & Furlong, C. (2009). Computer-assisted time-averaged holograms of the motion of the surface of the mammalian tympanic membrane with sound stimuli of 0.4-25 kHz. *Hearing Research*, 253(1-2), 83–96.
- Rosowski, J. J., Dobrev, I., Khaleghi, M., Lu, W., Cheng, J. T., Harrington, E., & Furlong, C. (2013). Measurements of three-dimensional shape and sound-induced motion of the chinchilla tympanic membrane. *Hearing research*, 301, 44–52.
- Rosowski, J. J., & Lee, C. Y. (2002). The effect of immobilizing the gerbil's pars flaccida on the middle-ear's response to static pressure. *Hearing research*, 174(1-2), 183–195.
- Rosowski, J. J., Mehta, R. P., & Merchant, S. N. (2003). Diagnostic Utility of Laser-Doppler Vibrometry in Conductive Hearing Loss with Normal Tympanic Membrane. *Otology & neurotology: official publication of the American Otological Society, American Neurotology Society [and] European Academy of Otology and Neurotology*, 24(2), 165–175.

- Rosowski, J. J., Nakajima, H. H., & Merchant, S. N. (2008). Clinical Utility of Laser-Doppler Vibrometer Measurements in Live Normal and Pathologic Human Ears. *Ear and hearing*, 29(1), 3–19.
- Rosowski, J. J., Ravicz, M. E., & Songer, J. E. (2006). Structures that contribute to middle-ear admittance in chinchilla. *Journal of Comparative Physiology A: Neuroethology, Sensory, Neural, and Behavioral Physiology*, 192(12), 1287–1311.
- Rosowski, J. J., Ravicz, M. E., Teoh, S. W., & Flandermeyer, D. (1999). Measurements of middle-ear function in the Mongolian gerbil, a specialized mammalian ear. *Audiology and Neurotology*, 4(3-4), 129–136.
- Rosowski, J. J., Teoh, S. W., & Flandermeyer, D. T. (1997). The effect of the pars flaccida of the tympanic membrane on the ear's sensitivity to sound. *ER Lewis, GR Long, RF Lyon, PM Narins, CR Steele and E Hect-Poiner. Diversity in Auditory Mechanics. World Scientific, New Jersey* (pp. 129–135).
- Sadé, J., & Ar, A. (1997). Middle ear and auditory tube: Middle ear clearance, gas exchange, and pressure regulation. *Otolaryngology-Head and Neck Surgery*, 116(4), 499–524.
- Salih, W. H. M., Buytaert, J. A. N., Aerts, J. R. M., Vanderniepen, P., Dierick, M., & Dirckx, J. J. J. (2012). Open access high-resolution 3D morphology models of cat, gerbil, rabbit, rat and human ossicular chains. *Hearing Research*, 284(1–2), 1–5.
- Schwab, S. A., Eberle, S., Adamietz, B., Kuefner, M. A., Kramer, M., Uder, M., & Lell, M. (2012). Comparison of 128-Section Single-Shot Technique with Conventional Spiral Multisection CT for Imaging of the Temporal Bone. *American Journal of Neuroradiology*, 33(4), E55–E60.
- Shapiro, R. (2014). *Vibration measurements of the pressurized eardrum in gerbils*. McGill University.
- Sim, J. H., & Puria, S. (2008). Soft Tissue Morphometry of the Malleus–Incus Complex from Micro-CT Imaging. *Journal of the Association for Research in Otolaryngology*, 9(1), 5–21.

- Sim, J. H., Puria, S., & Steele, C. R. (2007). Calculation of inertial properties of the malleus-incus complex from micro-CT imaging. *J. Mech. Mater. Struct*, 2, 1515–1524.
- Slama, M. C. C., Ravicz, M. E., & Rosowski, J. J. (2010). Middle ear function and cochlear input impedance in chinchilla. *The Journal of the Acoustical Society of America*, 127(3), 1397–1410.
- Soons, J. A., Aernouts, J., & Dirckx, J. J. (2010). Elasticity modulus of rabbit middle ear ossicles determined by a novel micro-indentation technique. *Hearing Research*, 263(1-2), 33–37.
- Stenfors, L., Carlsöö, B., & Winblad, B. (1981). Structure and healing capacity of the rat tympanic membrane after eustachian tube occlusion. *Acta Oto-Laryngologica*, 91(1-6), 75–84.
- Stuart, A., Yang, E. Y., & Green, W. B. (1994). Neonatal auditory brainstem response thresholds to air-and bone-conducted clicks: 0 to 96 hours postpartum. *Journal of the American Academy of Audiology*, 5(3), 163.
- Subhash, H. M., Nguyen-Huynh, A., Wang, R. K., Jacques, S. L., Choudhury, N., & Nuttall, A. L. (2012). Feasibility of spectral-domain phase-sensitive optical coherence tomography for middle ear vibrometry. *Journal of Biomedical Optics*, 17(6). Retrieved from <http://www.ncbi.nlm.nih.gov/pmc/articles/PMC3381045/>
- Suehiro, M. (1990). [Effects of an increase or decrease in the middle ear pressure on tympanic membrane vibrations (experimental study by holographic interferometry)]. *Nihon Jibiinkoka Gakkai Kaiho*, 93(3), 398–406.
- Sun, Q., Gan, R. Z., Chang, K. H., & Dormer, K. J. (2002). Computer-integrated finite element modeling of human middle ear. *Biomechanics and Modeling in Mechanobiology*, 1(2), 109–122.
- Takanashi, Y., Shibata, S., Katori, Y., Murakami, G., Abe, S., Rodríguez-Vázquez, J. F., & Kawase, T. (2013). Fetal development of the elastic-fiber-mediated entheses in the human middle ear. *Annals of Anatomy - Anatomischer Anzeiger*, 195(5), 441–448.
- Teoh, S. W., Flandermeyer, D. T., & Rosowski, J. J. (1997). Effects of pars flaccida on sound

- conduction in ears of Mongolian gerbil: acoustic and anatomical measurements. *Hearing research*, 106(1-2), 39–65.
- The Hearing Foundation of Canada. (2010). Newborn Hearing Screening. Retrieved September 29, 2010, from <http://www.thfc.ca/cms/en/ChildrenYouth/NewbornHearingScreening.aspx?menuid=106>
- Timoshenko, S. P., & Woinowsky-Krieger, S. (1959). *Theory of plates and shells* (Second.). New York: McGraw-Hill. Retrieved from <http://archive.org/details/TheoryOfPlatesAndShells>
- Tonndorf, J., & Khanna, S. M. (1968). Submicroscopic Displacement Amplitudes of the Tympanic Membrane (Cat) Measured by a Laser Interferometer. *The Journal of the Acoustical Society of America*, 44(6), 1546–1554.
- Tonndorf, J., & Khanna, S. M. (1972). Tympanic-Membrane Vibrations in Human Cadaver Ears Studied by Time-Averaged Holography. *The Journal of the Acoustical Society of America*, 52, 1221.
- Tos, M., & Poulsen, G. (1980). Attic retractions following secretory otitis. *Acta Otolaryngologica*, 89(3-6), 479–486.
- Tuck-Lee, J. P., Pinsky, P. M., Steele, C. R., & Puria, S. (2008). Finite element modeling of acousto-mechanical coupling in the cat middle ear. *The Journal of the Acoustical Society of America*, 124, 348.
- Von Unge, M., Decraemer, W., Bagger-Sjöbäck, D., & Van den Berghe, D. (1997). Tympanic membrane changes in experimental purulent otitis media. *Hearing research*, 106(1-2), 123–136.
- Von Unge, M., Decraemer, W. F., Bagger-Sjöbäck, D., & Dirckx, J. J. (1993). Displacement of the gerbil tympanic membrane under static pressure variations measured with a real-time differential moiré interferometer. *Hearing Research*, 70(2), 229–242.
- Vlaming, M., & Feenstra, L. (1986a). Studies on the mechanics of the normal human middle ear. *Clinical Otolaryngology & Allied Sciences*, 11(5), 353–363.
- Vlaming, M., & Feenstra, L. (1986b). Studies on the mechanics of the reconstructed human

- middle ear. *Clinical Otolaryngology & Allied Sciences*, 11(6), 411–422.
- Volandri, G., Di Puccio, F., Forte, P., & Carmignani, C. (2011). Biomechanics of the tympanic membrane. *Journal of Biomechanics*, 44(7), 1219–1236.
- Voss, S. E., Rosowski, J. J., Merchant, S. N., & Peake, W. T. (2000). Acoustic responses of the human middle ear. *Hearing Research*, 150(1-2), 43–69.
- Wada, H., Ando, M., Takeuchi, M., Sugawara, H., Koike, T., Kobayashi, T., Hozawa, K., et al. (2002). Vibration measurement of the tympanic membrane of guinea pig temporal bones using time-averaged speckle pattern interferometry. *The Journal of the Acoustical Society of America*, 111, 2189.
- Wada, H., Metoki, T., & Kobayashi, T. (1992). Analysis of dynamic behavior of human middle ear using a finite-element method. *The Journal of the Acoustical Society of America*, 92(6), 3157.
- Wang, X., Cheng, T., & Gan, R. Z. (2007). Finite-element analysis of middle-ear pressure effects on static and dynamic behavior of human ear. *The Journal of the Acoustical Society of America*, 122, 906.
- Whittemore Jr., K. R., Merchant, S. N., Poon, B. B., & Rosowski, J. J. (2004). A normative study of tympanic membrane motion in humans using a laser Doppler vibrometer (LDV). *Hearing Research*, 187(1–2), 85–104.
- Williams, K. R., & Lesser, T. H. J. (1990). A finite element analysis of the natural frequencies of vibration of the human tympanic membrane. Part I. *British journal of audiology*, 24(5), 319–327.
- Winerman, I., Nathan, H., & Arensburg, B. (1980). Posterior ligament of the incus: variations in its components. *Ear, nose, & throat journal*, 59(5), 227–231.
- Zhang, X., & Gan, R. Z. (2011). Experimental measurement and modeling analysis on mechanical properties of incudostapedial joint. *Biomechanics and modeling in mechanobiology*, 10(5), 713–726.
- Zhao, F., Koike, T., Wang, J., Sienz, H., & Meredith, R. (2009). Finite element analysis of the

- middle ear transfer functions and related pathologies. *Medical engineering & physics*, 31(8), 907.
- Zheng, Y., Ohyama, K., Hozawa, K., Wada, H., & Takasaka, T. (1997). Effect of anesthetic agents and middle ear pressure application on distortion product otoacoustic emissions in the gerbil. *Hearing Research*, 112(1-2), 167–174.
- Zwislocki, J. (1957). Some Impedance Measurements on Normal and Pathological Ears. *The Journal of the Acoustical Society of America*, 29(12), 1312–1317.
- Zwislocki, J. (1962). Analysis of the middle-ear function. Part I: Input impedance. *The Journal of the Acoustical Society of America*, 34(9B), 1514–1523.
- Zwislocki, J. (1963). Analysis of the Middle-Ear Function. Part II: Guinea-Pig Ear. *The Journal of the Acoustical Society of America*, 35(7), 1034–1040.